CHARACTERIZATION OF CELL-PENETRATING PEPTIDE COMPLEXATION AND INTERACTION WITH PLANT CELLS

JORDAN TAN PEPPER
Bachelor of Science, University of Lethbridge, 2013

A Thesis
Submitted to the School of Graduate Studies
of the University of Lethbridge
in Partial Fulfillment of the
Requirements for the Degree

MASTER OF SCIENCE

Department of Biological Sciences
University of Lethbridge
LETHBRIDGE, ALBERTA, CANADA

CHARACTERIZATION OF CELL-PENETRATING PEPTIDE COMPLEXATION AND INTERACTION WITH PLANT CELLS

JORDAN TAN PEPPER

Date of Defence: December 7, 2015

Dr. F. Eudes Co-supervisor	Research Scientist	Ph.D.
Dr. I. Kovalchuk Co-supervisor	Professor	Ph.D.
Dr. A. Ziemienowicz Thesis Examination Committee Member	Biologist	Ph.D.
Dr. P. Hazendonk Thesis Examination Committee Member	Associate Professor	Ph.D.
Dr. T. Burg Chair, Thesis Examination Committee	Associate Professor	Ph.D.

This Thesis is dedicated to my parents, Darren and Lei-Lian Pepper, and those many others who have helped me achieve my goals and stayed supportive through many trying moments with me.

Abstract

Cell penetrating peptides (CPPs) are short 8-30 amino acid polypeptides that are able to transit across the semi-permeable plasma membrane of living cells, and deliver bound cargoes to the cytoplasm and other subcellular locations (e.g. nucleus, plastid organelles etc). The use of CPPs in plant cells and tissues remains a small and little researched field compared with the greater body of animal based research imperatives. The present research describes firstly, the measured interaction of the chosen model CPP Tat_2 with the cell wall of microspores (i.e. microspore exine), secondly the reduction of the size and increase in regularity (measured as polydispersity) of Tat_2 nucleic acid polyplexes and the unique empirical derivation of pseudo-kinetic parameters of nucleic acid CPP aggregation. Additionally several attempts to apply the findings from this research in plant cells and tissues are presented and discussed throughout.

Acknowledgements

This work was not possible without the support of many individuals and colleagues. The members of the Eudes lab with Agriculture and Agri-food/Agriculture et Agroalimentaire Canada (AAFC-AAC), were all highly appreciated for their ideas, recommendations, affirmations, critiques, advice and encouragement. Specifically thanks may be given to Laboratory technicians Dr. Fengying Jiang and Kimberley Burton-Hughes, Post-Doctoral researchers Dr. Andriy Bilichak and Dr. Rakesh Sinha; to National Research Council (NRC) collaborators Dr. Elizabeth Marillia and Dr. Palak Kathiria. Especial gratitude for guidance and hands-on mentorship must be given to Dr. Priti Maheshwari, whose patience, wealth of knowledge and endearing encouragement was of great benefit to myself during difficult areas during the course of research.

Finally the criticism and direction provided by the members of the Thesis Examination Committee, Dr. Alicja Ziemienowicz and Dr. Paul Hazendonk; Dr. Ziemienowicz especially for her vast knowledge of transfection and hands-on guidance during the last months of research and Dr. Hazendonk for his unique intellectual contributions to the chemistry involved in many of the projects undertaken over the last two years.

Lastly, I must recognize and thank my two Co-supervisors, Dr. François Eudes and Dr. Igor Kovalchuk. Dr. Kovalchuk provided unerring encouragement during my time as a Master's student and helped greatly with his excellent classes and piercing questions. Dr. Eudes, as my principle supervisor, provided very direct and challenging research goals, while still allowing me the freedom to explore ideas and methods to achieve those goals, allowing me to develop my skills independently and freely.

Table of Contents

List of Tables

List of Figures

List of Abbreviations

ADP-RF – adenosine diphosphate ribosylation factor
AFM – atomic force microscopy
CDC – cell division control protein
cDNA – complementary DNA
CDS – circular dichroism spectroscopy
CIMC wash – a medium designed for induced microspore culture
Cn-AMP2 – an anionic CPP
CPP – cell-penetrating peptide
ddH_2O – double distilled water
D_H – hydrodynamic diameter
DLS – dynamic light scattering
DNA – deoxyribonucleic acid
DoE – design of experiment
dsDNA – double stranded DNA
dsRNA – double stranded RNA
ELS – electrophoretic light scattering
FDA – fluorescein diacetate
FITC – fluorescein isothiocyanate
GAG - glycosaminoglycan
GUS – β-glucoronidase enzyme
gus – β-glucoronidase gene
HIV-1 – human immunodeficiency virus 1
HR9 – histidine rich nona-arginine
I_c – ionic strength
$(KH)_9$-BP100 – a synthetic CPP derived from antimicrobial undecapeptide (BP100)
MβCD – methyl-β-cyclodextrin
MALS – multi-angle light scattering
MM – Maltose-mannitol solution
mRNA – messenger RNA
PDI – polydispersity index
PDS – phytoene desaturase enzyme
PEI – polyethylenimine
PQ-D16 – Poly[(3-methyl-1-vinylimidazolium chloride)-co-(1-vinylpyrrolidone)], Luviquat^{TM} FC-370
pVec – peptide vascular endothelial-cadherin
PVP – polyvinylpyrrolidone
R_g – radius of gyration
R_H – hydrodynamic radius
RLI – RNase L inhibitor protein
RSM – response surface methodology
RT-qPCR – real time quantitative polymerase chain reaction
RWM – reduced wash media
SEM – scanning electron microscopy
siRNA – short interfering RNA

SLS – static light scattering
SR9 – synthetic non-arginine
ssDNA – single stranded DNA
SUV – synthetic unilamellar vescicle
Tat – trans-activator of transcription
Tat_2 – sequence dimer of Tat
TBAB – tetrabutylammonium bromide
TBPB – tetrabutylphosphonium bromide
TEM – transmission electron microscopy
uv-vis – ultraviolet to visible wavelengths
V_H – hydrodynamic volume

1.0 Introduction

Cell-Penetrating Peptides (CPPs) are some of the most versatile non-biological methods known for delivering cargo into living cells (Bechara and Sagan 2013). This is owed in part to their ever increasing variety and also in part to their intrinsic chemical complexity. This chapter describes firstly the nature, identity and history of CPPs in a general sense, and secondly the methods of characterizing CPP:nucleic acid complexes (referred to as polyplexes). Thirdly, this chapter relates the use of CPPs in planta in detail, prefacing the main body of this thesis which has a particular emphasis on plant *in vitro* and *in vivo* systems.

1.1 Brief History of CPPs

CPPs are 8-30 amino acid residue polypeptides that display the ability to traverse the plasma membrane of living cells. The first two CPPs to be catalogued and studied were discovered almost simultaneously in sequences extracted from the transit domains of the trans-activator of transcription from HIV-1 and the Antennopedia homeodomain transcription factor. Both transit domain sequences were characterized by a high density of basic residues, particularly lysine and arginine. Furthermore, both were transcription activators, wherein the basic residues were crucial for import into the nuclei of cells, and DNA binding. This was the first evidence of highly hydrophilic substances transiting across the plasma membrane by a mechanism that was apparently independent of active or facilitated transport (e.g. receptors or protein channels)(Brock 2014). The transit domains were named penetratin in the case of the Antennopedia homeodomain transcription factor and Tat (or TAT) in the case of the trans-activator from HIV-1 (Madani, Lindberg et al. 2011). Both, especially Tat, now form a standard to which most

other similar CPPs are compared.

The discovery of Tat and penetratin allowed for the screening and identification of a large number of similar transit domains from a number of different species and protein origins, such as the BP series (Eggenberger, Mink et al. 2011), and pVEC (Mäger, Eiriksdottir et al. 2010). Furthermore, additional research into the essential elements of these naturally occurring sequences led to the synthesis of synthetic CPPs like ^{msr}(W/R) (Delaroche, Aussedat et al. 2007), synthetic nona-arginine, histidine-rich nona-arginine, Pep-1 and even more exotic modern inventions such as the NickFect (Oskolkov, Arukuusk et al. 2011) and PepFect series (Ezzat, Andaloussi et al. 2011) which incorporate stearyl moieties. This now large library of CPPs has been utilized primarily in human and animal cells, because of their potential for delivering therapeutics and dsRNA, which can potentially treat cancers (Bolhassani 2011). However, CPPs have been shown to also be functional in many other cell types, most notably plant cells, presenting an alternative approach to genetic engineering in economically relevant plant species (Chugh, Eudes et al. 2010).

Even with the fruitful history of CPP research, many questions are still open regarding their exact mechanism of entry and delivery of cargoes, and how to optimize them for different types of cells and *in vivo* systems.

1.2 Classification of CPPs:

CPPs may be classified according to several parameters, namely their mechanism of cellular entry, sequence of amino-acids, net charge and hydrophobicity. It has been shown that these physical characteristics are interrelated and allows for the definition of

four broad categories of CPPs; cationic CPPs, primary amphipathic CPPs, secondary amphipathic CPPs and anionic CPPs.

Cationic CPPs are by far the most familiar, due to their amenability in forming nanoparticle polyplexes with nucleic acids (Liu, Liou et al. 2013). The electrostatic interaction of lysine, histidine or arginine residues with the backbone phosphates of nucleic acids, allows for the compression of large fragments of DNA. This property is coupled with a retention of the cell-penetrating properties of the CPP, and it's interactions with the plasma membrane (Kawamoto, Miyakawa et al. 2012).

It has been shown that of the three positively charged amino-acids, arginine has the most cell-penetrating efficacy, which led to the development of synthetic nona-arginine (SR9), histidine rich nona-arginine (HR9) (Liu, Liou et al. 2013) based on peptides like Tat. Furthermore, the length of the polyarginine was also explored, and showed that a critical length was required for transduction of the peptide into living cells (Mizuno, Miyashita et al. 2009). This study showed that a minimum of six consecutive residues was required, and dropped off considerably with greater than twelve residues. This requirement for an optimal number of residues suggests other structural features of cationic peptides beyond the sequence, whereby a balance of phospholipid interaction and later entry into the cell requires a certain size.

Primary amphipathic CPPs are characterized by a larger sequence length, greater than fifteen residues and large numbers of tryptophan, leucine and isoleucine residues. While they also often include arginine as well, their unique properties have been traced to their hydrophobic residues (El-Andaloussi, Jarver et al. 2007). Unlike cationic CPPs

which must somehow transit across the plasma-membrane hydrophobic core as highly hydrophilic molecules, primary amphipathic CPPs have the advantage of high hydrophobicity which allows for direct interaction, not just with the head groups, but also with the fatty acid chains of phospholipids. This lowers the energy required for direct import through the plasma membrane (Deshayes, Plenat et al. 2004, Madani, Lindberg et al. 2011).

The categorical separation between cationic, primary amphipathic CPPs is bridged by the secondary amphipathic CPPs. Secondary amphipathic CPPs have sequences which have a mix of hydrophobic residues, and cationic residues. Penetratin displays features of secondary amphipathic CPPs, with a preponderance of tryptophan and leucine in addition to blocks of lysine and arginine. It has been surmised that the distribution cationic residues and hydrophobic residues within this class of CPPs allows for structural changes that occur at the plasma membrane, wherein the normally flexible random coil conformation converts to an α-helix which can infiltrate the lipid bilayer of the plasma membrane suggesting a mechanism for transit (Milletti 2012).

Lastly, the most uncommon class of CPPs are anionic CPPs, of which only a few examples exist. These particular CPPs are unique in that their net charge is anionic requiring interaction with zwitterionic phospholipid head groups, such as phosphotidyl choline, ethanolamine or serine (Yamada, Signorelli et al. 2015). Little is known about this class as their exploration is comparatively recent. Two prime examples, p28 (Yamada, Das Gupta et al. 2013) and Cn-AMP2 (Prabhu, Dennison et al. 2014) have been identified as anticancer and antimicrobial cell-penetrating peptides respectively, with no recorded nanocarrier properties. However, the lack of studies in which these

peptides are used as nanocarriers is likely due to the relative newness of exploration of these peptide and their most obvious uses as functional peptides.

The classification approach taken primarily deduces the categories of CPPs from their sequence and relative charge. It has been found that this particular method provides the best summation of the physical qualities and entry mechanisms of the present large library of CPPs. However, it must also be noted that synthetic and designed CPPs, particularly those that include non-classical amino-acids, or additional modifications and moieties, such as stearyl groups and phosphates, may diversify these classifications significantly (Mäe, El Andaloussi et al. 2009, Zhang, Song et al. 2013).

1.3 CPP Mechanisms of Cellular Entry

The debate over the cellular entry mechanisms of CPPs has been a central controversy within the field. This has been in part due to the large variety of CPPs, different cell types examined and the fact that they utilize multiple mechanisms of entry simultaneously which obscures the dominant mechanism of cellular entry (Mäger, Eiriksdottir et al. 2010, Jain, Yadav et al. 2015, Rodrigues, Andreu et al. 2015). It is, however, generally agreed that the primary manner of entry is through either an energy independent direct transport through the plasma membrane or through several forms of endocytosis (Brock 2014). While the first mechanism of direct transit is certainly the most intriguing, it seems to be favored in cases where CPPs act as singular molecules with no attached cargoes. When cargoes are affixed to the CPP endocytotic mechanisms seem to be more prevalent (Rodrigues, de la Torre et al. 2013). The following sections review the details of CPP entry mechanisms.

1.3.1 CPP Entry as Singular Molecules

The entry of CPPs into living cells is well documented from fluorescent studies, in which labelled peptides were used to detect the presence of the peptides in cells via fluorescent microscopy, particularly laser scanning confocal microscopy (Guterstam, Madani et al. 2009). These experiments have shown that as free molecules, the CPPs may transit across the plasma membrane and localize to the cytoplasm and nucleus, and may do so without inducing classical endocytotic pathways. However, because fluorescent studies are not always reliable, especially in the case of cationic CPPs as the addition of a highly amphipathic organic fluorophore like FITC or FDA, can and do change the chemical properties of the peptide, such that it does not accurately represent the activity of the peptide of interest (Lehto, Abes et al. 2010). Therefore, more creative measures must be used to determine their mechanism of entry with a high fidelity of accuracy. In particular, quantum dot conjugation which covalently attaches an inert inorganic fluorescent crystal to the peptide of interest. This conjugation does not affect the chemical properties of the CPP(s) as dramatically as attachment of a classical organic fluorophore (Liu, Huang et al. 2010).

Studies that have attempted to deduce the particular mechanism of entry for cationic CPPs such as Tat and oligo-arginines, have done so through knocking out endocytotic pathways, like clathrin and caveolin mediated endocytosis, through inhibitors such as chloroquinone, sucrose, genistein and MβCD (Rosenbluh, Singh et al. 2004, Minchin and Yang 2010). By knocking out various classical endocytosis pathways and observing little to no effect on CPP localization, it was proposed that all classes of CPPs must transit via direct penetration through the plasma membrane that does not require the

formation of endosomes. Additionally it was found that endocytotic mechanisms were preferred at physiological temperatures, but significant cooling of transfection reactions, to less than 20^{o}C, and as low as 4^{o}C, caused a predominance of direct translocation pathways (Chugh and Eudes 2008). Direct transfer has been proposed to proceed by no less than two distinct perturbations of the lipid bilayer; pore formation and inverted micelle formation.

Pore formation has been verified using membrane leakage assays, involving the release of a substrate from a synthetic lipid bilayer, that was then quantified over time and concentration of CPP used. An example is the use of ion flux as a result of CPP exposure, ionic strength, determined by media conductivity of the solution increasing due to leakage. This leakage has been linked to significant increases in cytotoxicity in cell culture at elevated concentrations of CPPs (Herce, Garcia et al. 2009). The manner in which cationic CPPs form pores in the plasma membrane has been linked directly to the activity of arginine and lysine, guanidinium and amine side chains respectively. These side chains penetrate the lipid bilayer and associate with the head groups of the cytosolic side of the plasma membrane, pulling the opposing phospholipids towards the extracellular side of the plasma membrane; multiple such interactions result in the formation of a pore. The pores formed are transient and are conjectured to last no more than the microsecond scale at lower concentrations of CPP, below 7 μM in the case of SR9. The pore formation pathway is not restricted to cationic CPPs, as secondary amphipathic CPPs like penetratin have demonstrated similar effects at higher concentrations (Guterstam, Madani et al. 2009).

Shuttling across the cell membrane via inverted micelles has largely been cited in

computation models, wherein molecular mechanics calculations were utilized. Molecular mechanics is a computational chemistry method designed to determine the features of large systems of intermolecular interactions by reducing the complex quantum nature of these interactions to classical physics counterparts. In this way, calculations involving tens of macromolecular structures may be approximated with relative efficiency, which would be extremely costly or impossible using *ab initio,* density functional theory or semi-empirical methods. This method has substantiated an otherwise difficult to detect or assay mechanism that shows the binding of the cationic residues in CPPs to the phospholipid head groups of a modelled lipid bilayer, subsequent induction of negative curvature in the upper leaflet of the bilayer and stabilization of a micelle within the membrane, before eventual release on the other side of the lipid bilayer restoring the bilayer. It has been concluded that this type of translocation induces a flip-flopping of phospholipids that was verified in synthetic unilamellar vesicles (SUVs) by ultraviolet to visible light (uv-vis) spectroscopy. This flip-flopping allowed for the determination of transient complex formation during curvature of the plasma-membrane between CPP cationic residues and phospholipids, forming structures similar to that of liposomes (Swiecicki, Bartsch et al. 2014). This facilitates the rapid internalization of the CPP. These studies do not, however, investigate the role of the inverted micelle mechanism in cell or tissue culture, only in non-biological systems, and therefore has not been as rigorously determined as a primary mechanism of entry as pore formation. The use of unilamellar vesicles vastly simplifies the composition of the plasma membrane, excluding transmembrane receptors, cytoskeletal tubulin and actin, glycosaminoglycans and peripheral proteins (Favretto, Wallbrecher et al. 2014). This renders such studies

useful, but far from comprehensive and explanatory (Takechi, Yoshii et al. 2011).

While these two mechanisms have been identified, it is not thought that they occur in exclusion of each other, but rather certain peptides may display a preference for one or the other. For example SR9 and Tat have been shown to favor pore formation, while penetratin and other secondary amphipathic peptides show a tendency towards inverted micelle formation for efficient delivery. This is further complicated by the cell type used, and the composition of the phospholipids, not to mention other membrane components.

1.3.2 CPP Entry as Nanocarriers:

CPPs have been largely explored for their use as nanocarriers, to deliver otherwise impermeable macromolecules into living cells. CPPs have acted as nanocarriers for proteins, circular and linear plasmid DNA, oligo-nucleotides, PCR product DNA, dsRNA, and bioactive small molecules (Chugh and Eudes 2008, Milletti 2012, Brock 2014). In general, for macromolecular cargoes the mechanisms of entry have been reduced to endocytosis, with little evidence of a strong contribution from direct translocation. This is likely due to a substantial increase in the size of the translocating particle, but also due to changes in the chemistry of the CPP upon association with the cargo of interest. In particular, polyplexes formed between CPPs and nucleic acids are quite large, usually averaging from 100-200 nm in diameter, compared to proteins which are usually less than 10 nm in diameter, with the lone CPP being smaller still (Jafari, Xu et al. 2014). This larger size makes translocation by a direct method energetically unfavorable. Instead, either classical forms for endocytosis (e.g. clathrin and caveolin) or another form of endocytosis, referred to as macropinocytosis, must often be invoked to

allow transit of these larger complexes (Jones 2007, Eggenberger, Mink et al. 2011).

Unlike classical ligand-receptor based forms of endocytosis, there is no currently defined receptor for macropinocytosis, as it relies instead on the remodeling of actin filaments near the plasma membrane to engulf particles that interact strongly with the plasma-membrane. In most examples this interaction is the same as that cited in the translocation of CPPs alone, an electrostatic binding between anionic or zwitterionic phospholipids with cationic CPP residues, primarily arginine. However, hydrophobic residues, particularly tryptophan are essential for translocation in some CPPs such as transportan, implicated in infiltrating the plasma membrane hydrophobic core. It is thought that the induction of curvature of the plasma membrane by the CPP-cargo conjugate or complex, stimulates the remodelling of actin filaments in an energy independent manner. This has been determined by observing endosome formation and release of cargo molecules in the cytoplasm of living cells at reduced temperatures and in the presence of classical endocytosis inhibitors (Shim, Eudes et al. 2012).

More recently it has been shown that the presence of a strongly negative glycocalyx consisting of heparin sulphate and other GAGs surrounding the cell membrane contribute to the internalization of CPP-cargo complexes and conjugates. It has been proposed that other than the obvious electrostatic interaction of the glycocalyx GAGs with the CPP, there is a sequestering of the GAGs on the outer leaflet of the plasma-membrane that leads to Rac-1 dependent actin reorganization, similar to macropinocytosis (Ziegler and Seelig 2011). With their involvement not completely understood, there is still debate as to whether they inhibit or enhance translocation of cargo bearing CPPs, as results have been contradictory.

Import via endosomes is only half the process of the nanocarrier properties of CPPs, as the cargo imported must also be released. Endosomal trafficking and escape as well as cargo release are essential to the functionality of CPPs as delivery agents. Endosomal escape has in fact been a major obstacle to the broader use of CPPs in practical areas, as the late endosome is often targeted towards lysosomes for degradation, where the functional cargo is often deactivated or destroyed. Arginine residues have shown some ability to deactivate lysosomes by rapidly raising the pH of the organelle due to arginine's basicity (Tanaka, Kanazawa et al. 2013). Additionally, this process may be assisted by destabilization of the endosome by the CPPs bound to the cargo molecule, invoking mechanisms similar to free peptide import. Lastly, cargo release must occur in the case of CPP:nucleic acid polyplexes, either by protease degradation of the CPP, or release due to structural changes brought on by cytoplasmic or target organelle conditions. Interestingly, it has been found that in plants the $(KH)_9$-BP100 CPP delivers nucleic acid cargoes more efficiently with less CPP proportionate to nucleic acid. This suggests that at least in the case of this CPP, the release of the cargo is facilitated by using less CPP (Lakshmanan, Yoshizumi et al. 2015).

1.4 Characterization Methods of CPP:Nucleic Acid Polyplexes

The formation of CPP:Nucleic acid polyplexes is of primary concern in a number of publications, and as a result, the need for adequate characterization of the nanoparticles formed from CPPs and nucleic acids has been required (Ezzat, Andaloussi et al. 2011). To accomplish this a range of analytical methods have been used, including high resolution microscopies like scanning electron microscopy (SEM) and atomic force

microscopy (AFM), circular dichroism spectroscopy (CDS) (Takechi, Yoshii et al. 2011) and even agarose gel electrophoresis assays (Chugh and Eudes 2008). These assays and methods are informative as to some parameters such as nuclease resistance in gel electrophoresis assays, or helical conformation versus beta-sheet or random coil conformation in CPPs with CDS and overall size of nanoparticles in AFM and SEM.

High resolution microscopies are very useful for determining the size and shape of hard or extremely compact polyplexes but fall short with looser conformations or polyplexes. Sample preparation for both AFM and SEM requires at minimum the deposition of the nanoparticles on the surface of a mesh or slide, eliminating any flexible features or complex shape the particles might have had while suspended in solution. It therefore only evaluates the size of nanoparticles once essentially compacted against a surface, introducing some inaccuracy regarding its true active state. Still, AFM, SEM and even transmission electron microscopy (TEM) remain valuable methods of nanoparticle identification and evaluation.

Agarose gel electrophoresis assays are quite common, but definitely the least powerful and most limited in determining properties of CPP:nucleic acid polyplexes, still useful information regarding the efficiency of complexation can be gleaned from this simple assay. Using very standard conditions of agarose gel electrophoresis (e.g. 0.5-1.0% gels, TAE buffer, ethidium bromide staining), a standard assay for efficiency of complexation may be performed by loading mixtures of ever increasing ratios of CPP to nucleic acid and observing exclusion of ethidium bromide due to blocking of intercalative interactions by CPP (Imani, Emami et al. 2015) or alternatively the retardation of electrophoretic shift can be used to gauge efficiency of complexation. The ethidium

bromide exclusion assay, in particular, can help determine the amount of CPP required to fully complex a given amount of the desired nucleic acid, by observing the dimming of the complexed bands compared to a control (Smith, Beck et al. 2015). Alternatively, nuclease digestion may be performed prior to running of the agarose gel, and the amount of degradation qualitatively determined from the intensity of lower weight bands in the gel; degradation that is inhibited by the compression and protection of the nucleic acid backbone by the CPP (Chugh and Eudes 2008).

Circular dichroism spectroscopy allows for quantification of the percentage of α-helix, β-sheet, or random coil conformation present in a given peptide, as well as the helicity of the nucleic acid involved. It cannot determine the location or distribution of the conformations, but may be used to determine changes in conformation over time or in different formation conditions. For this reason, it is a powerful technique for determining the general structure of the peptide alone and completely associated with the nucleic acid, with some options for real time analysis of the process of complexation (Ranjbar and Gill 2009).

Thus far the most useful set of methods for CPP:nucleic acid characterization and profiling have been light scattering methods. Apart from the already described techniques, this particular set is very common with the field of CPP research due to their relative ease of use and the quantity of data that can be acquired.

1.4.1 Light Scattering Methods

Light scattering methods generally revolve around the measurement of scattered laser light of a specific wavelength at specific angles of incident and detection. Within this general technical system there exists several common methods, particularly static

light scattering (SLS), dynamic light scattering (DLS), multi-angle light scattering (MALS), and electrophoretic light scattering (ELS) (Jafari, Xu et al. 2014). These methods fall squarely within the realm of particle characterization methods, capable of measuring the size, molecular weight and the zeta-potential of macromolecules and macromolecular complexes and polyplexes (see Table 1.1).

Table 1.1: Profiles of Light Scattering Methods

Technique	Parameter(s) Measured
Dynamic Light Scattering (DLS)	Hydrodynamic Diameter/Radius Polydispersity Index (PDI)
Static Light Scattering (SLS)	Molecular Weight, Radius of Gyration
Multi-angle Light Scattering (MALS)	Hydrodynamic Diameter/Radius, Absolute Molecular Weight, Radius of Gyration
Electrophoretic Light Scattering (ELS)	Zeta-potential, Electrophoretic Mobility

In most publications DLS and ELS are the primary methods of physical characterization of CPP:nucleic acid polyplexes. As CPP:nucleic acid polyplexes usually take the form of nanoparticles which are dominated by the CPP component, they are often best described by their size and their electrostatic interaction with their suspension media. Size is reflected in their hydrodynamic diameter or radius, while their electrostatic character is represented by a measure of their zeta-potential (Oskolkov, Arukuusk et al. 2011).

Hydrodynamic diameter or radius, D_H or R_H respectively, is not an exact measure of the size of the particle, but rather a reflection of the rate of diffusion of the particle in a specific solution. This means that the D_H or R_H measured is in fact the diameter or radius

of a so called “hard sphere” that diffuses at the same rate as the particle observed. As such, the shape of the particle is not taken into account as both rotational and translational degrees of freedom contribute to the measured value. Furthermore, in simple terms, since DLS measures diffusion of light scattering particles, the size is displayed as a distribution peak, and not a discrete number. Therefore, care must be taken when interpreting DLS data, because determining which size distribution is most significant becomes crucial, especially in multimodal systems (i.e. more than one peak) like those produced by CPP:nucleic acid polyplexes (Ezzat, Andaloussi et al. 2011, Quebatte, Kitas et al. 2013).

Polydispersity index or PDI, is another important parameter measured by DLS. PDI in the case of DLS is a quantitation of the heterogeneity of the sizes of the particles in a sample, based on the size distribution. The broader the distribution peak the more heterogeneous the size of the particles are within a sample, the narrower the distribution peak the more homogeneous the particles are within a sample. Generally, PDI values may vary between 0.0 and 1.0, with PDI values less than 0.1 representing extremely homogeneous particles and PDI values of 0.7 or higher being extremely heterogeneous particles. It has been found that polyplex forming CPPs like Tat maintain PDIs that are between 0.2 and 0.5, which is considered moderately polydisperse, but this is often dependent on the media used for formation and the nature of the nucleic acid. PDI lower than 0.2 is quite uncommon in CPP:nucleic acid polyplexes (Jafari, Xu et al. 2014, Lakshmanan, Yoshizumi et al. 2015).

Commonly, PBS, HEPES, TRIS and ddH_2O based media and buffers are used as suspension media for measuring size and PDI (Zhang, Song et al. 2013, Jafari, Xu et al. 2014, Yan, Gu et al. 2015). They are often chosen in order to measure and understand the

behavior of these polyplexes in solutions amenable to the cell or tissue culture of interest. This range of buffers and media however, bring up a degree of concern that must be addressed; the viscosity of the suspension medium. It must be remembered that, because DLS actually measures the diffusion of particles in suspension, the Einstein-Stokes equation used to calculate the size of the polyplexes must factor in the viscosity of the solution for accurate results. If the viscosity is not accurate, the size distribution will not be accurate either (Abe, Kawaguchi et al. 2013). Few publications concern themselves with detailing the use of a viscometer to determine medium viscosity, or state the calculated viscosity of their buffer based on the viscosity increments and decrements of the various salts in them. As a result DLS data must be used as a general idea of the size of a particular polyplex formulation and not interpreted as definite. Moreover, the same applies to refractive index, which is well influenced by solutes, and unless accounted for, can decrease the accuracy of measurements for larger particles.

ELS offers equally useful information regarding CPP:nucleic acid polyplexes, as the electrostatic character of the polyplex governs its ability to interact with the membrane of most typically used systems. ELS works by applying a voltage to a particle suspension, and then measuring, using laser Doppler velocimetry, the electrophoretic mobility of the particle in the solution. Laser Doppler velocimetry determines the rate at which the particles move towards the anode or the cathode exposed to the suspension. The faster the movement the more negatively charged or positively charged the particle is calculated to be. This charge is reflected in the zeta-potential value, a voltage which has a magnitude proportional to the electrostatic charge of the particle at its interface with the suspension medium. The zeta-potential is easily influenced by the nature of the

suspension medium in the same way DLS is, where viscosity and salt or surfactant content of the medium can influence the measurement unless carefully controlled and monitored. These factors must be worked out accurately in order for reliable information to be obtained.

Both SLS and MALS have seen less use in examining CPP:nucleic acid polyplexes, but have been used for similar systems wherein cationic polymers have been used to complex DNA. Both methods are capable of determining the molecular weight of polymers in solution, but only MALS is capable of determining radius of gyration. A radius of gyration is the distance from the axis of a rotating mass to its outermost point. SLS assumes that a particle scatters light uniformly regardless of the angle of detection and therefore assumes a particular shape (e.g. a sphere) and value of R_g, while MALS uses detection at multiple detection angles to accurately measure molecular weight of larger particles or non-Rayleigh scattering particles that have complex shapes. In combination with DLS, MALS allows the determination of a nanoparticles shape using a ratio R_g:R_H or ρ, where unity between the two numbers (Wattraint, Saadallah et al. 2013), a ratio of 1:1 indicates a perfect sphere and higher values indicate more elongated spheroid shapes, values much lower do not generally occur, as the radius of gyration always measures the distance to the most eccentric point .

Using these techniques in combination have allowed robust profiling of polyplexes and assisted in designing CPP based nanoparticles and determining the chemistry of complex formation.

1.5 Application of CPPs in Plant Systems

The use of CPPs for any purpose in plant cells has not received the same amount of attention as that performed in animal and human systems. Despite this the last seven years have proven to show remarkable progress in the field, despite only a handful of research groups being dedicated to the subject. Many of the same principles of CPP utilization in animal cell systems hold for plant cells and tissues, however large differences in the cellular biology of plants and animals have made the use of CPPs in plant systems more challenging. Almost universally, CPPs are less effective in plant tissues, both as singular molecules and as nanocarriers and it has been found that general rules for animal cell translocation and successful delivery of macromolecular cargoes are not always applicable or useful in plant cells.

In a comparative study and the first to report CPPs entering plant cells, the transfection efficiency of several fluorescently labelled CPPs (pVEC, TP10, penetratin and Tat) were compared in both Bowes human melanoma cells and SR-1 tobacco protoplasts. The findings were not encouraging, as it was found that all CPPs internalized in the Bowes human melanoma cells with nearly 100% of all intact cells transfected, while in the case of SR-1 tobacco protoplasts less than 16% (15.7% for transportan) of intact cells were transfected for all CPPs, and as low as 2.8% with penetratin (Mäe, Myrberg et al. 2005). Despite this, the verification of successful transfection indicated that CPPs were a plausible transfection agent for plant cells.

As a cargo carrier, the first indications that CPPs possessed qualities that would transfect plant cells were found through experiments where hexadimethrine bromide

(polybrene) and spermidine were used to transfect corn protoplasts and cotton suspension cell cultures. Hexadimethrine bromide, spermine and spermidine are net cationic compounds, a tertiary ammonium polycation in the case of hexadimethrine and polyamines in the case of spermine and spermidine. Because these compounds are known to bind DNA, and stick to the outside of plant cells, it was found that plasmid DNA could enter and transform plant cells when the cells were pre-incubated with these compounds, and could regenerate transgenic plants (Antonelli and Stadler 1990, Sawahel 2001).

Success in plant tissues and cell cultures may be considered of greater merit, as the delivery of cargo such as DNA or siRNA is often already applied in *in vivo* systems such as leaves, while CPP mediated delivery in animals is often bottlenecked at the organismal level (Nguyen, Xie et al. 2008).

1.5.1 Protein Delivery

In a 2004 publication it was shown that core histones could translocate across the plasma membrane of petunia protoplasts. Additionally, it was shown that BSA covalently bound to H2A was also able to translocate under the same conditions as histone alone. De-acetylated histones possess a large number of lysines and arginines required for nucleosome formation and demonstrated a similar pattern of cellular entry to that of CPPs, in that reduction of temperature during transfection to $4^{o}C$ and treatment with Nocodazole did not inhibit uptake (Rosenbluh, Singh et al. 2004).

After this initial indication, CPP-mediated protein delivery in plants has seen clear progress as the most successfully delivered cargo. However, all cargoes delivered to date have been marker proteins, such as GUS, aequorin, GFP and RFP, but the range of

tissues and species is extensive, from somatic tissues like leaves and root tips, to gametophytic tissue like cereal microspores and from onions to wheat (Ziemienowicz, Pepper et al. 2015).

The delivery of the β-glucoronidase enzyme (GUS), using simple complexation with Tat, Pep-1 and Tat_2, to triticale microspores was the first demonstration of gametophytic tissue CPP-mediated protein transfection with complexes formed from CPPs and protein (Shim, Eudes et al. 2012). Later, a fluorescent protein, Aequorin from *Aequorea victoria* was fused to Tat, and shown to translocate successfully into soybean suspension culture cells. Aequorin only fluoresces in the presence of calcium ions and this allowed for the observation of calcium ion concentration in the cells, demonstrating a possible assay for quantifying intracellular calcium concentration of plant cells (Zonin, Moscatiello et al. 2011).

Recently, mCherry delivery in wheat microspores using a cys-cys disulfide bond between cysteinated R9 and cysteinated mCherry demonstrated the highest translocation efficiency above that of simple complexes and fusion variants. It was also demonstrated that greater binding affinity to the microspore cell wall (exine) was essential for translocation as evidenced by confocal microscopy. The translocation efficiency was found to also be related to the amount of excess peptide used for disulfide bond formation, as larger ratios of R9 to mCherry increased translocation efficiency, implicating a combination effect between covalent linkage and complexation (Bilichak, Luu et al. 2015).

Due to the success of protein delivery in plant cells, reports of other more

functional proteins such as genome editors like zinc-finger nucleases, or gene regulators like TALES as CPP cargoes will likely appear in the near future.

1.5.2 DNA Delivery

The delivery of DNA has seen far less success in plant systems in terms of publications, than proteins. However, some success in recent years has been compelling, but also lacking in displaying high transfection efficiencies. In the same work that detailed the delivery of GUS protein in microspores, the delivery and expression of *gus* encoded on linearized plasmid was found to reach a maximum of 4% efficiency when complexed with Tat_2 versus much lower (less than 1%) efficiencies for a mutant Tat (M-Tat) and Tat (Chugh, Amundsen et al. 2009). This correlated well with findings in wheat zygotic embryos, that employed Tat_2 in concert with lipofectamine to deliver the same *gus* encoding linear plasmid at an efficiency of 12.7%. Unfortunately Tat_2 without the addition of lipofectamine was less effective at 8.3% efficiency (Chugh and Eudes 2008).

It may be conjectured that the reported low efficiencies may be due to the vast size and volume difference between CPP:DNA polyplexes and complexed or conjugated proteins; polyplexes often exceed 100 nm in diameter and globular proteins rarely exceed 10 nm in diameter (Wang, Fu et al. 2013, Zhang, Song et al. 2013). While this size difference does not necessarily affect translocation of polyplexes in animal cells, it can potentially hinder translocation via endocytosis or macropinocytosis in plant cells due to the cell wall. Still, recent research (as mentioned before) with $(KH)_9$-BP100 has actually shown that at least in *Arabidopsis* and *Populus* leaves, the use of larger less compact

polyplexes translocated at higher efficiencies than smaller more compact polyplexes. The delivery of plasmid DNA. These polyplexes have also been shown to be able to also target delivery of DNA to the mitochondria of *Arabidopsis*; when a mitochondrial targeting peptide was included (Chuah, Yoshizumi et al. 2015). The pore size of typical plant cell walls is approximately 10 nm (Sun, Hussain et al. 2014), and may occasionally dilate to 20 nm, yet translocation of polyplexes in excess of 200 nm has been successful, indicating other mechanisms at play besides simple membrane binding. Additionally these polyplexes were slightly negatively charged, which may imply that such polyplexes reduce adsorption to the cell surface during transfection and allowing portions of the polyplex to interact with the cell membrane. At this point it is unknown what exact mechanism allows the import of these large polyplexes (Lakshmanan, Yoshizumi et al. 2015).

1.5.3 siRNA Delivery

Finally the use of CPPs for the delivery of siRNAs, normally in the form of double-stranded 21-mer RNAs, has only two publications to date. The first detailed the delivery of 21-mer siRNAs complexed with dodeca-arginine dubbed POA, to tobacco suspension cells to silence the aadA GUS and NPTII transgenes. While analysis at the time showed that there was RNA degradation it was confirmed primarily through Northern blot, and RNase protection assay. RT-PCR is mentioned in the paper, but only gel electrophoresis is used to evaluate the PCR products with no normalization or reference genes. Due to this, the data is somewhat suspect, but gave an indication that siRNA delivery was possible using cationic CPPs (Unnamalai, Kang et al. 2004).

The second publication once again features $(KH)_9$-BP100 in delivery of siRNA to silence *yfp* (yellow fluorescent protein) in transgenic *Arabidopsis*, as well as the endogenous chalcone synthase gene. It was also applied to *Populus* in the silencing of the chalcone synthase gene. Silencing was verified by visual evidence (e.g. reduction in fluorescence, change in leaf colour) and western blot. It was shown that peak silencing was induced at nine hours after inoculation, afterwards beginning to restore control levels of apparent expression. Unfortunately, like the previous publication, RT-qPCR was not used to measure the degree of silencing, and hence the data remains suspect as some of the evidence could be artifacts of toxicity induced by the polyplexes, rather than direct targeting of the mRNA for degradation as has been found with post transcriptional gene silencing. However, the reduction of specific proteins in abundance evidenced through obvious phenotypic changes and western blot analysis presents relatively solid evidence of silencing (Numata, Ohtani et al. 2014). In the future it will be absolutely necessary to verify these results with proper real time methods.

1.6 Conclusions

The use of CPPs has become a very broad and complex field, and has begun to include a multitude of other non-viral and non-biological methods of cargo delivery into living cells. Indeed, one may include polymer and liposomal transfection methods as part of the field due to similar principles of cellular entry and cargo binding being involved. The following thesis endeavours to illustrate the value of the DLS and ELS in characterizing CPP:nucleic acid polyplexes, and the particular challenges that must be overcome in order the make CPPs a major method of plant genetic engineering and gene expression modulation.

The Interaction of the Cell-Penetrating Peptide Tat_2 and Polycation Luviquat™ FC-370 with Triticale Microspores

2.1 Introduction:

Microspores are the pre-gametophyte stage of pollen, and have proven to be a successful gametophytic tissue culture material. They have been primarily used in the production of doubled haploid (DH) plants for plant breeding; achieving homozygosity in a single generation. It has seen success in doubled haploid production of cereal crops such as wheat (*Triticum aestivum*), barley (*Hordeum vulgare*) and triticale (*Triticosecale spp.*) (Ferrie and Caswell 2010). Additionally, the transfection of microspores with plasmid and dsDNA using cell-penetrating peptides (CPPs) has also shown merit as a way to produce homozygous transgenic plants (Shim, Eudes et al. 2012).

Cell-penetrating peptides are a class of small peptides (5-30 amino-acids) that have the capacity to traverse the plasma membrane of living cells. Their usefulness comes from their complementary abilities to both bind various macromolecular cargoes, and shuttle them across the plasma membrane (Bechara and Sagan 2013). The cargoes that may be carried encompasses polynucleotides, proteins and small molecules, making them an attractive tool for biotechnology applications in plant tissue culture (Chugh, Eudes et al. 2010, Bolhassani 2011, Nam, Kim et al. 2011). At the current time however, plant cells, and in particular microspores, present a challenge to the efficacy of CPPs in delivering these cargoes (Ziemienowicz, Shim et al. 2012).

One of the primary obstacles to the transfection of microspores using CPPs is the microspore exine; a cell-wall-like layer that surrounds the microspore (Kim and Douglas 2013). It is largely believed that the CPPs must enter the cell via a small opening in the

exine called the micropore, where the CPPs may make contact with the plasma membrane and enter the cell. The chemical structure of the exine is complex and not completely characterized, but has been shown to consist primarily of a biopolymer called sporopollenin (Shi, Tan et al. 2011). Sporopollenin itself remains relatively uncharacterized because of its complexity, but physical data suggests it is composed of aliphatic carbon chains that are functionalized with hydroxyl groups, lactones, carboxyl groups and some phenylation. The other components of the exine are lipids, polysaccharides and phenols (Fang, Wang et al. 2008, Lallemand, Erhardt et al. 2013). This functionalization suggests an overall slightly negative charge. Since CPPs are typically characterized by positively charged lysine and arginine residues, the exine becomes an attractive target for binding of the CPPs via electrostatic interactions.

One possible method for limiting the interaction of cationic CPPs with the microspore exine is by blocking the electrostatic interaction using screening molecules. The best candidate screening molecules for this interaction are cationic surfactants, particularly polyquaterniums. Polyquaterniums are polymers characterized by quaternized ammoniums, and have previously been used in many applications including waste flocculation, hair conditioning and even as transfection agents themselves (Cumming, Hawker et al. 2010, Wang, Fu et al. 2013). Because of their physical similarity to CPPs in that they possess multiple cationic charges they may also present the same affinity for the microspore exine and thereby effectively block CPP-exine interactions.

Luviquat^{TM} FC 370 (polyquaternium-PQ-D16, hereafter PQ-D16) from Sigma-Aldrich, is a proprietary co-block polymer of polyvinylpyrrolidone and 3-methyl-

vinylimidazolium repeating units. This polymer was chosen due to its resemblance to polyvinylpyrrolidone (PVP), a relatively non-toxic polymer shown to a multitude of capabilities, including acting as a wetting and surfactant agent (Lakhwani and Rahaman 1999, Halake, Birajdar et al. 2014). In this study PVP, PQ-D16 and a mixture of PVP with PQ-D16 were tested in their ability to effectively neutralize exine charge. Additionally data was collected to illuminate the adsorption activity of Tat_2 to the triticale microspore exine at differing pH.

2.2 Materials and Methods:

2.2.1 Microspore Extraction:

Microspores were extracted from triticale (Sunray) using a modified version of a previously published extraction protocol (Asif, Eudes et al. 2013). Briefly, tillers were cut from donor plants at the early to mid uninucleate stage of microspore development, wrapped in aluminum foil and the stems were immersed in distilled water at 4^oC for 21±3 days. Glumes were harvested from two tillers, placed in a warring blender cup (VWR international, #58983-093) with 50mL extraction buffer and blended for two bursts of 7 s on low speed (18000 rpm). The homogenate was then strained through autoclaved mesh (1 mm^2 pores) and filtered through 100 μm sterile mesh (VWR international, #CA21008-950) into a 50 mL falcon tube. Microspores were pelleted at 100 g for 5 minutes at 4^oC, and the supernatant was decanted. All subsequent centrifugations were performed at 4^oC. The cells were then re-suspended in 15 mL of extraction buffer in a 15 mL tube and pelleted again at 100 g for 5 minutes. The pellet was then re-suspended in 15 mL CIMC wash and pelleted as before. The pellet was re-suspended again in 7 mL 20% maltose

solution and 1 mL of CIMC wash was layered on top in a 15 mL falcon tube, and centrifuged at 100 g for 13 minutes. At the interface of the CIMC wash and maltose, a band of viable microspores could be seen. These were removed with a 1 mL pipette and re-suspended in 15mL CIMC wash and pelleted at 150g for 5 minutes. The supernatant was decanted leaving at approximately 400 µL pellet of microspores at the bottom of the falcon tube. These cells were re-suspended with 1 mL of CIMC wash and subsequently quantified using a haemocytometer. The cells were then kept at 4^{o}C until suspension in dispersion media.

2.2.2 Dispersion Media Preparation:

Dispersion media was based on the composition of CIMC wash (Asif, Eudes et al. 2013). Due to the limitations of the Zetasizer Nano ZS software (v.7.02) several components of the CIMC wash could not be included in the software calculation of medium viscosity, dielectric constant, and refractive index. To accommodate this limitation, only maltose (90.000 g/L), mannitol (9.000 g/L), KNO_3 (1415 mg/L), $(NH_4)_2SO_4$ (232 mg/L), KH_2PO_4 (200 mg/L), $CaCl_2$ ●$2H_2O$ (83 mg/L) and $MgSO_4$●$7H_2O$ (93 mg/L) were included with ddH_2O as the solvent. All chemicals were purchased from Sigma-Aldrich.

The dispersion media (dubbed Reduced –Wash Media or RWM) was set to pH values of 5.4,6.0, 7.0 and 8.0 using 1N HCl and 1 M KOH. The dispersant was then filtered using a 5 mL syringe and 0.20 µm syringe filter in a laminar flow hood, to remove particulate from the dispersants.

2.2.3 Sample Preparation and Software Parameters:

Isolated microspores were suspended in 700 µL of the RWM dispersant at a concentration of ~21.4 cells/µL (15,000 cells per sample) in a rectangular 2 mL polystyrene cuvette. This concentration was determined in preliminary work to be sufficient for a high signal to noise ratio, while using a low density of microspores for more accurate measurements.

The same concentration of microspores as mentioned were prepared at a 2 mL volume and the absorbance was read at 633 nm, with a resultant OD of 0.003. Similarly refractive index of microspores was estimated to be approximately 1.53 based on the refractive index of pollen and sporopollenin (Charriere, Cuche et al. 2006). The RWM dispersant was found to have a calculated refractive index of 1.345, a dielectric constant of 78.5 and a viscosity of 1.399 mPa·µs. These parameters were calculated using the complex dispersant editor available with the Zetasizer software (Malvern). All samples were measured using the "Universal 'Dip' Cell" (ZEN1002) provided with the Zetasizer Nano ZS. Measurements were made using the Smoluchowski approximation for electrophoretic mobility, using Laser Doppler Velocimetry (LDV).

2.2.4 Zeta-Potential Measurement of Tat_2 Adsorption to Tritcale Microspore Exine:

In order to determine what range over which to measure the zeta-potential change of the microspore exine due to Tat_2 (RKKRRQRRRRKKRRQRRR, Canpeptide), a plateau was found by adding 0.2 µg amounts of Tat_2 in single microliter volumes, with Tat_2 dissolved in the appropriate pH of RWM. Between each addition was an incubation period of 15 minutes to allow for complete adsorption. This was done at pH=6.0 and 7.0

RWM; in the case of pH 6.0 it was found that the plateau was reached before the second addition, and was subsequently followed up with a similar trial using 0.04 μg increments (1/5 of 0.2 μg). Once a plateau was observed for each pH in these trial runs, the point of saturation was divided into seven equal increments to investigate the change in zeta-potential of the microspores with addition of Tat_2. Identical increments for pH 6.0 and 7.0 were used for pH 5.4 and 8.0 respectively for ease of comparison. This was 0.04ug for pH 5.4 and 6.0; and 0.6ug for pH 7.0 and 8.0. Seven replicates were performed in pH 5.4, 6.0 and 7.0, with three replicates in pH 8.0. As with the trial runs, 15 minutes of incubation time was used between additions. Seven replicates of each experiment were completed.

2.2.5 Formulation of Pol-1:

PVP and PQ-D16 were mixed in RWM at various ratios extending from 1/9 through to 9/1 PVP:PQ-D16 in volumes of 1 mL at 5mg/mL total polymer compounds. Using a quartz low volume cuvette (ZEN2112) for measurements of size on a Zetasizer Nano ZS, 20 μL of polymer mix was measured for particle size with 173^{o} backscatter. Both Z-average size and PDI (polydispersity index) were recorded for three measurements. These were averaged and standard deviation was calculated. Both PVP and PQ-D16 alone at 5 mg/mL were measured as controls.

2.2.6 Titration of Microspores with PVP, PQ-D16 and Pol-1:

Microspores were extracted as previously described (2.2.1) and titrated over a range of 0 to 10 μg/mL with each polymer (PQ-D16, PVP and Pol-1) at 1 μg/mL increments measuring zeta-potential at each increment. Microspores were suspended in

RWM supplemented with 5 mM trisodium citrate to act as a low capacity buffer due to greater volume. Samples consisted of 10 mL of microspore suspension of 214,000 cells, and utilized the MPT-2 autotitrator for all titrations. Three measurements were taken for each increment, and two titrations were performed for each polymer. Microspores were re-circulated between measurements at 80% pump capacity and samples were kept suspended by a magnetic stir disk at 20% maximum drive. Titrants consisted of 5 mg/mL solutions of each polymer in RWM+5mM trisodium citrate. Each measurement was considered a repetition. Data was plotted and non-linear regression by minimizing total squared deviation was used to determine specific values of constants in equation (**2.1**). Equation (**2.1**) was modelled as an analogue of the Michaelis-Menten equation evaluating hyperbolic saturation trends.

$$\zeta + |\zeta_i| = \frac{(\zeta_{max}+|\zeta_i|)[P]}{[P]+[P]_{1/2}} \qquad \textbf{(2.1)}$$

Prior to non-linear regression the parameters ζ_{max} and $[P]_{1/2}$ were approximated using an analogue of the Hanes-Woolf rearrangement (see Eq (**2.2**)).

$$\frac{[P]}{\zeta+|\zeta_i|} = \frac{1}{\zeta_{max}}[P] + \frac{[P]_{1/2}}{\zeta_{max}} \qquad \textbf{(2.2)}$$

In equations (**2.1**) and (**2.2**) ζ is the zeta-potential, ζ_i is the initial zeta-potential, ζ_{max} is the maximum or plateau zeta-potential at saturation, [P] is the concentration of polymer and $[P]_{1/2}$ is the polymer concentration at half the ζ_{max}. Using the parameters determined, isoelectric point or concentration at which zeta-potential is 0 mV for microspores was also calculated as well as the number of elementary charges per

microspore was calculated based on the PQ-D16 molecular weight of 100 kDa and charge density of 2.0 meq/g (DeWolf Chemicals). These two values were also calculated based on best guess approximations from the Tat_2 adsorption work.

2.3 Results:

2.3.1 Effect of Tat_2 on Triticale Microspore Exine Zeta-Potential:

The adsorption of Tat_2 to microspore exine was examined using zeta-potential measurements of the cells when incubated with increasing concentrations of Tat_2 at different pH. The behavior of Tat_2 adsorption varied considerably among the various pH levels tested. Using zeta-potential as a measure of this behavior, it was shown that both pH 5.4 and pH 8.0 followed a similar pattern of adsorption over the experiment, having a nearly hyperbolic trend (see Fig. 2.1 (a) and (b)). Adsorption in RWM at pH 7.0 followed a nearly linear pattern throughout, showing a very large degree in variation as indicated by standard deviations exceeding 2.0 mV at 0.6, 1.2 and 4.2 µg of Tat_2. Adsorption behavior in RWM at pH 6.0 followed an evidently sigmoidal pattern. The initial zeta-potential for all pH levels except pH 5.4 was not significantly different, averaging to -11.9±1.3 mV. Microspores in RWM at pH 5.4 however showed a less negative initial zeta-potential of -7.7±1.4 mV. Specific initial values are displayed in Table 2.1. In controlling for possible change over time, it was found that no significant change occurred over the course of 1.75 hrs, or the course of a single experiment, at any of the pH levels.

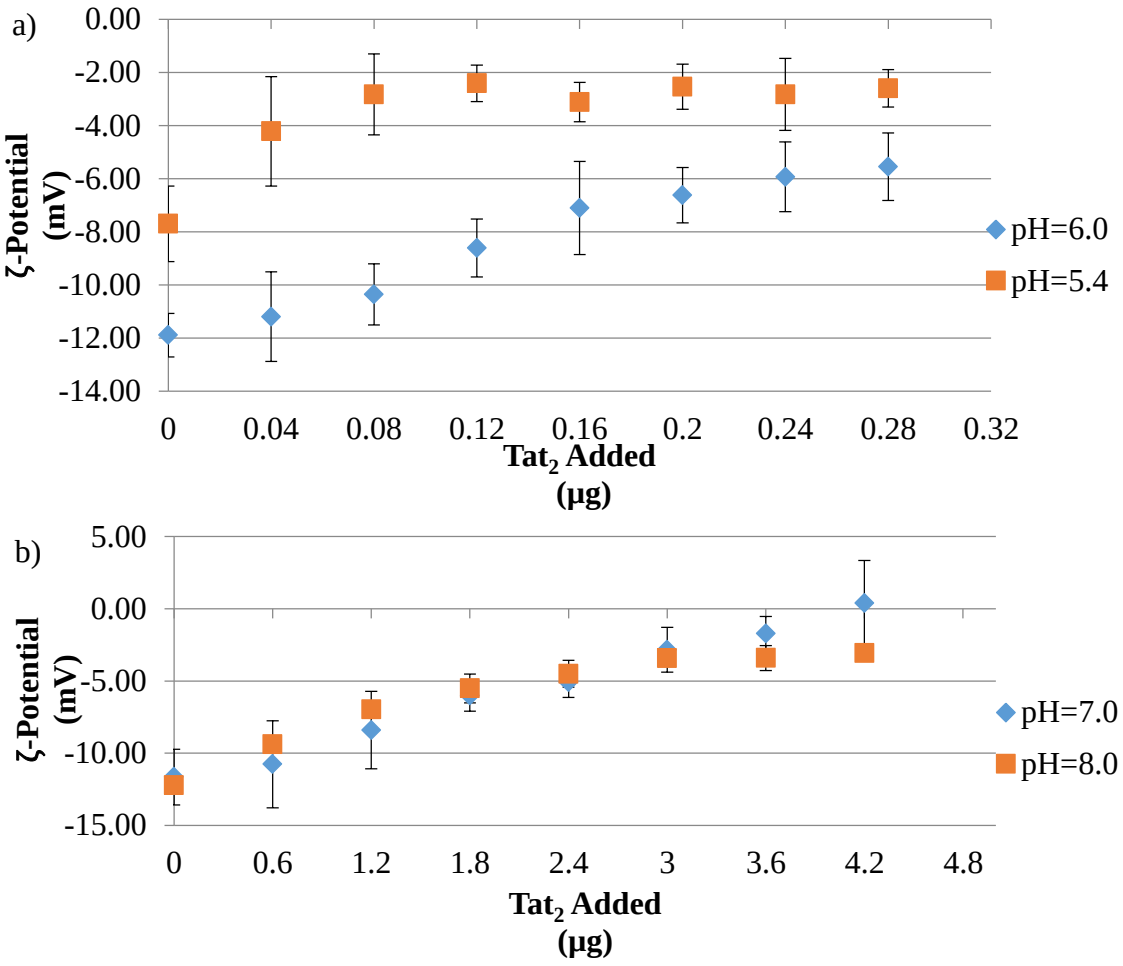

Figure 2.1: Zeta (ζ)-potential of triticale microspores with the addition of Tat_2 at different pH. Performed in RWM at pH=6 and pH=5.4 (a), and pH=7 and pH=8.0 (b). Data plotted are means±stdev (n=7, pH 8.0 n=3).

Table 2.1 displays the specific initial, plateau and change in zeta-potential with the addition of Tat_2. In the case of pH 7.0 a plateau appears to occur near 3.0 µg, however there is significant variation beyond that point which obscures the veracity of the plateau, suggesting that the plateau may be at a mass of greater than 4.0 µg. It can be shown that there was a high similarity between the changes in zeta-potential between the pH 5.4 and pH 6.0 trials, as well as between the pH 7.0 and 8.0 trials. In the case of pH 5.4 and 6.0, the change was ~+5.3 mV, and in the case of pH 7.0 and 8.0 the change was ~+8.8 mV

(Table 2.1). However, the plateau zeta-potential was highest in pH 6.0 at -6.62±1.04 mV, contrasting significantly with the other pH levels. Overall it was found that the pH at which the least amount of Tat_2 was required to reach a plateau in zeta-potential was pH 5.4.

Table 2.1: Initial, Plateau and Change in Zeta-Potentials for Triticale Microspores Due to Tat_2 Addition

pH	Mass of Tat_2 to Plateau (µg)	ζ_i (mV)**	ζ at Plateau (mV)**	$\Delta\zeta$ (mV)**
5.4	0.12	-7.70±1.42	-2.41±0.69	+5.29±1.58
6.0	0.20	-11.89±0.82	-6.62±1.04	+5.27±1.32
7.0	>4.00*	-11.66±1.93	-2.84±1.55	+8.82±2.48
8.0	3.00†	-12.23±0.59†	-3.23±0.23†	+8.81±0.63†

*Required Tat_2 may be greater than 4.00 µg due to significant variation.
**Data displayed are means±s.d. (n=7).
†Sample size n=3.

2.3.2 Measurement of Pol-1:

Mixtures of PQ-D16 and PVP K29/32 were suspended in RWM at varying ratios (w/w) at 5 mg/mL, and read for Z-average size and PDI. The results show that the lowest size particles formed from these mixtures and lowest PDI was at the 2/8 ratio (i.e. 1/4) (see Fig. 2.2). The size was 15.48 nm and PDI was 0.291, contrasted to PQ-D16 alone with 25.81 nm and PDI 0.630, and compared with PVP with 13.95 nm and PDI 0.189. It is interesting to note that despite similarity in size between the 2/8 mixture and PVP control that the 1/9 mixture (90%) PVP had a more similar size to PQ-D16 alone, with at 26.49 nm. The 2/8 mixture described was labelled Pol-1 and used for titrations of microspores (see Fig. 2.2).

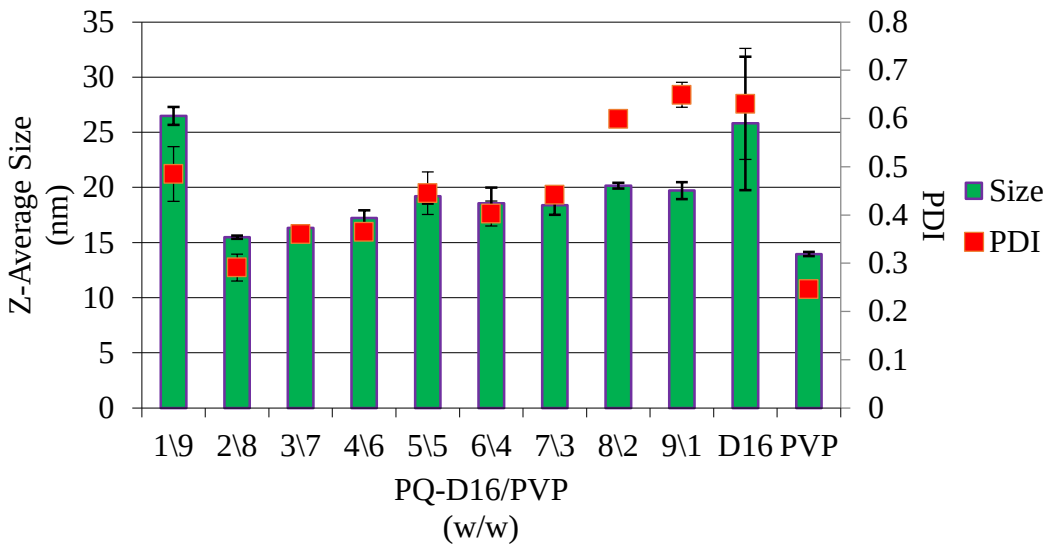

Figure 2.2: Dynamic light-scattering (DLS) measurements of polymer mixtures composed of ratios of Luviquat^{TM} FC 370 (PQ-D16) to polyvinylpyrrolidone K29/32 (PVP). Both diameter in terms of Z-average size (overall size) and polydispersity index (PDI) are displayed. Data shown is the average of three measurements of a 5 mg/mL solution composed of the ratios shown (from 1/9 to 9/1).

2.3.3 Polycation Adsorption to Triticale Microspores:

Triticale microspores were titrated with PQ-D16, PVP and Pol-1 to determine their affect on microspore exine zeta-potential (Fig. 2.3). PVP K29/32 was shown to have virtually no relevant effect on the zeta-potential of Triticale microspores, with no distinctive change but a high variation in zeta-potential overall varying between -15 to -20 mV. It must be noted there is a discrepancy between the values displayed for the initial zeta-potential with each titration versus that of the microspores from the Tat_2 treatments. The pH was 7.0 for all titrations and this gives a maximum discrepancy of up to 13 mV. However, standard deviations for all samples were high, up to 5 mV, and for this reason the 0 and 1 µg/mL increments were discarded in all regression analyses. A hyperbolic trend is noted in the case of both Pol-1 and PQ-D16 titrations (see Fig. 2.3(a)). The curves were substantially similar as shown by the linearized plots, showing that non-

linear regression was necessary to sufficiently differentiate the parameters of each curve.

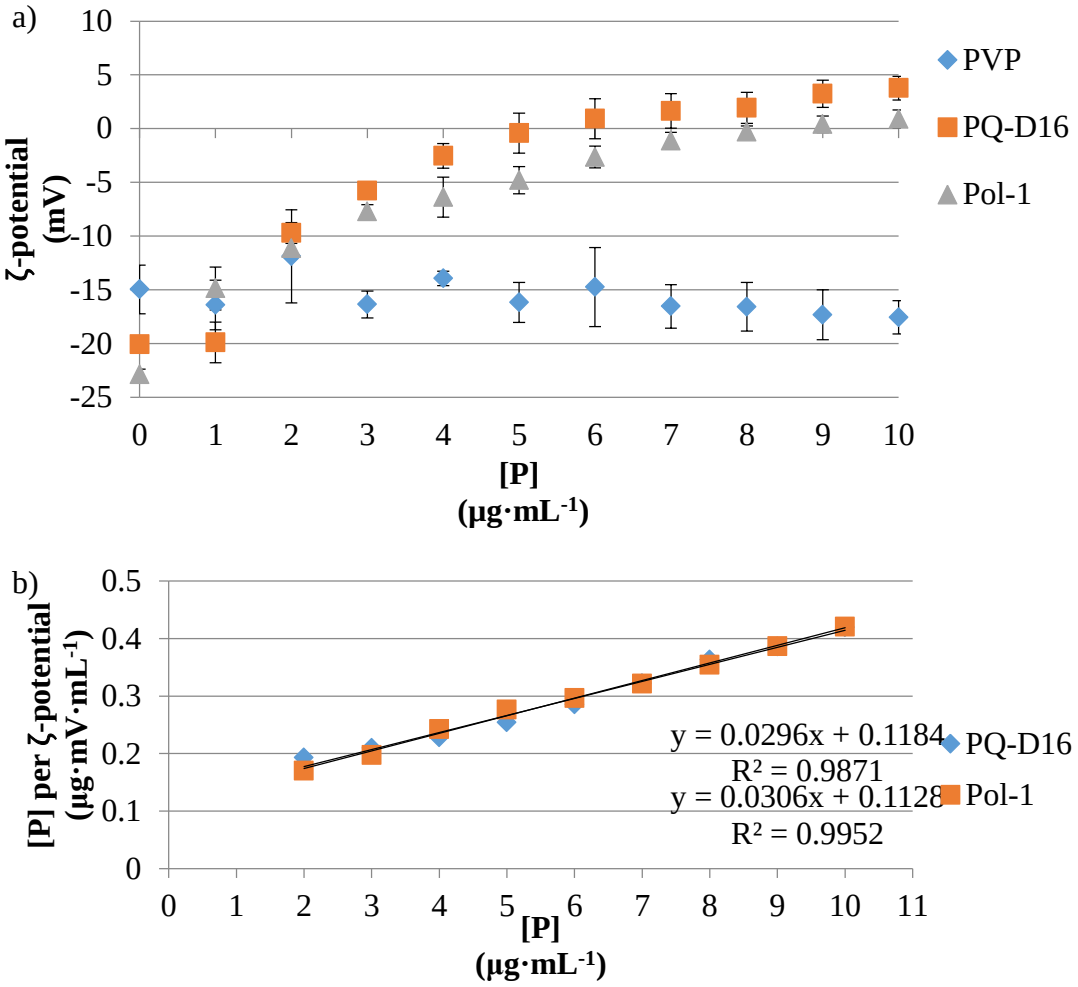

Figure 2.3: Titration curves (a) and linearized plots (b) of ζ-potential change of triticale microspores when titrated with to PVP, PQ-D16 and Pol-1. Titration with PVP served as a negative control. Linearized plots from a Hanes-Woolf analogue with accompanying trend-lines and linear regression fits are shown for display purposes (b), and goodness of the linearization strategy.

The parameters ζ_{max}, I_p and $[P]_{1/2}$ were derived from the non-linear analysis of the saturation curves, and are displayed in Table 2.2. The data shows a significant difference in ζ_{max} and I_p, with a difference of 3.9 mV and 2.8 µg/mL. However, it was also shown that the $[P]_{1/2}$ value for both Pol-1 and PQ-D16 were substantially similar with only a difference of 0.25 µg/mL. Furthermore, under the assumption that all added polymer or

polycation adsorbed to the microspores, the calculated number of elementary charges per microspore at pH=7.0 was also significantly different as well as the mass of total polymer required to reach the I_p, differences of $2.4 \cdot 10^{14}$ charges and 131 pg per microspore respectively. Unsurprisingly more total polymer was required from Pol-1 than from pure PQ-D16, but was approximately 67% as effective at neutralizing the charge based on the mass required, despite a predicted 25% efficacy based on the amount of PQ-D16 used during titration. Similarly for ζ_{max}, Pol-1 has a predicted value 71% that of pure PQ-D16, showing a substantially similar pattern for overcharging of the microspores. For PQ-D16, the number of elementary charges per microspore was calculated at a greater number than for Pol-1, under the assumption of complete complementarity of negative moieties on the exine surface and the positive charges in PQ-D16. Further to comparison, Tat_2 was shown to require a similar mass to neutralize the charge of microspores at pH=7.0 of approximately 266 pg, and also predicted approximately $1.3 \cdot 10^{16}$ elementary charges per microspore, two order of magnitudes above that of the other values (see Table 2.2).

Table 2.2: Derived Parameters from Polymer Titrations of Triticale Microspores

Polymer Additive	ζ_{max} (mV)	I_p (µg/mL)	$[P]_{1/2}$ (µg/mL)	# of Elementary Charges per Microspore	Mass of Polymer per microspore to reach I_p (pg)
PQ-D16	13.7	5.8	3.94	$7.4 \cdot 10^{14}$	271
Pol-1	9.80	8.6	3.69	$5.0 \cdot 10^{14}$	402
Tat_2*	-	~4.3	-	$1.3 \cdot 10^{16}$	266

*Derived from the best guess from Figure 2.1 (b) (4.00 µg/15,000 microspores)

2.4 Discussion

It was found that the exine of Triticale microspores had variable affinities for the CPP Tat_2 based upon the pH of the suspension solution. The data found there to be a

substantial approximately ten-fold decrease in the amount of Tat_2 that could apparently adsorb and neutralize the exine charge, between the pH values of 6 and 7. The amount of Tat_2 adsorbed further decreased between pH 6 and 5.4. However, the initial zeta-potential was substantially similar for pH 6, 7 and 8 at approximately -12 mV. This suggests a change in the available number of elementary charges on the exine but not a change in the total number of charges between the pH values of 6 and 7. However, as the pH was decreased below 6 to 5.4, the zeta-potential was reduced in magnitude to -7.71 mV, indicating a reduction in the number of charges total. This suggests that structural changes occur at the exine from pH 6 to pH 7 (see Table 2.1). It has been shown that lactone moieties present in the exine have a pKa range of 4.0-7.0 (Barrier 2008), where protonation results in ring opening and changes in sporopollenin overall structure, the change in available charges may have been a result of structural changes between the pH increments (see Fig. 2.4).

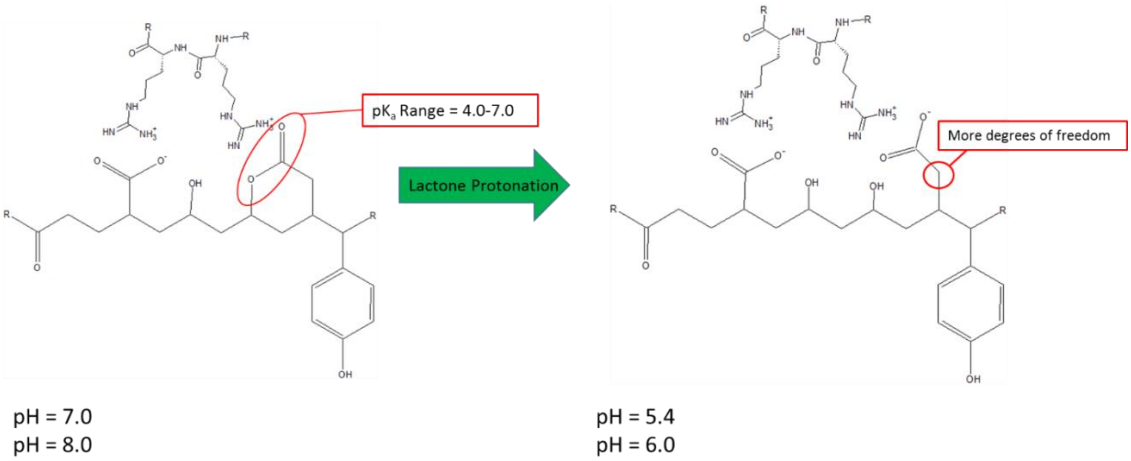

Figure 2.4: Projected model of how lactone protonation may affect adsorption of Tat_2 to the microspore exine. The lower chemical structure represents a hypothetical sporopollenin fragment, and the upper a fragment of arginines in Tat_2. Electrostatic interactions are shown for both carboxyl and lactone functionalities, with red rings indicating points of interest.

Another possibility that could be affected by pH is the internalization of Tat_2, as the cells were alive during the experiment. It has previously been shown that protonation of the cell membrane can induce invaginations and endocytosis (Ben-Dov and Korenstein 2012, Ben-Dov and Korenstein 2013). This effect could potentially lead to internalization of peptides before they adsorb to the exine surface explaining why the plateau zeta-potential of the pH=6 increment is more negative than at the pH=5.4, a difference of approximately 4 mV, as invaginations would start forming at this pH, and more surface moieties would be neutralized by protonation at pH 5.4. However, the molecular structural explanation seems the most complete of the possibilities, as the lower pH levels also reached a plateau at lower amounts of peptide, which does not support intake of the peptides, though a combination of factors remains likely.

Another layer of complexity in the adsorption of Tat_2 has to do with the microchannels present in microspores and pollen (Atkin, Barrier et al. 2011, Tsou, Cheng

et al. 2015). These microchannels are large enough to accommodate Tat_2 within them, allowing for more apparent charges on the microspore exine. The adsorption of polycations to the microspore exine revealed that the number of apparent elementary charges of the microspore exine increases significantly when Tat_2 at pH 7 was used to determine the number of charges to reach I_p (see Table 2.2), a 17.6 fold increase in apparent charges over PQ-D16 and 26 fold over Pol-1. This seemed to indicate that Tat_2 was accessing anionic charges that could not be accessed by PQ-D16 and Pol-1, which may be those located within the microchannels of the microspore. However, overcharging was not observed with Tat_2, even at lower pH levels where the plateau was extended over a large concentration range, particularly in pH 5.4 (see Fig. 2.1 (a)), although the concentrations applied were not as high as that applied with PQ-D16 and Pol-1.

A comparison of the parameters derived from the non-linear regressions of the saturation curves of Figure 2.3, shows that PQ-D16 has a higher ζ_{max} of 13.6 mV versus Pol-1 which has a value of 9.80 mV, however the $[P]_{1/2}$ was nearly identical between the two polymer titrants, showing that the adsorption affinities were similar, but with different end points of overcharging. This suggests a different structural character between pure PQ-D16 and its admixture with PVP, Pol-1. It is known that highly hydrophilic polycations like PQ-D16 usually have a solution state conformation of a random coil or string (Dobrynin, Deshkovski et al. 2001, Dobrynin and Rubinstein 2005). This well explains the data presented as PQ-D16 possessed a Z-average size of >25 nm and has a molecular weight of 100 kDa, it would not have been able to enter the microspore exine microchannels, but would have spread over the microspore instead. Because Pol-1 was smaller in particle size, it may be suggested that as a polymer blend

its adsorption may have had more complexity at the surface recruiting otherwise non-adsorbing (if adsorbing then not affecting zeta-potential) PVP to the cell surface, in a synergistic effect that is not unprecedented with PVP blends (Hidalgo-Alvarez, Martin et al. 1996, Lipatov 2002).

In this study the data collected is of a highly novel character as no investigation into the solution electrochemical properties of a living plant cells has been performed before. It is especially important as the cells that were under investigation were observed under conditions similar to their culturing environment for somatic embryogenesis, but also because pollen exine has been investigated as a microencapsulation technology (Barrier, Diego-Taboada et al. 2011), where the modification of the surface with specificity may be a point of investigation in the future. Furthermore it is only the second reported investigation of zeta-potentials in plant cells, the first investigating the salt dependency of surface zeta-potentials of rice roots (Li, Liu et al. 2014), and one of only a few published works on living cells, in bacteria (Shevchuk and Klimenko 2010, Ciesla, Bieganowski et al. 2011) and human cell cultures (Bondar, Saifullina et al. 2012). The hoped application of this data will be towards the enhancement of CPP:cargo uptake in microspores, which has hitherto been low in efficiency likely due to the high degree of exine adsorption as verified in this report, especially when one considers that 4+ µg of Tat_2 adsorb and effectively become biologically inactive with only 15,000 cells, much less the standard experimental replicate for Triticale microspores of 100,000, and that only 1-2 µg of Tat_2 was ever used in transfection (Shim, Eudes et al. 2012). Increasing bioavailability may now be possible through this better understanding of the electrochemical character of the triticale exine, whether by blocking agents or medium

modification.

2.5 Conclusion

While the data presented here does not implicate any practical application, it does provide information regarding a little understood part of CPP transfection in plant cells, the interaction of CPPs and polycations with cell-wall type structures, and its effect on those structures.

3.0 The Use of Tetrabutylphosphonium Bromide as a Size and Polydispersity Reducing Agent for Tat_2:Nucleic Acid Polyplexes and as a Transfection Adjuvant for Tat_2:siRNA Polyplexes in Triticale Leaf Tissue

3.1 Introduction:

Cell-penetrating peptides (CPPs) are non-viral vectors often derived from the transduction domains of various proteins, and usually consist of 8-30 amino-acids. Often, they are characterized by the presence of a net cationic charge originating from the arginine and lysine residues of the peptide's sequence (Brock 2014). Because of the several characteristics of binding nucleotide cargoes through electrostatic interactions, the ability to traverse the cell membrane, and targeting of specific organelles, these peptides have been used for the delivery of negatively charged polynucleotides into both plant and animal cells. The delivery of plasmid DNA, dsDNA, ssDNA and dsRNA (e.g. siRNA) using CPPs has been successful in various plant and animal cell-culture systems (Chugh and Eudes 2008, Liou, Liu et al. 2012). The success of these systems, however, is based heavily on the physicochemical characteristics of the nano-complexes, often called polyplexes, formed between the nucleic acids and the CPPs. The three principle characteristics that apparently govern the transfection efficiency of these nano-complexes are size-distribution, polydispersity, and zeta-potential (Cardoso, Trabulo et al. 2013, Liu, Liou et al. 2013).

To address these particular parameters, the standard analysis tool is dynamic light scattering. Dynamic light scattering (DLS) is a photometric technique that analyzes the Rayleigh scattering of monochromatic laser light by colloidal particles in a dispersion medium (Jafari, Xu et al. 2014). This may be used to determine size distribution via the

Stokes-Einstein equation or the zeta-potential based on electrophoretic mobility of the particles. In this study, DLS has been used to characterize and optimize the conditions for formation of nano-complexes for delivery into plant cell culture systems. Since the conditions that effect nano-complex formation are multitudinous, the purpose of this study was to explore and discover conditions that minimize size and PDI, while increasing zeta-potential through different ionic strengths, cationic charge to anionic charge molar ratios, and quaternary ammonium and phosphonium additives.

The manner of entry of CPPs into the cell has remained a subject of controversy due to conflicting data from a number of reputable sources (Bechara and Sagan 2013). However, it has been generally agreed that the process of CPP complex uptake either acts through direct transport, using interactions with the cell membrane phospholipids, or through various forms of endocytosis (Ziegler and Seelig 2011). In the case of the latter the process must be two-fold, endosomal formation followed by endosomal release. In order to take advantage of both endocytotic and direct transduction pathways, phase catalysts may improve transfection efficiency. For this purpose the formation of stable ternary complexes of CPPs, nucleic acids and tetrabutylammonium bromide (TBAB) or tetrabutylphosphonium bromide (TBPB), was also explored. The cationic component of these salts have already been shown to complex with DNA , and are also documented phase-catalysts, binding and moving anions from aqueous hydrophilic environments to non-aqueous hydrophobic environments, something of possible benefit to membrane transduction or endosomal release (Di Profio, Germani et al. 2010). Polymers with tertiary ammoniums and phosphoniums have been utilized as well for delivery of nucleic acid cargoes in animal cells (Ornelas-Megiatto, Wich et al. 2012), and phosphonium salts

have been shown to have mitochondrial targeting properties (Muratovska, Lightowlers et al. 2001). Also the addition of these salts can reduce the need for large amounts of CPP to complex nucleic acids, as the charge ratio load for complete binding may be reduced.

Most the work performed with CPPs has focused on delivery in animal cells, mammalian cells in particular, which have shown high efficiency delivery of a number of cargoes conjugated or non-covalently bound to CPPs. The same cannot be said for plant cells, due to factors inhibiting uptake, such as the cell wall, differing rates of macropinocytosis and differences in membrane physicochemistry. One particular difference not previously investigated is the composition of plant tissue culture media and its effect on complex formation and stability. Because of the overriding dominance of animal cell culture systems as research platforms for CPP investigation, the relevant media investigated has frequently been PBS or serum based media (Hemp, Smith et al. 2012, Jafari, Xu et al. 2014). As a result very little information gathered from other complex formation studies is applicable to plant tissue culture systems which use high sugar media.

Tat_2 (RKKRRQRRRRKKRRQRRR) was evaluated in its complexation of 21mer dsRNA, 0.5, 1, and 3 kb dsDNA as well as a circular plasmid (5556 bp) with and without TBAB or TBPB or $CaCl_2$. Lastly some work was completed with regards to experimenting in delivering TBPB modified siRNA polyplexes to triticale leaf tissue.

3.2 Materials and Methods

3.2.1 Nucleic acid preparations:

The 1kb ladder from Invitrogen was used as the source of all linear dsDNA fragments. Ladder was prepared according to manufacturer instructions and run on a 1.0% agarose gel stained with Gel Red (0.5x) for 1 hour in 1xTAE buffer at 90 V. The desired linear dsDNA fragments (0.5, 1 and 3 kb) were visualized using an ultraviolet light and extracted from the gel using a scalpel. The DNA fragments were then purified from the agarose using the Qiagen gel extraction kit, following the manufacturers instructions, eluting all final fragments from columns using Ultrapure Water (Sigma-Aldrich). Isolated DNA stocks were diluted to 20 ng/µL.

The pMS plasmid with a segment of 3033 bp inserted at the multiclonal site (total length 5.556 kb), was used for study of pDNA size and PDI in complex with Tat_2. The plasmid was cloned using *E.coli*, strain DH5α. *E.coli* containing pMS were taken from a glycerol stock and cultured overnight in 200 mL of LB media and purified from cells using a plasmid maxiprep kit according to the manufacturers instructions (Sigma-Aldrich). Plasmid was eluted from the included columns using Ultrapure water (Sigma) and diluted to 20 ng/µL for use in complex formation.

The dsRNA was ordered from IDT with the sequence,5´-CAUGGAGACGCCGUCGUU-3´ and complementary strand 5´-CGAGGACGGCGUCUCCAUGUU-3´, producing a duplex with double U overhangs and a molecular weight of 13368.1 Da. The lyophilized product was dissolved in Ultrapure Water and subsequently diluted to a stock concentration of 2.0 µM (26.7

ng/μL).

Final concentrations of all nucleic acids were determined by a NanoDrop 8000 UV-Vis spectrophotometer (Thermo Scientific).

3.2.2 Polyplex Sample Preparation and Size Analysis:

3.2.2.1 Polyplex Preparation and Measurement:

Sample preparation and analysis methods were based on a previous work involving siRNA polyplexes (Jafari, Xu et al. 2014). Individual samples were prepared in a PCR well plate. Maltose-mannitol (MM, 90 mg/mL maltose, 9 mg/mL mannitol) solutions with varying amounts of $CaCl_2$ (0.00 mM, 78.43 mM, 156.86 mM, 235.29mM, 313.73 mM and 392.16 mM) were prepared in ddH_2O at pH 7.0 and filtered twice through 0.2 μm cellulose syringe filters (VWR) using a 5 mL syringe. From these stock solutions 17 μL were aliquoted into well plates for each $CaCl_2$ concentration and 1 μL of stock dsRNA or DNA was added. Finally, 1 μL of the appropriate amount of peptide was added and 1 μL of MM solution with no $CaCl_2$ was added to bring the final volume to 20 μL. The reaction mixtures were allowed to incubate for 15 minutes. In the case of the addition of tetrabutylbammonium bromide (TBAB, Sigma) and tetrabutylphosphonium bromide (TBPB, Sigma), instead of MM, 1 μL of 8.4 nmol/μL TBAB or TBPB dissolved in MM was added after 10 minutes of incubation time and allowed a further 5 minutes of incubation time. This was a +/- 100:1 molar charge ratio of N^+ or P^+ to backbone phosphates. These preparations resulted in 20 μL samples with final $CaCl_2$ concentrations of 0.0, 66.6, 133.3, 200.0, 266.6 and 333.3 mM, corresponding to ionic strengths of 0.0, 0.2, 0.4, 0.6, 0.8 and 1.0 M respectively. The final concentrations of TBAB and TBPB

were 420 μM, contributing little to ionic strength of solution. Only the 8:1 charge ratio and TBPB were tested with DNA samples.

Size analysis was carried out immediately after incubation in a wetted (with 200 μL MM solution) low volume quartz sizing cuvette (ZEN 2112). The entire sample was loaded into the cuvette and measured on a Zetasizer Nano ZS (Malvern) with a 633 nm laser at 173^{o} backscatter. Data was analyzed using the CONTIN algorithm in the Zetasizer software v.7.02 (Malvern). Three repeat measurements were made of each sample and means and standard deviations of both the primary particle size distribution peak, and PDI were calculated and plotted.

3.2.2.2 Advanced Size Analysis

Hydrodynamic diameters (mean measured sizes, D_H) from formulations which resulted in minimally sized polyplexes for each size of nucleic acid were used to calculate hydrodynamic volumes (V_H) under the assumption of a near spherical shape for all polyplexes. V_H was plotted as a function of the approximate length of the nucleic acid based on the assumption of 0.33 nm/bp. In the case of circular plasmid the length was halved to account for supercoiling and circular shape. Linear regression was used to determine a mathematical relationship between nucleic acid length and polyplex volume, and the slope was used to determine the goodness of fit of each individual data point.

3.2.3 Zeta-potential Analysis:

Zeta-potentials (symbol-ζ) were analyzed for circular plasmid, and for 21-mer dsRNA in formulations as previously described but with an increase in the concentration of nucleic acid and Tat_2 by five-fold (5 ng/μL, nucleic acid). This was done at a 1:1, 4:1

and 8:1 N:P ratio for each with and without TBPB (100:1 +/- molar ratio), as well as nucleic acid alone. Zeta-potential of samples were read using a capillary zeta-cuvette with gold electrodes in a Zetasizer-Nano (Malvern). The samples were prepared to a volume of 700 µL to fill the cuvette.

3.2.4 Delivery of siRNA in Young Triticale Leaf Tissue:

3.2.4.1 Treatment of Plant Material and Sample Collection:

Seeds of *Triticosecale sp. Whittmack cv* Sunray, were planted in 8x4 root trainers and allowed to grow in a growth cabinet at 12-15^{o}C, and a photoperiod of 19 hr/day at an intensity of 300 µE/m^2/s. At 13 days post planting, at the two leaf stage, plants were inoculated using a 1 mL sterile syringe (VWR) to inject a formulation of one of the following in either ddH_2O or maltose-mannitol solution; solution only (Control), TBPB only, siRNA only, Tat_2 only, TBPB+Tat_2, TBPB+siRNA, siRNA+Tat_2, Tat_2+siRNA+TBPB, scsiRNA (scrambled siRNA), and Tat_2+scsiRNA+TBPB. Together there were a total of eighteen treatments performed in a minimum of four replicates, where a single repetition consisted of eighteen individual plants. A total of 250 pmol of siRNA in 100 µL was injected in all siRNA treatments, with TBPB and Tat_2 being added proportional to the siRNA at the 8:1 N:P ratio of Tat_2 to siRNA and TBPB at the +/- 100:1 ratio of phosphonium ions to phosphates. The injections were directed towards the base of the youngest leaf on the bottom side. Plants were placed back into their prior growth conditions until sample collection 24 hours later.

The siRNA duplex (IDT) was targeted to the phytoene desaturase (PDS) endogenous gene and was designed using pssRNAit online tool provided by the *Zhao*

Bioinformatics Laboratory based on a chinese spring wheat PDS mRNA sequence (acc. FJ517553.1) with the sequence 5′-CAUGUUGUGAAGACACCCGAG-3′ (sense) and 5′-UCGGUGUCUUCACAACAUGGU-3′ (anti-sense).

To generate the scsiRNA duplex (5′-AGCCGGUACGAAUAGTGAGUC-3′ and 3′-UCGGCCAUGCUUAUCACUCAG-5′), the siRNA sense sequence was scrambled using the Genscript® online sequence scrambler; with rice being used as a reference genome. Both strands of the resultant sequence were tested for potential off-target sequence alignment with the *Ensembl Plants* database (*Triticum aestivum* and *Hordeum vulgare* genomes), as well as the general *NCBI* database using BLASTn.

3.2.4.2 RNA Extraction, cDNA synthesis, and RT-qPCR Analysis:

The tip of the inoculated leaves (3-4 cm length by 1 cm width) was cut using scissors and placed into screwcap "tough tubes" (VWR) with 3 stainless steel beads (3 mm width) and immediately frozen in liquid nitrogen and stored at -80^{o}C. To extract RNA the Nucleomag RNA 96 well plate (Macherey-Nagel) extraction kit was used, according to the manufacturers instructions with automation of extraction on a Biosprint 96 well plate robot (Qiagen). Purified RNA was quantified using UV-vis spectroscopy on a Nanodrop 8000 (ThermoFisher Scientific). cDNA was synthesized using a Superscript® VILO cDNA synthesis kit (ThermoFisher Scientific) according the manufacturers instructions with a total of 1.2 µg of RNA template per 20 µL reaction. RT-qPCR analysis was performed using SYBR-Green master mix (Life Technologies) with 40 ng of template cDNA per PCR reaction in 96 well plates. Each treatment and

biological replicate was evaluated in three technical PCR replicates, with primers (500 nM forward and reverse) designed to amplify the target cDNA phytoene desaturase (PDS) and for three reference genes; ADP-ribosylation factor (ADP-RF), cell division control protein (CDC) and RNase L inhibitor protein (RLI) (see Table 3.1 for details). Thermocycling conditions were the following; 95^{o}C for 15 min, and 40 cycles of 15 s of 95^{o}C, 30 s of 60^{o}C and 30 s of 72^{o}C, followed by a melting temperature series to evaluate amplicon content; 15 s at 95^{o}C, 15 s at 60^{o}C and 15 s 95^{o}C. Reference genes were analyzed for stability by global averages of Ct-values and the most stable was used for normalization of the target PDS gene expression level, based on the ΔΔCt method as amplification efficiencies were substantially similar (within <2%). Data was displayed as relative expression of PDS using $2^{-\Delta\Delta Ct}$ for conversion.

Table 3.1: Primer-set Sequences for RT-qPCR

Gene	Forward Primer Sequence (5′-3′)	Reverse Primer Sequence (5′-3′)	Source
PDS	AAAGCAGGGTGTTCCTGAT	CATGGATAACTCGTCAGGGTTTA	Geneious software alignment with NCBI FJ517553.1
ADP-RF	TCTCATGGTTGGTCTCGATG	GGATGGTGGTGACGATCTCT	(Gimenez, Piston et al. 2011)
CDC	CAGCTGCTGACTGAGATGGA	ATGTCTGGCCTGTTGGTAGC	
RLI	TTGAGCAACTCATGGACCAG	GCTTTCCAAGGCACAAACAT	

3.2.4.3 Statistical Analysis of RT-qPCR:

Data was analyzed using ANOVA and unpaired t-test to detect significant differences between pairs of means, with calibration of all treatments to an n=3 group of

untreated controls. Repetitions that were furthest from the mean were removed from the data set to a minimum of four biological repetitions prior to ANOVA and t-test. This was done to maintain a balanced system for ANOVA. Statistical significance was rated at the 95% and 99.99% confidence interval, $p<0.05$ and $p<0.0001$ respectively. Two way ANOVA was applied twice to evaluate factors affecting relative expression of PDS. The first application evaluated sample treatment (Control, TBPB, siRNA, Tat_2, Tat_2+siRNA, siRNA+TBPB, Tat_2+siRNA+TBPB, scsiRNA and Tat_2+scsiRNA+TBPB), and solvent used (ddH_2O of maltose-mannitol). The second application of two way ANOVA gauged possible interaction between sample treatments (Control, siRNA, Tat_2, Tat_2+siRNA and scsiRNA) with and without TBPB. In cases where ANOVA could not show statistical significance between factors, or interaction of factors, data sets were combined and reduced again to a minimum of eight biological replicates for display purposes and Student's t-test.

3.3 Results:

3.3.1 Tat_2 Complexation with dsRNA:

Hydrodynamic diameters and polydispersity indices (PDI) of Tat_2:dsRNA polyplexes were measured using DLS. Tat_2 complexation with 21-mer dsRNA showed significant reduction in size and PDI upon the use of TPBP as an additional agent. It can be seen from Figure 3.1 that at all charge ratios of Tat_2:dsRNA, TBPB at a +/- 100:1 molar charge ratio decreased the size of the polyplexes but was most effective at the 8:1 Tat_2:dsRNA charge ratio, producing polyplexes with a D_H of ~10 nm without addition of $CaCl_2$ (see Fig. 3.1). Generally it can be seen that PDI correlates with size, lower sizes existing at lower PDI measurements. A PDI of ~0.1 indicates a strongly homogeneous

size of the particles, and was only achieved using TBPB, with TBAB only improving complex formation at an ionic strength of 0.6 M before it was indistinguishable from the effect of $CaCl_2$ alone. This trend was observed with $CaCl_2$ throughout. It can be seen that as ionic strength increases, the addition of TBPB had a less dramatic effect that was indistinguishable from the effect of $CaCl_2$ alone at I_c exceeding 0.6 M (see Fig. 3.1).

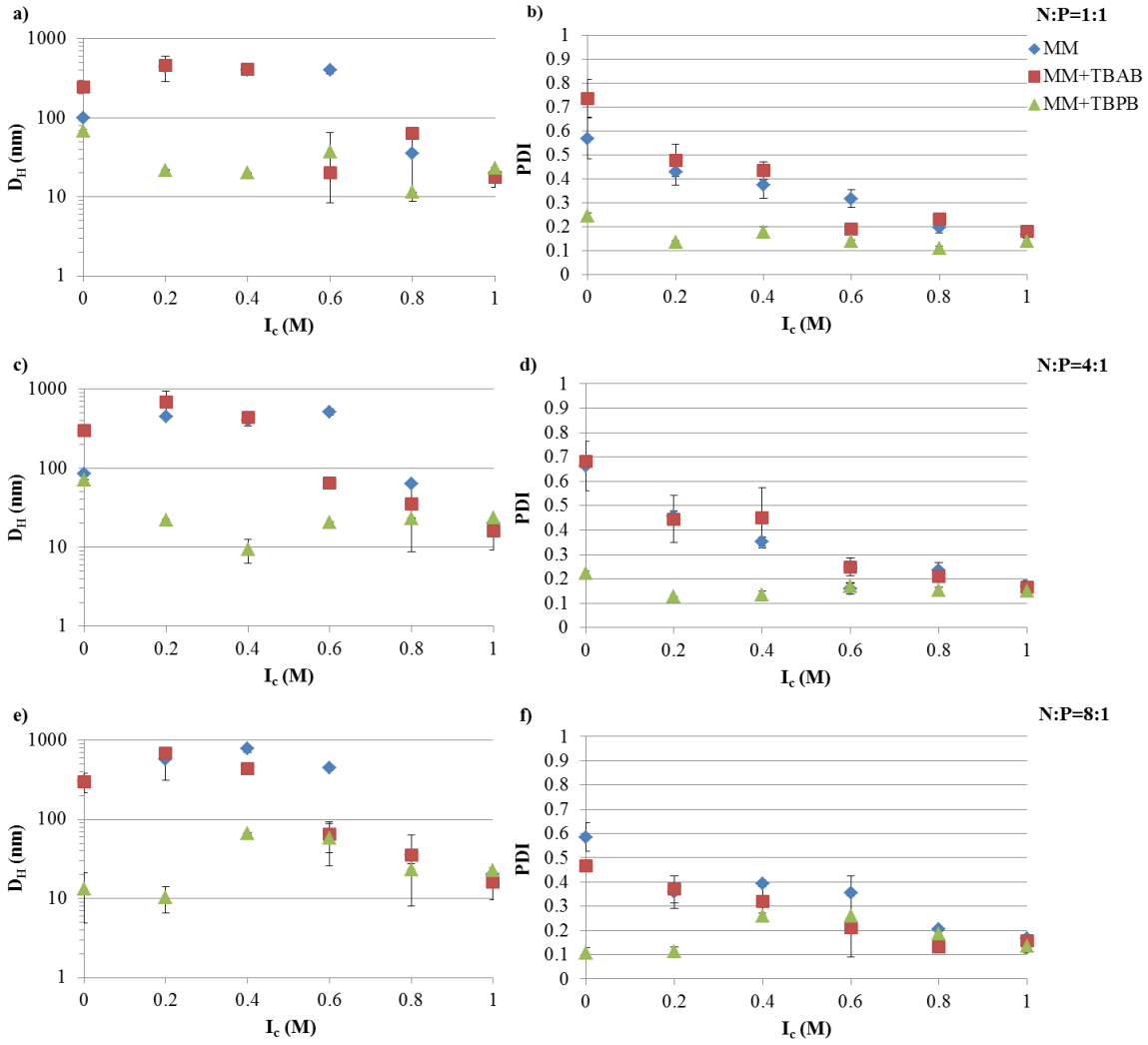

Figure 3.1: Hydrodynamic diameters (D_H) and PDI at different Tat_2:dsRNA +/- molar charge ratios and ionic strength using $CaCl_2$. Charge ratios used were 1:1 (a,b), 4:1 (c,d) and 8:1 (e,f). Data plotted are means±s.d. (n=3) using the CONTIN algorithm.

3.3.2 Tat_2 Complexation with DNA:

Tat_2:DNA polyplex hydrodynamic diameters (D_H) were measured under different ionic strengths of $CaCl_2$ and in the presence or absence of TBPB. The addition of TBPB to Tat_2:DNA polyplexes showed a noted lesser effect than that observed with dsRNA (see Fig. 3.1 and Fig. 3.2). However the behavior of linear DNA did not strongly resemble the patterns observed with dsRNA. In the case of 0.5 kb, it was shown that TBPB had a weak effect on PDI, but reduced the size by ~50%, from 189.3 nm to 96.0 nm. This effect became more pronounced with an increase in ionic strength, however, at ionic strength of 0.8 the size increased to 811 nm, with reduction to a minimum in size at an I_c of 1.0 M of 46.95 nm. The PDI was found again to generally correlate inversely with I_c with a reduction to 0.155 at an I_c of 1.0 M.

In the case of the 1 kb DNA fragment (see Fig. 3.2-b), a true disparity in size and PDI can only be seen at the 0.0 M ionic strength limit, where size was at a minimum (62.6 nm) for the TBPB formulation and PDI was 0.538. A similar minimum was reached for formulation without TBPB at 0.4 M ionic strength with a size of 72.6 nm. The PDI was generally too high at all ionic strengths higher than 0.0 M for appropriate analysis.

At 3 kb both MM and MM+TPBP produced nearly identical results in regards to PDI, while size was generally reduced to 90-120 nm under all ionic strengths except for 0.2 M where MM and MM+TPBP formulas showed the same size particles (~250 nm) and 0.6 M, where the MM only formulation was shown to be significantly smaller (135.9 nm) and the MM+TBPB formula was substantially larger (461.5 nm). A complete divergence in size was noted after I_c 0.8 M.

For circular plasmid, the results show a close correlation in size under both MM and MM+TBPB condition, up to 0.2 M ionic strength and at 0.6 M. PDI was lowered substantially by addition of TBPB (a reduction of 0.3), but became smaller and more similar between MM and MM+TBPB formulations after 0.4 M ionic strength.

Generally it was shown that TBPB decreases particle size marginally, while often having a more significant effect on PDI up to <3 kb sized linear DNA and has less impressive effects at 3 kb linear DNA, in combination with Tat_2. Increasing ionic strength generally decreases PDI, but is highly dependent on the size of the nucleic acid. Additionally, large sizes can be observed to occur at anomalous positions, particularly with 0.5 kb linear DNA, where the 0.8 M I_c increment was substantially larger than all other formulations (nearly eight-fold). As can be seen by comparing the TBPB positive samples to the TBPB lacking samples, the size of polyplexes was more affected at the smaller size ranges, with the effect becoming very slight with circular plasmid, though all minimized sizes were found only in the TBPB positive samples.

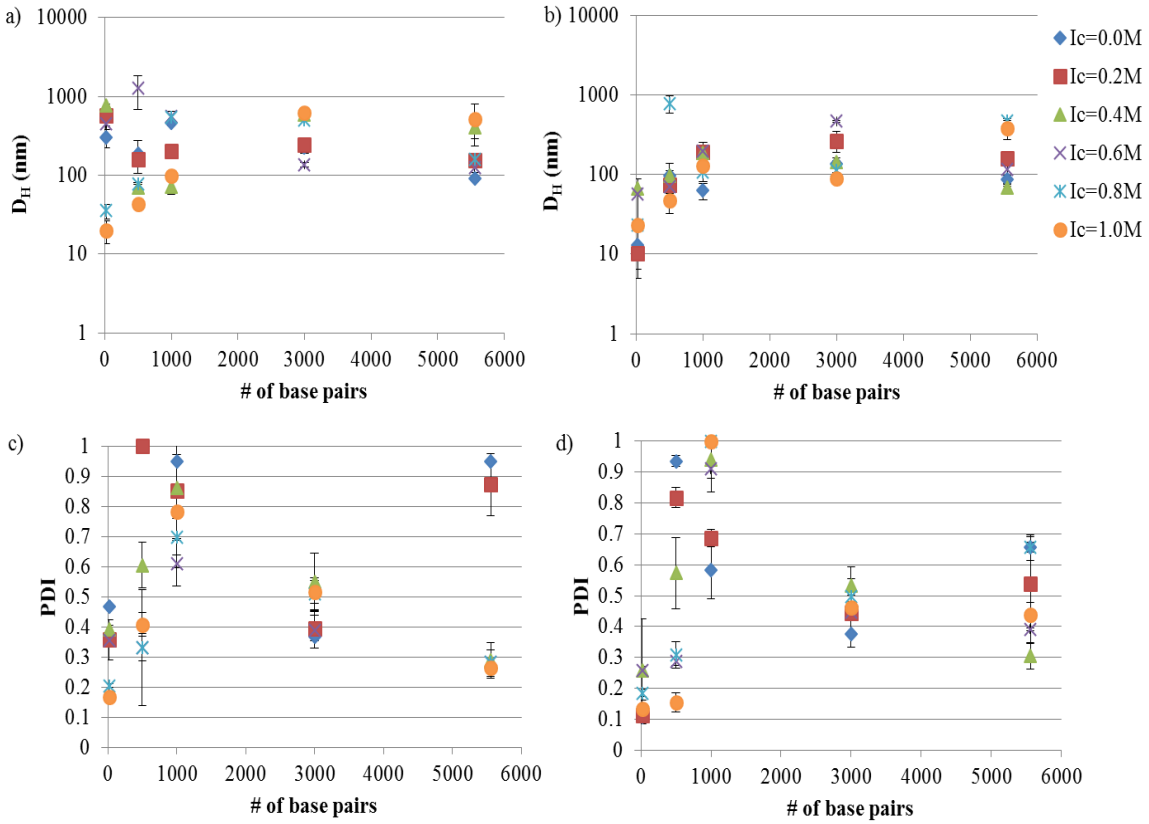

Figure 3.2: Hydrodynamic diameters (D_H) and PDI measurements of DNA-Tat_2 polyplexes in MM media with (b, d) and without TBPB (a, c). The 8:1 Tat_2:dsRNA charge ratio is also shown for comparison. The relationship between the size of the nucleic acid in terms of # of base pairs and the size of the polyplexes is shown. Data plotted are means±s.d. (n=3), evaluated using CONTIN.

3.3.3 Advanced Size Analysis:

Hydrodynamic Volumes (V_H) were calculated from the smallest Tat_2 polyplex sizes measured for each nucleic acid under their specific conditions (see Table 3.2). The volumes allow for a robust linear regression when related to the length of the nucleic acid (see Fig. 3.3). It was also interesting that the approximation of the size of the circular plasmid to one half of its actual sequential length to account for secondary structure and circular shape, was well approximated to the regression shown (see Fig. 3.3).

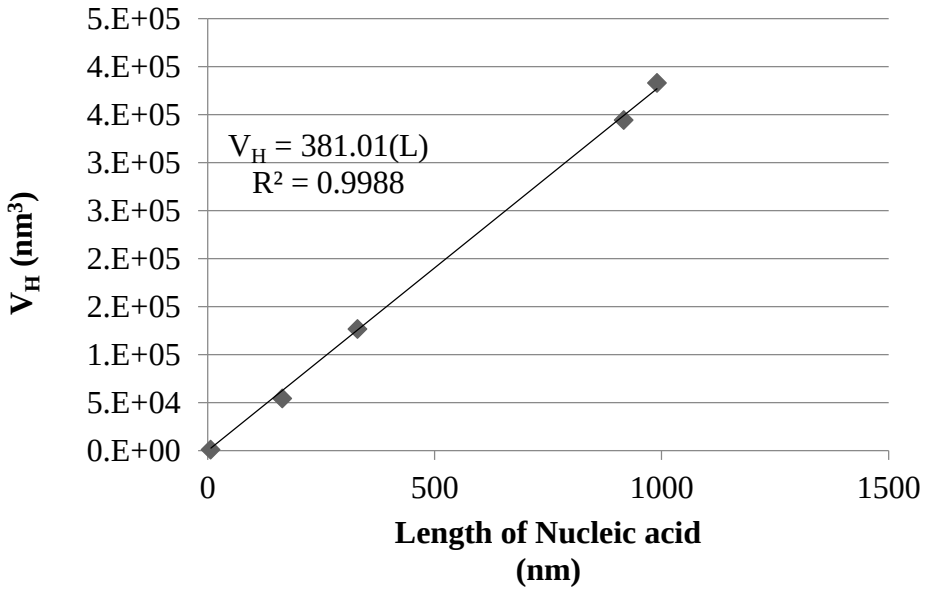

Figure 3.3: Hydrodynamic Volume (V_H) of size minimized polyplexes of different lengths of nucleic acid. Data shown is a conversion of the mean polyplex size to hydrodynamic volume under the approximation of a sphere. The linear regression was forced through zero to better reflect the fact that a length of 0 nm would result in a polyplex of 0 nm^3. R^2 and regression equation shown, where "L" is the length of the nucleic acid.

By solving for the slope of the linear regression fit based on the equation V_H=380.01(L) or the quotient of V_H over L, one can roughly gauge how well the calculated values of V_H correspond to the spherical approximation (see Table 3.2). Additionally, all the smallest measured polyplexes (numerical values in Table 3.2) required the use of TBPB, though other formulations at high I_c were also found to give similar results (see Fig. 3.2). The poorest fit was found for 21-mer dsRNA at 21% similarity to the slope, when the length and volume were used as calculated (i.e. 572.0/6.93= 82.5).

Table 3.2 Minimally Sized Polyplexes and Formulations

Nucleic acid: Length & Type (nt/nm)	I_c $CaCl_2$* (M)	Minimal D_H (nm)	Calculated V_H (nm^3)	Goodness of Regression fit (% of slope)
dsRNA (21/6.93)	0.2	10.29	572.0	21
Linear dsDNA (500/165)	1.0	46.95	$5.419 \cdot 10^4$	86
Linear dsDNA (1000/330)	0.0	62.30	$1.266 \cdot 10^5$	100
Circular plasmid (5.556/916.7)	1.0	86.96	$3.443 \cdot 10^5$	99
Linear dsDNA (3000/990)	0.4	90.10	$3.830 \cdot 10^5$	101

*All formulations required TBPB

3.3.4 Zeta-Potential Analysis:

Zeta-potentials of Tat_2:circular plasmid and Tat_2:dsRNA polyplexes were measured at different N:P ratios, both with and without TBPB**.** At low N:P ratios (1:1 and 4:1), zeta-potential was greatly affected by TBPB, where circular plasmid was found to have virtually no change at the 1:1 N:P ratio level in the presence of TBPB while without TBPB a change of 22.2 mV occurred with the addition of Tat_2. With dsRNA the addition of TBPB had no effect on zeta-potential at the 1:1 N:P ratio, with a measure of approximately -24 mV. At the 4:1 N:P ratio, the circular plasmid was overcharged to a zeta-potential of 30.9 without TBPB but significantly less at 22.0 mV with TBPB. The opposite trend was observed in the case of 21-mer dsRNA, as the 4:1 ratio without TBPB resulted in a zeta-potential of neutralization at -0.241 mV, while with TBPB the potential was measured at 4.54 mV. Overcharging continued at the 8:1 ratio in the case of circular plasmid and dsRNA without TBPB to 30.9 mV and 33.6 mV respectively. Increase in

zeta-potential was shown in the case of circular plasmid up to 38.4 mV in the presence of TBPB at the 8:1 N:P ratio. The increase in zeta-potential was comparatively marginal in the case of dsRNA at an average of 8.56 mV, an increase of only 4.02 mV compared to circular plasmid's increase of 16.4 mV (see Fig. 3.4).

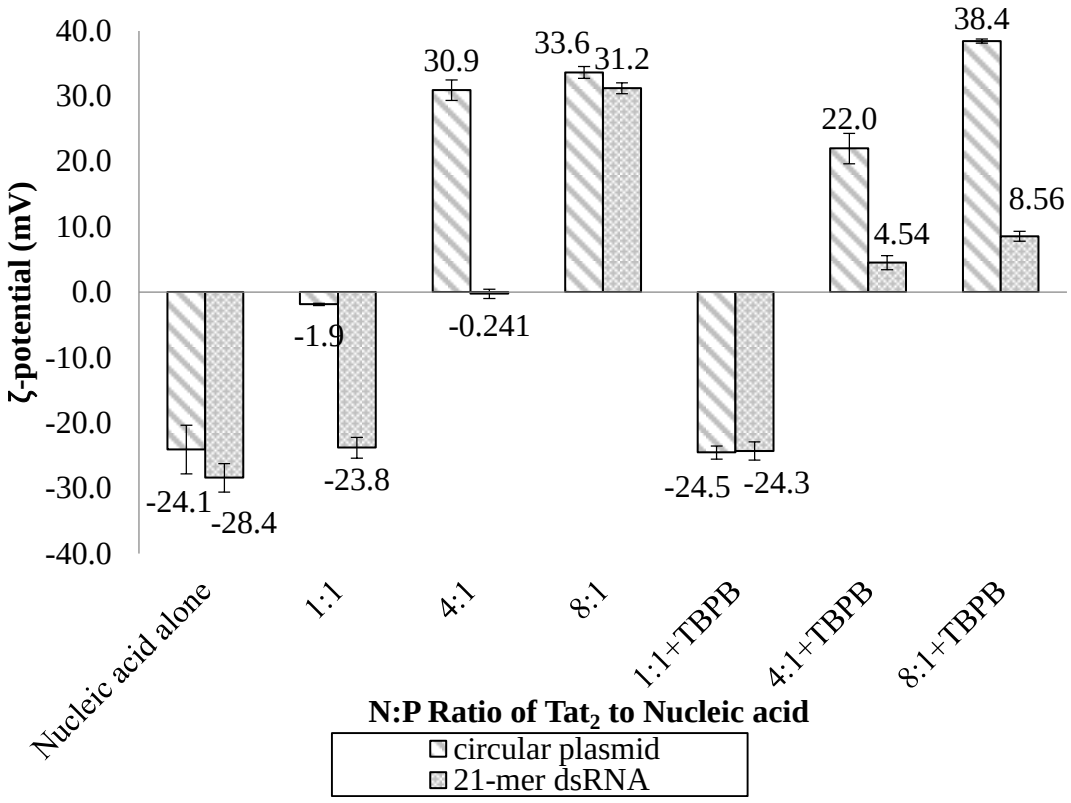

Figure 3.4: Zeta (ζ) potential analysis of circular plasmid and dsRNA samples with and without TBPB in MM medium at the 1:1, 4:1 and 8:1 N:P ratios with Tat_2. Circular plasmid was preferred over the linear dsDNA due to the higher concentration required for zeta-potential measurements. Numbers displayed are the values of the bars in mV, with striped bars indicating circular plasmid samples and patterned bars indicating 21-mer dsRNA. Data displayed represent means±s.d calculated from triplicate measurements of a single sample.

3.3.5 RT-qPCR of Inoculated Triticale Leaf Samples:

The expression level of the phytoene desaturase gene was evaluated using RT-qPCR, and converted to relative expression values using the $2^{-\Delta\Delta Ct}$ method. A reduction in expression by 20-30% was observed in all samples that were treated by injection. Samples treated with TBPB, showed up to 45% reduction in expression with Tat_2+TBPB, TBPB+siRNA and Tat_2+scsiRNA+TBPB showing significances of $p<0.05$. An approximately 75% reduction in PDS expression ($p<0.0001$ compared to control) was only observed in treatments that possessed siRNA, TBPB and Tat_2 (see Fig. 3.5). Additionally, only the Tat_2+siRNA+TBPB treatment was found to show a statistical difference from all other samples except for TBPB alone ($p=0.068$) in unpaired comparisons using Student's t-test (see Table 3.3). Furthermore, it must also be noted that an especially high degree of statistical significance was noted between the Tat_2+siRNA+TBPB treatment and the Tat_2+scsiRNA+TBPB treatment at $p=4.21 \cdot 10^{-4}$. This was noteworthy as these two treatments were the closest in composition, the only difference being the sequence of the RNA duplex, yet the scsiRNA variant was indistinguishable from the other controls (see Table 3.3).

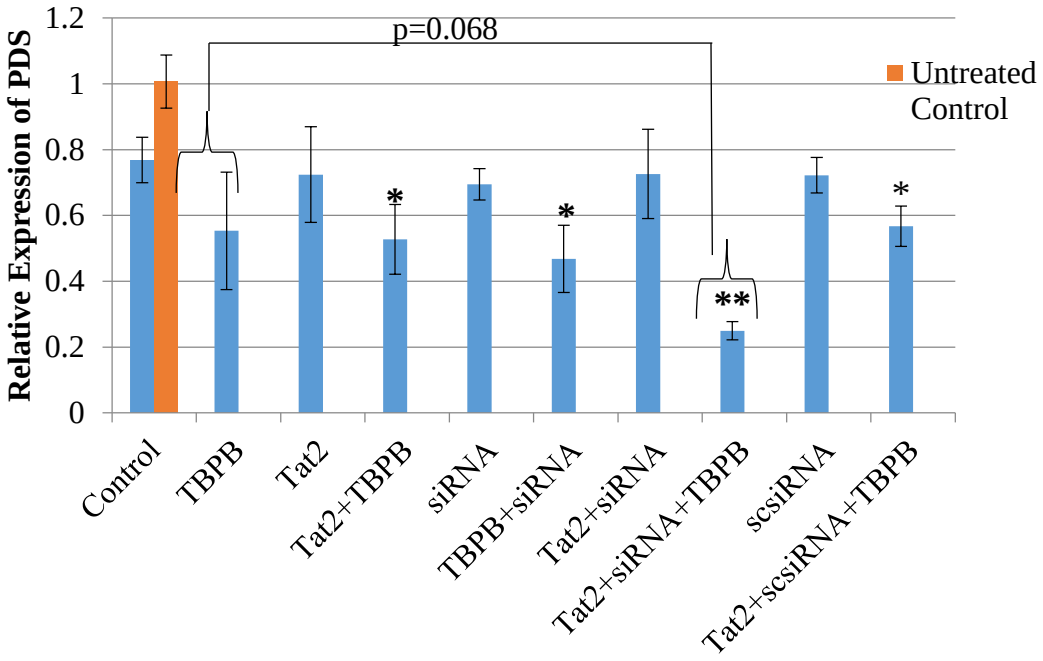

Figure 3.5: Relative expression of PDS from seedling Triticale (Sunray) leaves converted from ΔΔCt values, normalized against ADP-RF. All data was calibrated against an untreated control (Red, n=3). No statistical significance was found to be contributed by the solvent used (maltose-mannitol or ddH_2O) according to Two-way ANOVA. A significance level of p=0.00024 was found for the difference between treatments containing TBPB and those without. The (*) and (**) indicate a significance of $p<0.05$ and $p<0.0001$ between the designated treatment and the Control (solvent only), based on Student's t-test. Tat_2+siRNA+TBPB was found to be significantly different ($p<0.05$) from each other sample except TBPB alone (p=0.068, shown above). Data displayed are means±s.e. n=8.

Table 3.3: Table of p-Values for Unpaired Student's t-Tests of RT-qPCR Samples

	1	**2**	**3**	**4**	**5**	**6**	**7**	**8**	**9**	**10**
1		0.145	0.395	0.041	0.198	0.016	0.394	$3.22 \cdot 10^{-5}$	0.304	0.024
2			0.235	0.452	0.233	0.343	0.227	0.068	0.196	0.471
3				0.147	0.426	0.086	0.496	$6.18 \cdot 10^{-3}$	0.495	0.173
4					0.091	0.347	0.135	0.018	0.067	0.376
5						0.036	0.416	$2.97 \cdot 10^{-6}$	0.354	0.063
6							0.077	0.036	0.025	0.211
7								$4.47 \cdot 10^{-3}$	0.489	0.156
8									$7.63 \cdot 10^{-6}$	$4.21 \cdot 10^{-4}$
9										0.040

Key: 1- Control (solvent only), **2**-TBPB, **3**-Tat_2, **4**-Tat_2+TBPB, **5**-siRNA, **6**-TBPB+siRNA, **7**-Tat_2+siRNA, **8**-Tat_2+siRNA+TBPB, **9**-scsiRNA, **10**-Tat_2+scsiRNA+TBPB

ADP-RF expression was found to be the most stable reference for normalization, with CDC and RLI being far less stable. Table 3.4 shows the raw Ct values for 42 of the samples collected. ADP-RF had a standard deviation amongst all tested samples of less than 1 Ct, while all other reference genes displayed standard deviations of greater than 1.3 Ct. Additionally it was found that for CDC and RLI samples that utilized TBPB had significantly lower Ct values than those without, with differences of up to 5 Ct, which represents an approximately 2^5 fold difference in expression level. In the case of CDC this was a difference of 22-24 Ct to 19-22 Ct, and the case of RLI a change from 24-26 Ct to 20-22 Ct and as low as 18 Ct.

Table 3.4: Ct value Analysis of Target (PDS) and Reference Genes from RT-qPCR of Triticale Leaves

MM=Maltose & Mannitol		Target Gene		Reference Genes					
		PDS		ADP-RF		CDC		RLI	
		Water	MM	Water	MM	Water	MM	Water	MM
Control	R1	25.97506	25.27929	23.69714	23.64619	24.89149	24.59786	27.55565	26.8921
	R2	24.09459	22.97824	22.32155	22.68338	22.50624	22.97363	25.32632	25.50647
	R3	24.89621	25.0647	23.08394	24.07086	23.60398	25.33332	26.07088	27.85261
TBPB	R1	23.8075	26.51612	23.5131	23.30975	19.80063	24.19953	24.34309	28.25299
	R2	25.19291	23.16497	22.32155	22.94547	21.94078	21.53990	25.55262	25.74529
	R3	24.78741	21.99968	23.08394	22.30749	20.68024	19.86071	25.14708	23.17134
Tat_2	R1	24.83638	24.98278	23.89314	23.05583	24.19563	23.67613	26.60516	26.46833
	R2	25.98721	24.48807	24.27212	24.70116	24.78406	24.94172	27.22974	26.97839
	R3	23.59364	22.32445	21.86751	21.99121	22.8027	22.26852	25.40135	24.36699
Tat_2+TBPB	R1	23.53142	24.62914	21.57527	22.68105	19.31091	21.34158	22.80724	25.29072
	R2	24.90273	22.93241	23.09212	22.63462	24.23861	20.6065	25.99182	24.88507
	R3	22.69374	21.69301	20.92079	21.20382	19.69844	22.30575	22.00518	18.81472
siRNA	R1	23.6736	23.10535	22.51141	21.20382	22.75313	22.30575	25.13446	24.36139
	R2	24.3346	24.86552	22.63000	22.78061	23.72576	23.80411	25.76133	26.07446
	R3	25.12562	22.92009	22.77035	20.993	24.643	20.16918	26.48736	23.5526
TBPB+siRNA	R1	23.95464	22.99029	21.96783	21.23991	19.47517	18.81622	23.77386	22.70514
	R2	27.65538	23.44015	24.70874	22.83608	23.18448	20.70164	26.23117	25.17861
	R3	22.77532	26.3533	21.36877	22.93817	18.8543	22.43513	23.76294	26.85483
Tat_2+siRNA	R1	23.69739	24.94946	22.79139	23.28964	23.56374	23.79088	26.56873	26.37328
	R2	23.36801	22.79671	22.14104	22.68721	22.49702	23.12447	25.34292	25.88212
	R3	26.69707	22.90538	23.55313	22.94949	24.65446	23.57826	26.85719	25.81883
Tat_2+TBPB+siRNA	R1	25.5705	24.87389	22.25095	21.67845	21.568	19.85769	26.00412	24.39663
	R2	25.13404	24.65055	22.59306	23.53069	20.51949	21.75225	25.47359	26.23117
	R3	25.40095	23.65055	23.52309	21.59999	21.22104	19.96935	26.25145	24.3767
General average		**24.65358**	**23.89809**	**22.76883**	**22.62324**	**22.29639**	**22.24792**	**25.48689**	**25.25128**
General STDEV		**1.21450**	**1.31722**	**0.92368**	**0.95134**	**1.94878**	**1.81074**	**1.34342**	**1.95342**

3.4 Discussion:

It must be understood that the principle size being measured is a hydrodynamic diameter, which reflects better the diffusion of particles in a medium rather than its actual size and shape. Therefore, its best application is in determining relative sizes of particles in different formulations and gauging PDI. It is with this in mind that these results must be evaluated.

In this study it has been shown with relatively high confidence that TBPB acts to help reduce both size and PDI of Tat_2:nucleic acid polyplexes, while TBAB shows little significant impact. Because several sizes of nucleic acid were utilized, the mechanism by which this chemical acts may be elucidated. It may be hypothesized that it acts through the charge neutralization of phosphates on the backbone of nucleic acids, whereby compaction of the nucleic acids may be increased by the phosphonium cations. However, this cannot be the case, as 21-mer dsRNA has no structure beyond its sequence, therefore nothing to compress. However, small ~10 nm polyplexes were formed with the addition of TBPB, while without it polyplexes were 300 nm for the +/- 8:1 ratio of Tat_2:dsRNA. It is therefore proposed that TBPB acts as a low effective concentration chaotropic, as shown previously (Harrison, Sader et al. 2006), breaking apart larger aggregates into smaller particles. This mechanism of action is substantiated as it is shown to only display substantial effects with linear dsDNA smaller than 3 kb, since only the mass concentration of DNA was held stationary (1 ng/μL) the molarity of the DNA was reduced with increasing DNA length, meaning molar charge ratio was not the main contributor to size reduction but likely bulk molar ratio of particles to TBPB. Furthermore, the PDI measured for small polyplexes was usually itself low (<0.3) Zeta-

potential data also shows that the impact of TBPB was more significant with dsRNA, showing a substantially lower zeta-potential for dsRNA at the 8:1 N:P ratio (see Fig. 3.4). This difference was nearly 30 mV, indicating that the chaotropic effect was more significant in the case of dsRNA, and was able to disrupt but not abolish intermolecular interactions between Tat_2 arginines and dsRNA phosphates. Interactions of tertiary phosphonium and ammonium cations of various types have been shown to interact strongly with DNA (Chatterjee and Moulik 2005, Dehkordi, Bordbar et al. 2012), and similar interactions with dsRNA (Crnolatac, Tumir et al. 2013). However previous work used phenyl substituted phosphoniums, and observed intercalative interactions with as well as electrostatic interactions, with similar organic groups forming hydrophobic interactions. While intercalative interactions are unlikely, hydrophobic shells and charge screening may have contributed to the formation of highly stabilized particles.

Calcium chloride concentration in terms of ionic strength was shown to reduce PDI in the case of dsRNA, 0.5 kb linear DNA and circular plasmid. Calcium chloride has already been shown to reduce CPP:nucleic acid sizes, but was not tracked for effect on PDI (Khondee, Baoum et al. 2011). In the case of Tat_2 it can be seen that $CaCl_2$ did not significantly affect size except in the case of dsRNA. While it is known that divalent cations can complex and precipitate DNA, it has also been shown that Ca^{2+} ions can bridge zwitterionic lipids with DNA to form liposomes (Antipina and Gurtovenko 2015). It must be remembered that there exist two anionic glutamate residues in Tat_2, and a similar adapter role for Ca^{2+} may explain the increased homogeneity, by occupying these residues and preventing aggregation. From this it can be inferred that $CaCl_2$ has less a chaotropic role in complex formation, and more of a stabilization role as it maintains the

uniformity of the size of the particles, but does not actively reduce the size of the particles. It may do so through electrostatic screening of the polyplexes as well.

This is the first time that a small molecule phosphonium salt has been used to reduce the size and PDI of CPP:nucleic acid polyplexes, albeit with varying efficacies. It also illustrated the first formulation of CPP:nucleic acid polyplexes in a medium high in maltose and mannitol. Polyphosphonium polymers have shown promise as low cytotoxicity transfection agents superior to their ammonium analogues, able to effectively complex nucleic acids at 1:1 molar charge ratios (Hemp, Allen et al. 2012, Hemp, Smith et al. 2012). It has been proposed that this highly efficient complexation is due to the higher localization of cationic charge on the phosphorus atom of the quaternary phosphonium versus the quaternary ammonium nitrogen atom (Wang, Liu et al. 2011). This may also contribute to the apparent chaotropic activity of TBPB.

It was also found that the minimal D_H of the polyplexes, for each length of nucleic acid was related linearly to the volume of the polyplex. The correlation was strong (see Fig. 3.3), and showed that for each nm of nucleic acid there was an increase of approximately 380 nm^3 in volume. It was also shown that the length of circular plasmid fit with the other data points when reduced to half its length to account for secondary structure (916 nm vs 1032 nm). This suggests that circular plasmid folds along a particular geometry that is functionally equivalent to a linear DNA half its length. It has been shown that polyplexes of protamine and plasmid DNA form fasciculated structures, where DNA strands are located side by side after condensation (Motta, Brocca et al. 2013). A similar structural formation may be the pattern observed with Tat_2. Furthermore, it was found that 21-mer dsRNA D_H=10.29 polyplexes represented the least well fit data

point under the spherical volume approximation, indicating a different shape than that of the other nucleic acid lengths. Since dsRNAs of only 21-mer in length form relatively inflexible rods, which would not form spheres at a small size such as 10 nm in diameter if it follows the fasciculated pattern, and would instead form small prolate spheroids. However, other studies with electron microscopy will be necessary to fully confirm the sizes and possibly shapes of the formed polyplexes (Kato, Nakamura et al. 2014). It can be conjectured, however, that the found linear relationship points to only a single nucleic acid molecule being involved in individual polyplexes when size was minimized.

All data being considered, these explanations do not account for the seemingly anomalous non-correlating points found during this study. Most notable would be the 0.5 kb sample at 0.8 M I_c $CaCl_2$ and TBPB which measured at ~800 nm in diameter (see Fig. 3.2). This was much larger, nearly ten fold, that of the non-TBPB formulation (~80 nm). No clear explanation for this exists, except that the patterns were more consistent with 21 mer dsRNA in all cases than what was found at larger nucleic acids, and even showed more consistent patterns with circular plasmid. This suggests that long linear DNA, expectedly, has more degrees of conformational freedom and may not always conform in the same manner when conditions change, due to more complex structural dynamics. However, caution must be applied in these cases, as errors in measurement could also account for these differences.

The RT-qPCR data was able to show reasonably well that the use of TBPB was necessary in conjunction with Tat_2 to induce silencing of the PDS gene with 21-mer siRNA. Additionally, it was demonstrated that the silencing must have been systemic, as the portion of leaf tissue sampled was at the tip, while injections were performed at the

base of the leaf. This implies that siRNA must have travelled via plasmadesmata or another vascular mechanism to induce silencing in the distally located tissue (Melnyk, Molnar et al. 2011). It was also interesting to note that no significant difference in the expression of PDS was found between treatments using a maltose-mannitol solution as compared to simple ddH_2O. This was surprising, because uptake of sugar solutions may be assisted through stimulation of phloem loading and unloading in plant vasculature (Lalonde, Tegeder et al. 2003, Peuke, Gessler et al. 2015). This implies that the mechanism of siRNA polyplex tissue dispersion and cell entry was not affected by the solvents used in these experiments, but instead was primarily affected by the formulation of the polyplexes.

A possible reason why the Tat_2+siRNA+TBPB treatment was the only one that showed profound down regulation of PDS (up to 75-80%) may be due to the reduced size of polyplexes in that treatment. At a size of between 10-20 nm, the size was within the scope of the pores in plant cell walls. The pores of the cell wall of most plants do not exceed 20 nm (Chichiriccò and Poma 2015) and since CPPs require contact with the plasma membrane to mediate import, smaller polyplexes may increase efficiency. This is contrary to results in a prior study that show large polyplexes exceeding 200 nm in diameter were able to transfect dicot plant cells with siRNA (Numata, Ohtani et al. 2014).

Similar to prior results in plant cells, lower zeta-potentials also seemed to have enhanced efficiency. Additionally it may not be only import into the cells, but the subsequent release of the cargo which was enabled by the TBPB, as the reduced zeta-potential compared to that without TBPB, indicates less bound Tat_2. This is further supported by the fact that the larger polyplexes studied previously were also less bound

by CPP (Lakshmanan, Yoshizumi et al. 2015).

Another possible contributing enhancer of transfection may be due to the potential for TBPB to slightly solubilize cellulose. It has been shown that with high concentrations (40% v/v) of its hydroxide variant (Abe, Fukaya et al. 2012) and with other similar ionic liquids (Kagimoto, Fukumoto et al. 2006) that they are capable of dissolving cellulose. Some slight dissolution of the cellulose in the leaf cell wall may have caused Likely the explanation is a combination of all noted factors that allowed for the observed down-regulation.

The PDS gene was chosen due to its role in carotenoid synthesis, and previous use as a marker in virus-induced gene silencing (VIGS) in *Triticeae* species (Holzberg, Brosio et al. 2002, Budak, Jiao et al. 2015) where silencing was usually indicated by a photobleaching of the leaves. However, endemic silencing must be necessary to observe photobleaching, because such no photobleaching was observed in any plants up to 3 weeks after inoculation. It is also worth noting that the PDS primers used for this study amplified a region of the PDS coding sequence 601 nucleotides upstream of the target site of the siRNA and therefore first site of mRNA cleavage. Since the VILO kit uses both oligo-dTs and random hexamers as primers for cDNA synthesis, the entire body of mRNA was reverse transcribed. Because of the upstream point of amplification during RT-qPCR, even transcripts that were not translatable into functional protein were amplified. The functional transcript abundances could therefore be much lower than what was measured. Future work may require the inclusion of a primer set that amplifies over the region targeted by the siRNA.

While ADP-RF was the most stable reference gene and hence the one used for normalization of PDS expression levels, CDC and RLI showed interesting effects in samples treated with TBPB. One possible reason for the measured differential and instability of these reference genes that was systematically found in the TBPB samples was because TBPB is related to long known growth retardant and regulator used in agriculture, known as phosphon (Balczewski, Biczak et al.). Also, it was reported that growth retardation of *Hordeum vulgare* and *Raphanus sativus* L. was caused by the similar ionic liquid salts triphenyl-hexadecylphosphonium iodide and triphenylmethyl-phosphonium iodide, which was observed as reduced growth height (Biczak, Bałczewski et al. 2014). It is likely that these two genes were upregulated as a stress response, particularly CDC which plays a role in cellular division (Gimenez, Piston et al. 2011), which was also upregulated the most, up to 2^5 times the expression level of the treatments without TBPB (see Table 3.3). Due to this effect, it is likely that other chemicals similar to but less toxic than TBPB may need to be explored when applied to other genes of interest.

3.5 Conclusions

The work presented in this chapter opens the door to the use of similar formulations for dsRNA polyplexes for gene silencing in plants. Additionally, information was discovered that for the first time made a strong mathematical relationship between polyplex size and the length of the nucleic acid, resulting in a regression fit that indicated a 380 nm^3 volume increase for every nm of nucleic acid for the CPP Tat_2. It may be possible to extend this study to other peptides and determine whether substantially similar trends are observed, or whether this is unique to Tat_2.

Finally this is the first (to our knowledge) report of polyplexes of siRNA that may only include a single siRNA molecule with a size between 10-15 nm in terms of D_H. This has not been accomplished by any other method. Still more work will need to be done to fully confirm all results reported herein, in particular more studies of siRNA delivery and gene-silencing.

4.0 Temporal Evolution of CPP:5bp dsDNA Polyplexes Monitored Using Dynamic Light Scattering

4.1 Introduction:

Nanocarrier technologies have grown to become a leading method of gene delivery in both *in vitro* and *in vivo* systems. Human, mammalian, and plant cell systems have all shown susceptibility to nucleotide delivery via cell-penetrating peptides (CPPs) and other cationic polymers and dendrimers (Kadlecova, Rajendra et al. 2013). This study was undertaken to evaluate a little studied phenomenon of particular application to CPPs, polyplex aggregation and time evolution. The most prevalent method for characterizing the size of CPP-nucleotide polyplexes has been dynamic-light scattering (DLS) (Kato, Nakamura et al. 2014), due to its relative ease of sample preparation compared to the more robust direct microscopy methods, atomic force microscopy (AFM) and scanning electron microscopy (SEM) (Di Profio, Germani et al. 2010). It was with this particular fact in mind that this study was initiated, to develop an empirical relationship and mathematical model between polyplex aggregation (in terms of hydrodynamic diameter) and time, using DLS as the basic method. Furthermore, there currently exists no mathematical model for predicting points of formulations of high stability, with reduced size increase of polyplex over time. Often formulations for CPP-nucleotide polyplexes take the form of a so called N to P ratio (*R*) or the molar ratio of cationic nitrogen bearing residues on the CPP (lysine and arginine) to negative phosphate groups on the nucleic acid. Thus far it has been shown that higher *R* usually results in smaller polyplex size and increased stability for not only CPP:nucleic acid polyplexes (Nam, Kim et al. 2011) but those formed with PEI and other polycations (Perevayazko, Bauer et al. 2012).

In many cases, CPP-nucleic acid polyplexes have only been evaluated over short time courses (one to two hours), or longer time courses (two days) with large gaps between measurements. Since transfection often occurs over time periods less than one hour, it may seem redundant to observe polyplex aggregation over time periods greater than what is necessary for transfection. However this may not be the case in plant tissue culture systems where polyplexes may remain in a state of dynamic equilibrium between adsorption to the cell-wall and free in solution, for periods of time well beyond the 1 hour treatment. Furthermore, in monocot plants it has been shown that lower *R*, as low as 1:1, were more successful in transfection with both circular plasmid (Chuah, Yoshizumi et al. 2015) and siRNA (Numata, Ohtani et al. 2014). Moreover, a measure of the stability of a CPP-nucleotide polyplex evolution over time may be useful to projects in which lyophilisation and preservation of the polyplex is the goal (Steele, Zhao et al. 2012).

Because it was not abundantly clear in all cases what value of *R* will yield the most favorable results, having a predictive landscape from which to derive the appropriate formulation for a given cell type may be used in conjunction with prior data to optimize the transfection efficiencies of CPPs.

The system was simplified substantially for observation of very fundamental properties of aggregation due solely to the characteristics of the peptide, for this reason 5 bp dsDNA was used. For peptides, R9 was used as a representative of a simple highly cationic CPP, and Tat_2 as a representative of a complex cationic CPP. By simplifying the system, variations arising from the degrees of freedom of motion inherent in larger nucleic acids were avoided (Battistini, Hunter et al. 2010).

It was found that over an observed time scale of 4 to 5 hours, the Z-average hydrodynamic diameters of polyplexes followed 3rd-order polynomial patterns, characterized by an initial aggregation phase, a stationary stable phase of consistent size and a secondary less drastic aggregation phase. Furthermore it was found that the coefficients of the 3rd-order polynomial fits were related to the natural logarithm of the *R* value by a secondary 3rd-order polynomial fit. This series of polynomial fits allowed for direct comparison of temporal properties across CPPs, and fitted these schemes to a very direct method for characterizing CPP:nucleic acid interactions without the use of more advanced methods (Wattraint, Saadallah et al. 2013).

4.2 Materials and Methods:

4.2.1 Oligonucleotide Preparation:

All oligonucleotides were purchased from Integrated DNA Technologies (IDT). To prepare 5 bp dsDNA, 5-nucleotide synthetic (no 5′-phosphate) oligonucleotides with the sequences 5′-AGTCC-3′ and 5′-GGACT-3′, were dissolved in Ultrapure H_2O (Sigma) to a concentration of 10 mg/mL and combined in equimolar ratios for annealing. The combined oligonucleotide solution was mixed gently by pipetting and heated to 40^{o}C for 10 minutes and then allowed to cool to room temperature, and were then placed at 4^{o}C to assist in annealing. The stock 5 bp DNA was diluted ten-fold for quantification by UV-vis absorbance using an ND-8000 Nanodrop system (Thermoscientific). The DNA stock solution was confirmed to anneal using high density agarose gel electrophoresis. A 50 mL, 4% MetaPhor Agarose^{TM} (VWR) gel was prepared using 1x TAE buffer and 5 µL 10,000x GelRed stain (Biotium), with thin well combs. Samples of both the stock 5 bp

DNA and the 5′-GGACT-3′ (5 nt) samples were loaded on the gel at mass amounts of 10 µg (1 µL of DNA solution, and 2 µL of 10x loading dye), as well as the Low Range DNA Gene Ruler Ladder (Thermofisher Scientific) and run for 40 minutes in 1x TAE buffer at 80V. The gel was visualized using an AlphaImager Pro HP system. Stable annealing was judged by the maintenance of band brightness after electrophoresis taking advantage of GelRed's 2-fold greater binding sensitivity with dsDNA versus ssDNA.

4.2.2 Peptide Preparation:

Peptides were purchased from Canpeptide, which used stationary phase synthesis and provided peptides as lyophilized products. R9 (RRRRRRRRR) and Tat_2 (RKKRRQRRRRKKRRQRRR) were reconstituted using Utrapure H_2O (Sigma) to concentrations of 5 mg/mL and 4 mg/mL respectively. These stock concentrations were used for all experiments.

4.2.3 Polyplex Sample Preparation:

Polyplexes were formed directly in the cuvettes used for measurement, which were disposable low volume plastic sizing cuvettes from Malvern. Firstly 10 µL of 500 mM potassium phosphate ($K_xH_yPO_4$) buffer calibrated to pH 7.0 using 1M KOH, was added to the cuvette and a volume of Ultrapure H_2O (Sigma) appropriate to dilute the sample to ~50 mM potassium phosphate was added. The exact volume of water required was adjusted by a few microliters depending the *R* ratio of the polyplex formulation. Then 10 µg of oligonucleotide was added and the appropriate amount of peptide solution was added to reach the desired *R* value. For R9, *R* values of 1, 2, 3, 7, 10, 20 and 30 were prepared. For Tat_2 the same was performed with the exception of R=7. Upon addition of

peptide, the final volume of each sample was 100 μL, and was pipetted several times to mix the components completely. The complexation reactions were allowed to proceed for 15 minutes at room temperature (25^{o}C) before the first DLS measurement was taken.

4.2.4 Time Evolution Analysis of Polyplexes with DLS:

Polyplexes were analyzed using a Zetasizer ZS Nano (Malvern), using 173^{o} NIBS backscatter with a 633 nm He-Ne laser. The CONTIN algorithm included with the Malvern Zetasizer software v7.4 was used to evaluate the raw correlation data. All samples were measured at 25^{o}C with no agitation between measurements or time points. With each sample three size measurements were taken every 30 minutes for 4 to 5 hours, and the Z-average was recorded and standard deviation of the measurements were calculated. Since measurements at each time point required up to 6 minutes total to complete, all subsequent time points were read exactly 30 minutes from the beginning of the previous measurement. All samples evaluated were monomodal, and did not necessitate 13^{o} forward scatter for evaluation.

4.2.5 Data Analysis:

Upon collection of data, Z-average size as hydrodynamic diameter in nanometers was plotted as a function of time in hours. A 3rd-order regression fit was found to be the best representation of the data over the observed time courses. Regression fits were approximated using Microsoft Excel. However, because polynomial regression fits often increase in R^2 value with an increase in the degree of the independent variable, the fit was kept to a 3rd-order regression in all cases to represent the overall pattern of the most

extreme cases, and evaluate attenuation of the coefficients as the pattern became less representative in some samples.

4.3 Results:

4.3.1 Confirmation of 5-mer DNA Annealing

DNA was found to be stably annealed as judged by agarose gel electrophoresis and precast GelRed stain. The 5 nt band was greatly diminished in brightness compared to the 5 bp band. Furthermore, the electrophoretic shift was at the expected size limit, though extensively diffuse due to large amounts of DNA loaded.

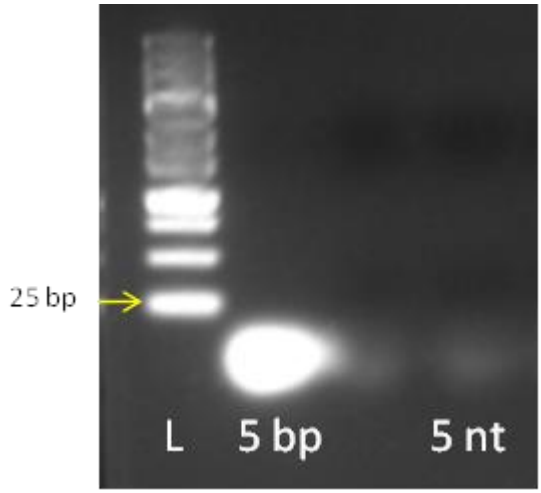

Figure 4.1: Confirmation of 5 bp annealing using 4% MetaPhor agarose and GelRed precast stain. Lanes denoted in picture are L-Low Range Gene Ruler Ladder, 5 bp-annealed 5 bp DNA and 5 nt- 5 nucleotide ssDNA 5´-GGACT-3´. Gel was run at 80 V for 40 minutes in 1xTAE buffer. The bottom band (25 bp) of the ladder has been denoted for comparison to the 5 bp band. The mass loaded for samples was 10 µg. The 5 nt band shows much less intensity compared to the 5 bp band.

4.3.2 Mathematical Analysis of Polyplex Time Evolution Trends

The modelling of the evolution of the polyplexes over time allowed for the subsequent plotting of the polynomial coefficients a, b, c, and d for the various 3rd –order fits of the different *R* values as dependents on the natural logarithm of the *R* value (see

Fig. 4.1 and 4.2). This allowed for secondary modelling of the pattern as a function of *R*, utilizing another series of 3rd-order fits. Again 3rd-order polynomial fits were maintained in all cases to observe attenuation of the coefficients as patterns became more quadratic or linear. In this manner both the primary and secondary 3rd-order regressions could be compared across peptides by arranging the secondary 3rd-order regression coefficients into matrices (see Eq (**4.1**), (**4.2)** and (**4.3**)); where each row of the matrix contains the secondary coefficients defining the 3rd-order function of a particular primary coefficient of the time course regression. Row sum operations on these matrices were used as a basis of non-arbitrary comparison between the different peptides, at an $R=e$. Further operations derived from an apparent relationship between the change of polyplex size and the peptide used.

It was found that all *R* values in R9 were well fit over the time course of 4 hours to a 3rd-order polynomial (see Fig. 4.2). While in the case of Tat_2 the fit was less representative at higher *R* ratios and required observation of up to 5 hours to confirm 3rd-order behavior at the $R=10$. The pattern resembled a quadratic fit at $R=20$ and a nearly linear decrease in Z-average hydrodynamic diameter at $R=30$ (see Fig. 4.3). In the case of R9 the polyplexes initial size was found to range from 218 to 570 nm and 161 to 371 nm in the case of Tat_2. In all cases and values of *R*, plateaus were observed at 1.5 to 3.0 hrs except in the case of the $R=20$ and $R=30$ for Tat_2.

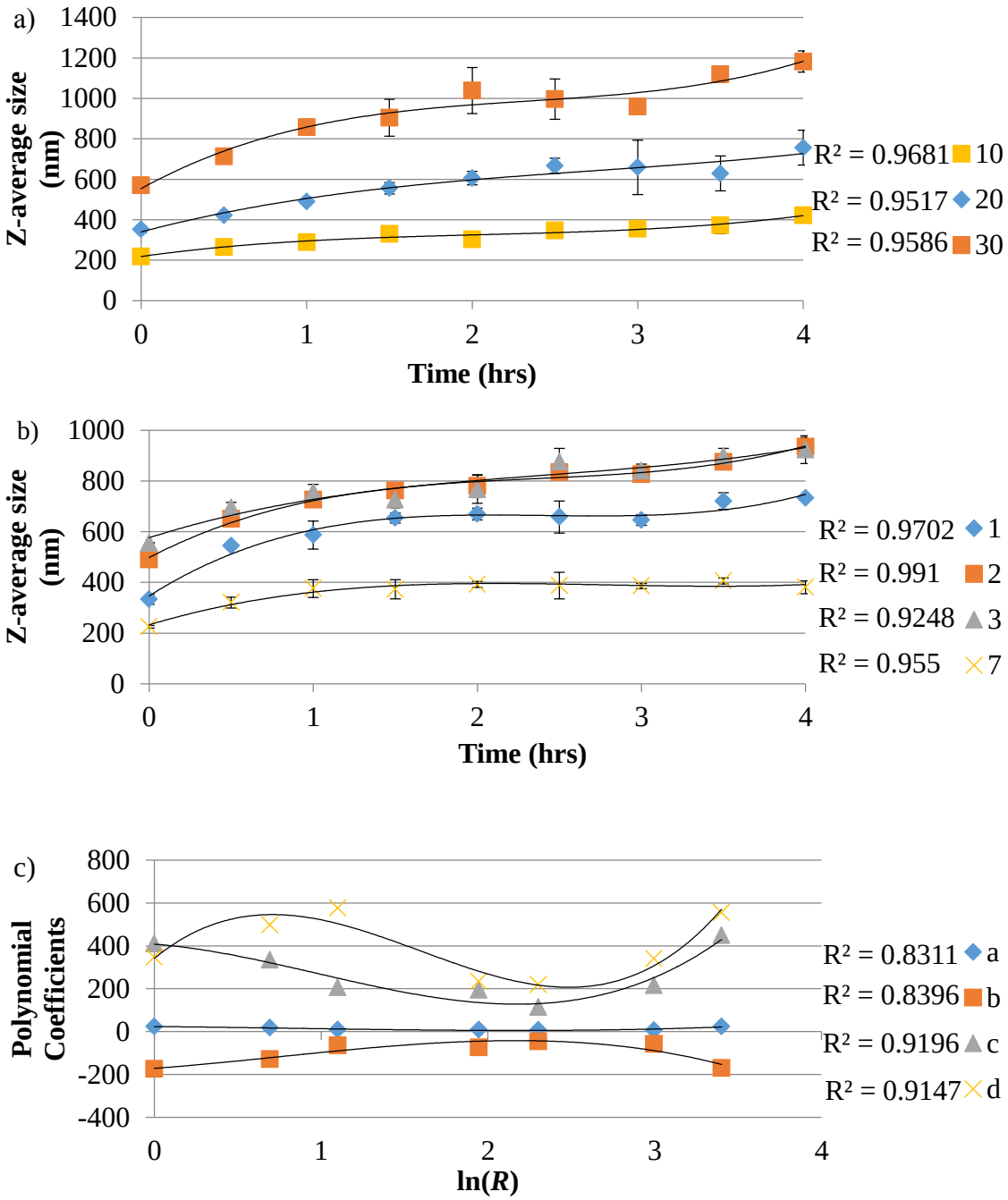

Figure 4.2: Trend in Z-average size of polyplexes consisting of R9 and 5-mer dsDNA over time with third order polynomial fits. R^2 values are displayed next to respective legend entries. Error bars are standard deviation about a mean of triplicate measurements of a single sample (a and b). Trend in coefficients of primary third order polynomials plotted against the natural log of the N:P ratio (*R*) with third order fits to the trends (c).

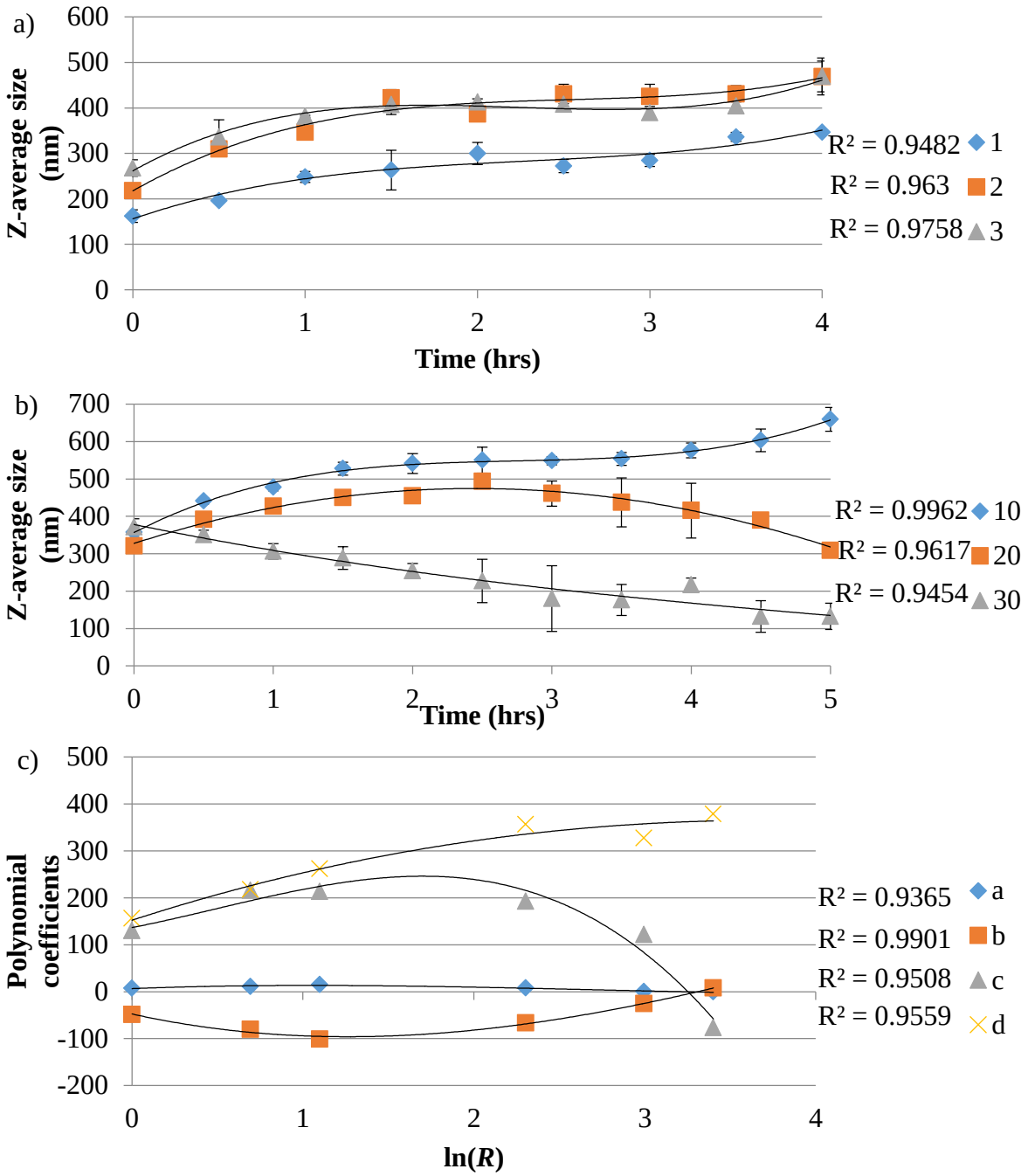

Figure 4.3: Trend in Z-average size of polyplexes consisting of Tat_2 and 5 mer dsDNA over time with third order polynomial fits. R^2 values are displayed next to their respective legend entries. Error bars show standard deviation about a mean of triplicate measurements of a single sample (a and b). Trend in coefficients of primary third order polynomials plotted against the natural log of the N:P ratio (*R*) with 3rd-order fits to the trends (c).

The coefficients for each 3rd – order regression were then plotted against the natural logarithm of *R*, yielding secondary 3rd-order patterns. It was shown, however, that the polynomial coefficient plot for Tat_2 showed patterns that could also be well fit by quadratic regression, but 3rd-order regressions were utilized to maintain consistency for later evaluation (see Fig. 4.2 and 4.3, panel c in both). The values for the d-coefficient calculated for R9, which correlates to the initial size of the polyplexes, was observed to have a trend of increase (from 218.6 to 576.1) to decrease (from 576.1 to 218.3) and back to an increase (from 218.3 to 554.2). This contrasted heavily with the overall trend of increase for the d-coefficient of Tat_2. Notwithstanding, these regression fits to the experimental data allowed for the derivation of an empirical approximation formula (see Eq. 4.1).

$$\boldsymbol{D_{HPP}(\Delta t_i, R) \approx (a_a \ln^3(R) + b_a \ln^2(R) + c_a ln(R) + d_a)\Delta t_i^{\,3} + (a_b \ln^3(R) + b_b \ln^2(R) + c_b ln(R) + d_b)\Delta t_i^{\,2} + (a_c \ln^3(R) + b_c \ln^2(R) + c_c ln(R) + d_c)\Delta t_i + a_d \ln^3(R) + b_d \ln^2(R) + c_d ln(R) + d_d} \quad \textbf{(4.1)}$$

Where D_{HPP} is the Z-average hydrodynamic diameter of the polyplexes in nm, Δt_i is the change in time (in hours) after initial complex formation (i.e. 15 minutes post mixing), and *R* is the molar ratio of the cationic residues of the peptide to the phosphate groups on the oligonucleotide. All coefficients from a_a to d_d are empirical constants derived from the secondary 3rd-order fits that relate the natural logarithm of *R* to the primary 3rd-order coefficients; a_a to d_a defines the *a* term with units in nm/hr^3, a_b to b_b defines the b term with units in nm/hr^2, a_c to d_c defines the *c* term with units in nm/hr and a_d to d_d defines the d term with units in nm. From this equation it becomes apparent that

the behavior of each polyplex may be defined according to a 4×4 matrix such that each primary coefficient is defined by each row of the matrix shown in equation (**4.2**).

$$\boldsymbol{P(N,B,pH)} = \begin{bmatrix} \boldsymbol{a_a} & \boldsymbol{b_a} & \boldsymbol{c_a} & \boldsymbol{d_a} \\ \boldsymbol{a_b} & \boldsymbol{b_b} & \boldsymbol{c_b} & \boldsymbol{d_b} \\ \boldsymbol{a_c} & \boldsymbol{b_c} & \boldsymbol{c_c} & \boldsymbol{d_c} \\ \boldsymbol{a_d} & \boldsymbol{b_d} & \boldsymbol{c_d} & \boldsymbol{d_d} \end{bmatrix} \tag{4.2}$$

Where the matrix is designated by the peptide name "*P*", with the values of the matrix being as yet undetermined functions of the nucleic acid identity "*N*" (number of nucleotides and double or single stranded, RNA or DNA) the buffer or media conditions "*B*" and the pH of the solution "*pH*". This matrix arrangement of the constants allows for the simplification of equation **(1)** to a product of that coefficient matrix and vector matrices of $ln^3(R)$, $ln^2(R)$, $ln(R)$ and 1, as well as $\Delta t_i{}^3$, $\Delta t_i{}^2$, Δt_i and 1 (see Eq (**4.3**)).

$$\boldsymbol{D_{HPP}(\Delta t_i, R)} \approx \begin{bmatrix} \boldsymbol{\Delta t_i}^3 & \boldsymbol{\Delta t_i}^2 & \boldsymbol{\Delta t_i} & \mathbf{1} \end{bmatrix} \left(\begin{bmatrix} \boldsymbol{a_a} & \boldsymbol{b_a} & \boldsymbol{c_a} & \boldsymbol{d_a} \\ \boldsymbol{a_b} & \boldsymbol{b_b} & \boldsymbol{c_b} & \boldsymbol{d_b} \\ \boldsymbol{a_c} & \boldsymbol{b_c} & \boldsymbol{c_c} & \boldsymbol{d_c} \\ \boldsymbol{a_d} & \boldsymbol{b_d} & \boldsymbol{c_d} & \boldsymbol{d_d} \end{bmatrix} \begin{bmatrix} \boldsymbol{ln^3(R)} \\ \boldsymbol{ln^2(R)} \\ \boldsymbol{ln(R)} \\ \mathbf{1} \end{bmatrix} \right) \tag{4.3}$$

Using the form of matrix representation shown in equation (**4.2**), equations (**4.4**) and (**4.5**) show the empirically determined matrices for R9 and Tat_2 using the designation of $dsDNA_5$ to represent a double-stranded 5-bp oligonucleotide.

$$R9(\boldsymbol{dsDNA_5, 50\ mM\ K_2HPO_4, 7.0}) = \begin{bmatrix} \mathbf{2.005} & \mathbf{-4.824} & \mathbf{-7.419} & \mathbf{23.72} \\ \mathbf{-13.23} & \mathbf{29.65} & \mathbf{57.54} & \mathbf{-171.3} \\ \mathbf{41.60} & \mathbf{-121.9} & \mathbf{-60.29} & \mathbf{407.8} \\ \mathbf{120.8} & \mathbf{-578.4} & \mathbf{637.3} & \mathbf{341.6} \end{bmatrix} \tag{4.4}$$

$$\boldsymbol{Tat_2(dsDNA_5, 50\ mM\ K_2HPO_4, 7.0)} = \begin{bmatrix} \mathbf{1.050} & \mathbf{-8.423} & \mathbf{14.19} & \mathbf{6.575} \\ \mathbf{-2.278} & \mathbf{36.16} & \mathbf{-80.38} & \mathbf{-47.48} \\ \mathbf{-19.75} & \mathbf{29.27} & \mathbf{71.75} & \mathbf{136.6} \\ \mathbf{0.2142} & \mathbf{-17.08} & \mathbf{117.8} & \mathbf{152.3} \end{bmatrix} \quad \textbf{(4.5)}$$

Row sums of each matrix were used as a non-arbitrary comparison between peptides and their evolution with a specific nucleic acid over time. The top row was designated the "a" row and proceeded in alphabetical order to "d" with the bottom row (see Table 4.1). These sums normalize the coefficients under the assumption of $R=e$ such that $ln(R)=1$.

Table 4.1: Row Sums of Matrices with Respective Units for Peptides with 5-bp dsDNA

Peptide	Sequence	a-Row Sum (nm/hr^3)	b-Row Sum (nm/hr^2)	c-Row Sum (nm/hr)	d-Row Sum (nm)
R9	RRRRRRRRR	13.48	-97.38	267.2	521.2
Tat_2	RKKRRQRRRRKKRRQRRR	13.39	-93.98	217.9	253.3

Despite apparently large differences in their behavior at high R values, it was found that the a-coefficient row sum was nearly identical between the two peptides having a value of 13.48 nm/hr^3 for R9 and 13.39 nm/hr^3 for Tat_2. Similarly, row sums for the b-coefficients (a_b through d_b) were found to be -97.38 and -93.98 nm/hr^2 for R9 and Tat_2 respectively. However they differed substantially in both c- and d- row sums with Tat_2 being smaller in both cases, by 49.3 nm/hr in the c-row sum and 267.9 nm in the d-row sum (see Table 4.1).

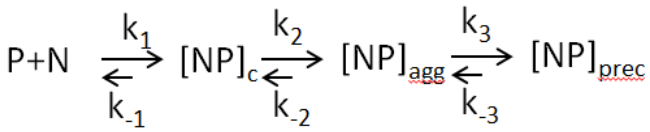

Figure 4.4: Kinetic Scheme for the aggregation of polyplexes composed of cationic nitrogenous peptide "N" and anionic phosphate bearing nucleotide "P". Definitions for the objects above are: $[NP]_c$, nucleotide-peptide complex, $[NP]_{agg}$ nucleotide-peptide aggregate, $[NP]_{prec}$ nucleotide-peptide precipitate and designation "k" for all kinetic constants. This is under the assumptions that *R* ratio equals to or exceeds a value of 1 and that $k_1 > k_{-1}$, $k_2 > k_{-2}$ and $k_3 > k_{-3}$.

Given the scheme for aggregation described previously (Zheng, Niu et al. 2014), where polyplex aggregation and evolution proceed through three primary stages, it may be assumed under the equilibrium scheme in Figure 4.4, that the sum of the kinetic rate equation for growth in terms of kinetic constants k_2 and k_3 may be proportional to the contributions of the cubic scaled of the "*a*" row sum and the linearly scaled "c" row sum. Likewise the kinetic constants k_{-2} and k_{-3} were proportional to the row sum "b", in cases where $k_1 >> k_{-1}$ (see Eq (**4.6**) and (**4.7**)).

$$\boldsymbol{v_{Pg}} = [[\boldsymbol{NP}]_{\boldsymbol{c}}]\boldsymbol{k_2} + \left[[\boldsymbol{NP}]_{\boldsymbol{agg}}\right]\boldsymbol{k_3} \propto$$

$$\begin{bmatrix}\Delta \boldsymbol{t_i}^{\boldsymbol{3}} & \boldsymbol{0} & \Delta \boldsymbol{t_i} & \boldsymbol{0}\end{bmatrix}\left(\begin{bmatrix}\boldsymbol{a_a} & \boldsymbol{b_a} & \boldsymbol{c_a} & \boldsymbol{d_a}\\ \boldsymbol{a_b} & \boldsymbol{b_b} & \boldsymbol{c_b} & \boldsymbol{d_b}\\ \boldsymbol{a_c} & \boldsymbol{b_c} & \boldsymbol{c_c} & \boldsymbol{d_c}\\ \boldsymbol{a_d} & \boldsymbol{b_d} & \boldsymbol{c_d} & \boldsymbol{d_d}\end{bmatrix}\begin{bmatrix}\boldsymbol{ln^3(R)}\\ \boldsymbol{ln^2(R)}\\ \boldsymbol{ln(R)}\\ \boldsymbol{1}\end{bmatrix}\right) \qquad \textbf{(4.6)}$$

$$\boldsymbol{v_{Pd} = [[NP]_{agg}]k_{-2} + [[NP]_{prec}]k_{-3} \propto}$$

$$\left|\begin{bmatrix}\mathbf{0} & \Delta t_i^{\,2} & \mathbf{0} & \mathbf{0}\end{bmatrix}\left(\begin{bmatrix}a_a & b_a & c_a & d_a\\ a_b & b_b & c_b & d_b\\ a_c & b_c & c_c & d_c\\ a_d & b_d & c_d & d_d\end{bmatrix}\begin{bmatrix}ln^3(R)\\ ln^2(R)\\ ln(R)\\ \mathbf{1}\end{bmatrix}\right)\right| \qquad \textbf{(4.7)}$$

Where v_{Pg} is the rate of polyplex growth and v_{Pd} is the rate of polyplex dissociation under the conditions described. With this proportionality holding within proscribed limits the ratio of the rates of polyplex precipitation and polyplex dissociation are propotional to their respective row sums from equations (**4.6**) and (**4.7**) (see Eq (**4.8**)).

$$\frac{\mathbf{v_{Pg}}}{\mathbf{v_{Pd}}} = \frac{[[\mathbf{NP}]_c]\mathbf{k_2}+[[\mathbf{NP}]_{agg}]\mathbf{k_3}}{[[\mathbf{NP}]_{agg}]\mathbf{k_{-2}}+[[\mathbf{NP}]_{prec}]\mathbf{k_{-3}}} \propto$$

$$\frac{(\mathbf{a_a\,ln^3(R)+b_a\,ln^2(R)+c_a ln(R)+d_a})\Delta\mathbf{t_i}^3+(\mathbf{a_c\,ln^3(R)+b_c\,ln^2(R)+c_c ln(R)+d_c})\Delta\mathbf{t_i}}{|(\mathbf{a_b\,ln^3(R)+b_b\,ln^2(R)+c_b ln(R)+d_b})\Delta\mathbf{t_i}^2|} \qquad \textbf{(4.8)}$$

Given this proportionality an additional value, here referred to as "Ɨ", can be calculated given as the ratio of the definite integrals of each component over the observed time and ratio spans:

$$\text{Ɨ} =$$

$$\frac{\int_{R_i}^{R_f}\int_{\Delta t_{i,i}}^{\Delta t_{i,f}}(\mathbf{a_a\,ln^3(R)+b_a\,ln^2(R)+c_a ln(R)+d_a})\Delta\mathbf{t_i}^3+(\mathbf{a_c\,ln^3(R)+b_c\,ln^2(R)+c_c ln(R)+d_c})\Delta\mathbf{t_i}\;d\Delta\mathbf{t_i}dR}{\left|\int_{R_i}^{R_f}\int_{\Delta t_{i,i}}^{\Delta t_{i,f}}(\mathbf{a_b\,ln^3(R)+b_b\,ln^2(R)+c_b ln(R)+d_b})\Delta\mathbf{t_i}^2\;d\Delta\mathbf{t_i}dR\right|}$$

(4.9)

Because these definite integral ratios are proportional to equation (**4.8**)**,** it follows that Ɨ is proportional to $\frac{v_{Pg}}{v_{Pd}}$ (Eq. (**4.10**)):

$$\frac{v_{Pg}}{v_{Pd}} \propto Ɨ \qquad \textbf{(4.10)}$$

With this relationship Ɨ is an approximate measure of the tendency of the polyplex system to precipitate over time under the specified parameters. Higher values of Ɨ indicate a greater tendency to aggregate and precipitate over the N:P ratios (i.e. *R*) considered and time course of observation.

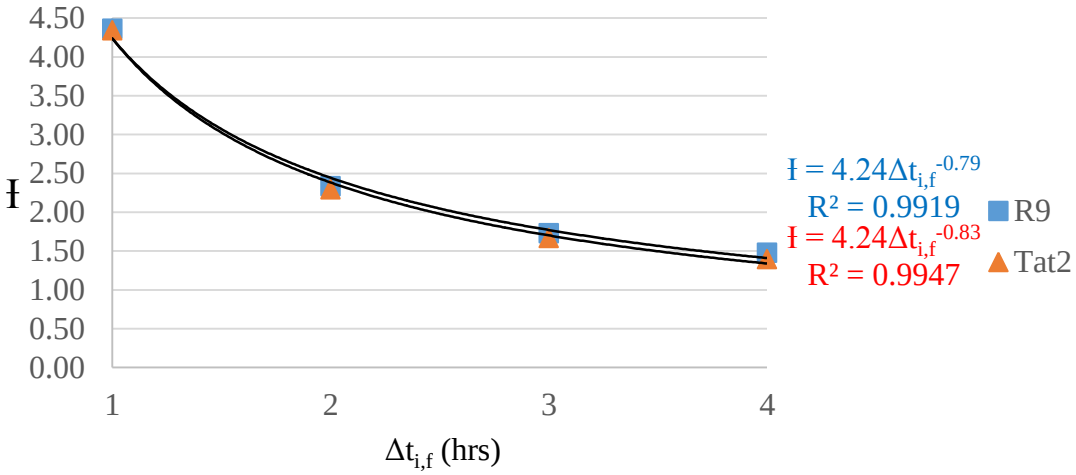

Figure 4.5: Plot of Ɨ values calculated at different values of $\Delta t_{i,f.}$ Based on a $\Delta t_{i,i}$ of 0 hrs and R_i of 1 and R_f of 30.
Trend lines shown indicate a power regression for which the equations and R^2 values are shown, blue for R9 (blue squares) and red for Tat_2 (red triangles).

The values of Ɨ for incrementally higher $\Delta t_{i,f}$ values (1, 2, 3 and 4 hrs) was found to follow a decaying power function, where the regressions show a high degree of similarity between that for R9 and Tat_2. Divergence may be noted as $\Delta t_{i,f}$ values were increased, showing that Tat_2 has generally lower values of Ɨ, with greatest divergence at

$\Delta t_{i,f}$ = 4 hrs, with 1.39 and 1.47 for Tat_2 and R9 respectively. The variable exponent may be pointed out as representative of the divergence, with -0.79 for R9 and -0.83 Tat_2 (see Fig. 4.5).

4.4 Discussion

Here, it was shown that the behavior of polyplex evolution over time was related to 3rd-order polynomial patterns and produced a matrix of constants unique to the peptide in question, which themselves were presumed to be a function of the nucleic acid size and character, the media or buffer composition and the pH. Prior to this study it was shown that the evolution of polyplexes formed from poly-L-lysine and 21 bp dsDNA or 2 kb dsDNA over time consisted of a minimum of three phases; initial formation, aggregation and finally precipitation (Zheng, Niu et al. 2014) each governed by kinetic constants (see Fig. 4.4).

In the present work it has been shown that the aggregation and precipitation phases were observable via DLS, but also revealed other parameters of how the hydrodynamic diameter of the particles change over time. It has been shown that there is at minimum one term related to growth over time, one term related to deceleration of that growth and one term that is a "jerk" term describing the change in the acceleration of growth. These parameters were best represented by the row-sums of the peptide matrices, with the a-row sum representing the magnitude of the jerk term, the b-sum representing the magnitude of the deceleration of growth, the c-row sum representing the rate of polyplex growth and the d-row sum representing the initial size of the polyplex as a hydrodynamic diameter (D_H). Each row sum value may be considered a multiplier that acts upon the natural logarithm of *R*, and may further be related to the evolution kinetics

of the system.

It was interesting that 3rd-order fits characterized polyplex evolution over the 4-5 hour time course of observation, as it noted a significant contribution of aggregate dissociation in the b-row sum, which manifested as a prolonged state of roughly stable polyplex size at R=7 for R9 while in the case of Tat_2 this led to a decrease in Z-average size at R>20. This may have been a function of the composition and pH of the buffer as well as the peptide used. In the case of interest, 50 mM potassium phosphate was used to buffer the system, which may have allowed for charge screening and retardation of the aggregation stage of polyplex time evolution (Zhu, Sheng et al. 2011). The similarity of this parameter between the two peptides studied suggests that its contribution at higher R is less significant and therefore may be governed primarily by buffer concentration and composition, due to higher concentrations of peptide being less inhibited by charge screening.

The "jerk" parameter of the a-row sum was also shown to be highly similar between the two peptides, with values of 13.48 nm/hr^3 and 13.39 nm/hr^3 for R9 and Tat_2 respectively, suggesting that this parameter may be dependent on the size and type of oligonucleotide used. This parameter may have some contribution from the buffer, again from charge screening, but since this parameter fundamentally reverses the effects of the b-row sum in the cases studied, it must be closer related to size increase, suggesting that it was primarily related to the common nucleic acid size between each peptide.

The primary growth rate term derived from the c-row sum may likely be related to the binding of the peptide to the nucleic acid, as both peptides were characterized by

high cationic charge this term was also similar between the two peptides, but not nearly as similar as the a- and b-row sums. Still, this significant difference between the two values for R9 and Tat_2 may be related to their respective abilities to complex and subsequently shield oligonucleotides from further interaction with other polyplexes (Dey, Kumar et al. 2014). This would explain why Tat_2 had a lower c-row sum as it would be more efficiently wrapped around the 5-mer oligonucleotide, due to its greater length over R9 (eighteen residues as opposed to nine residues).

Finally, the d-row sum displays a multiplier of the initial size of the polyplex, which was less than half as large (~48%) in the case of 5-mer dsDNA as R9, at 253.3 nm for Tat_2 compared to 521.2 nm for R9. This nearly exactly 50% difference conspicuously points to the difference in molecular weight and residue length of each peptide, as Tat_2 has eighteen residues at a molecular weight of 2.6612 kDa, and R9 has nine residues at a molecular weight of 1.4237 kDa. This may mean that this parameter was related directly to the size of the arginine rich peptide, as extension of particular moieties (e.g. polyethyleneglycol) has been shown to increase temporal stability of polyplexes using PEI (Millili, Selekman et al. 2010, Smith, Beck et al. 2015).

As noted in the results (section 4.3), the values for the d-coefficient correlate with initial sizes of the different peptide to nucleic acid ratios (symbol *R*). This poses some interest as it was found that R9 had a pattern of initial increase in size that dropped off heavily at $\ln(R)>1$, and was followed by a progressive increase in value from $\ln(R)>2$ (see Fig. 4.2). This phenomenon was not observed with Tat_2, where a gradual increase in the d-value was noted at increasing values of *R*. This suggests that in the case of R9, the peptide was able to stabilize the polyplex size through charge screening and effective

complexation, but that massive increases in peptide content (R>10) the peptide began to add more mass to the polyplexes. In Tat_2 this phenomenon was not observed. This may have been because either, the search space did not cover the range over which the d-value reduction occurs (3>R<10), or Tat_2 proceeds to a pattern of peptide build-up on formed polyplexes with little to no point of polyplex size reduction. It is worth noting however that the Tat_2 d-value did show a slight dip at R=20, which may have been an indication of a similar trend to R9 over a range between R=10 and R=30.

It was shown that Tat_2 has less tendency towards aggregation and precipitation than R9 by using the values for Ɨ; however, the difference between the two peptides was vanishingly small (see Fig. 4.5), suggesting highly similar complexation patterns over the time course of observation and even the values of R evaluated. This was surprising given the highly dissimilar matrix values and the different patterns of aggregation observed (see Fig. 4.2 and 4.3). It was also interesting to note that the value for Ɨ decreases substantially as the value of $\Delta t_{i,f}$ was increased, showing an inverse relationship between the tendency towards aggregation and the time that has elapsed. However, the metric may only be valid in comparison between peptides, whereby the divergence observed at increasing $\Delta t_{i,f}$ indicated a point of decreasing similarity between the two peptides in their aggregation behaviour.

Optimization of DNA:polycation systems has been attempted before, where 2 kDa branch PEI was used to complex plasmid DNA. In that work response surface methodology (RSM) and design of experiment (DoE) analysis, were used in a similar fashion to the method described here to optimize the pH, PEI concentration and DNA concentration to achieve maximum stability of the formed polyplexes (Clima, Ursu et al.

2015). Particularly RSM, was applied in a manner very similar to the present work, wherein, where here R, $\Delta t_{i,}$ and Ɨ were used create a search space or landscape of temporal polyplex behaviour. This was found to relate to the kinetics of polyplex formation as has been suggested in several other works (Nam, Kim et al. 2011, Dey, Kumar et al. 2014).

4.5 Conclusions

The parameters discovered using the experimental and mathematical set-up described allows for the characterization of polyplexes, in terms of the particular peptides involved, oligonucleotide size and identity and buffering conditions. Furthermore, the introduction of the empirical value Ɨ allows for independent measurement of polyplex evolution dynamics over time with attention to the entire scope of the experiment. Future work will require more peptides and sizes of nucleic acid to be evaluated as well as temperatures and pH increments. It is likely these parameters may impact polyplex behaviour and allow for more rigorous estimation of optimized conditions and comparison between various polyplex types.

5.0 Summary

In this thesis, three chief discoveries were underscored in relation to CPPs and their interaction with plant cells. First, the adsorption of CPPs and similar molecules to the surface of microspores, which revealed a portion of the charge character of microspores, showing a particularly high adsorption affinity for the CPP Tat_2. Secondly, a demonstration of the use of a phosphonium salt, TBPB, as a CPP:nucleic acid polyplex chaotropic and stabilizer, as well as a transfection adjuvant in leaf tissue. Thirdly, that there exists a robust mathematical relationship between the aggregation of CPP:nucleic acid polyplexes, time and the ratio of CPP to nucleic acid, that leads to the calculation of a non-arbitrary value ("Ғ") that characterizes a particular combination of CPP and nuclei-acid under a specific set of conditions. These three discoveries were punctuated by the demonstration of the versatility of an extremely basic pair of techniques for measuring charge character or zeta-potential and nanoparticle size, in ELS and DLS respectively. The extensive use of these techniques allowed for the detection of heretofore unknown changes in the charge character of microspore exine due to pH and methodologically simple profiling of the aggregation character of CPP:nucleic acid polyplexes. Lastly this research presents the first use of proper RT-qPCR in detecting the silencing of an endogenous plant gene with CPP delivered siRNA.

6.0 Future Directions

While the studies presented within this thesis may be deemed relatively complete, there remains several confirmatory studies which must be carried out. Most of these are noted within the discussion sections of the preceding chapters (see sections 2.4, 3.4 and 4.4). Future work will likely take the shape of application of the basic science findings discussed in this thesis, namely taking advantage of the charge character of the microspore exine to improve transfection, applying siRNA delivery formulations in the field and designing of peptides or other nanocarriers specialized for delivery in plant cells.

In the case of microspore exine, pH must be investigated further, as well as how microspores can be buffered to prevent the presumably adverse effects of CPP adsorption to their surface, thereby increasing the soluble portion of CPPs and CPP:cargo complexes. With the high affinity that the CPP Tat_2 has for the exine surface, nearly all CPP introduced during a standard transfection may adsorb to the exine and never interact with the cell membrane and thereby transfect the microspore. Lowering pH below a value of 7.0 appears to be a viable option, but other effects on the CPP:nucleic acid polyplexes that result from pH reduction must be investigated in tandem to properly utilize the information presented here. Alternatively, the strong adsorptive properties of cationic CPPs to the microspore exine may be used to the advantage of transfection by coating the microspore exine in CPPs, thereby inducing internalization mechanisms through saturation, before addition of CPP:cargo complexes or polyplexes. With this, steps must be taken to minimize cytotoxicity, and optimize the process.

In transfecting plants in the field with siRNA two major hurdles must be overcome; the infiltration method and the toxicity of the adjuvant TBPB. In Chapter 3.0, the infiltration method was injection, and for application in the field individual injection would present extreme tediousness and expense, necessitating the demonstration of the formulation to work as a foliar spray, where dosage would be less controlled as well as less concentrated. It was shown (tentatively) that TBPB and Tat_2 were necessary for delivery of siRNA into triticale leaves, with TBPB being an environmentally toxic chemical (Biczak, Bałczewski et al. 2014). Two routes may solve this problem, either reduction of the concentration of TBPB in the formulation or its replacement with a safer chemical that shows similar properties, which may be other organo-phosphonium based ionic liquids. Should success be fully demonstrated with these two hurdles, applications beyond plants may become relevant, as common pests, parasites and weeds may also become targets for siRNA treatment with the purpose of environmentally safe extermination.

Finally, application of the methodological set-up described in Chapter 4.0, may be used to define peptides on a quantitative scale, and lead to design of CPPs specifically for use with plants and plant based tissue culture. By employing DLS as a primary high throughput tool, other factors may be incorporated into the method to fully profile CPP:nucleic acid polyplex aggregation; namely temperature, CPP sequence, CPP isoelectric point, CPP molecular weight, pH, buffer concentration or ionic strength, buffer viscosity, buffer composition, nucleic acid length, nucleic acid type (DNA or RNA, single stranded versus double stranded) and transfection efficiency. All of these factors may be freely integrated into the equations outlined using polynomial regression to model the

behavior of each polyplex formulation, and quantitatively compare them. By creating a comprehensive landscape from the listed factors, prediction of sequences of maximum transfection efficiency may be able to be accurately predicted. Furthermore response surface methodology may also be applied to reduce the required data points for this comprehensive landscape, allowing for more rapid determination of the multi-factor landscape (Clima, Ursu et al. 2015, Mostafaei, Ghobadian et al. 2015).

7.0 Bibliography

Abe, M., Y. Fukaya and H. Ohno (2012). "Fast and facile dissolution of cellulose with tetrabutylphosphonium hydroxide containing 40 wt% water." Chem Commun (Camb) **48**(12): 1808-1810.

Abe, T., T. Kawaguchi, T. Saito and I. Satoh (2013). "Molecular dynamics analysis for the brownian motion of nano bubble." Particle-Based Methods III: Fundamentals and Applications: 569-576.

Antipina, A. Y. and A. A. Gurtovenko (2015). "Molecular mechanism of calcium-induced adsorption of DNA on zwitterionic phospholipid membranes." J Phys Chem B **119**(22): 6638-6645.

Antonelli, N. M. and J. Stadler (1990). "Genomic DNA can be used with cationic methods for highly efficient transformation of maize protoplasts." Theoretical and Applied Genetics **80**(3): 395-401.

Asif, M., F. Eudes, H. Randhawa, E. Amundsen, J. Yanke and D. Spaner (2013). "Cefotaxime Prevents Microbial Contamination and Improves Microspore Embryogenesis in Wheat and Triticale." Plant cell reports **32**(10): 1637-1646.

Atkin, S. L., S. Barrier, Z. Cui, P. D. Fletcher, G. Mackenzie, V. Panel, V. Sol and X. Zhang (2011). "UV and visible light screening by individual sporopollenin exines derived from Lycopodium clavatum (club moss) and Ambrosia trifida (giant ragweed)." J Photochem Photobiol B **102**(3): 209-217.

Balczewski, P., R. Biczak and B. Pawlowska Use of ionic salts containing phosphonium cation and halide anion, as herbicide for selectively or totally eradicating unwanted plants or weeds e.g. heartsease, and in chemical, pharmaceutical and food industries and electrochemistry areas, AKAD JANA DLUGOSZA (IMJA-Non-standard) AKAD JANA DLUGOSZA CZESTOCHOWIE (IMJA-Non-standard): 11.

Barrier, S. (2008). Physical and Chemical Properties of Sporopollenin Exine Particles. Doctor of Philosophy, University of Hull.

Barrier, S., A. Diego-Taboada, M. J. Thomasson, L. Madden, J. C. Pointon, J. D. Wadhawan, S. T. Beckett, S. L. Atkin and G. Mackenzie (2011). "Viability of plant spore exine capsules for microencapsulation." J. Mater. Chem. **21**(4): 975-981.

Battistini, F., C. A. Hunter, E. J. Gardiner and M. J. Packer (2010). "Structural mechanics of DNA wrapping in the nucleosome." J Mol Biol **396**(2): 264-279.

Bechara, C. and S. Sagan (2013). "Cell-penetrating peptides: 20 years later, where do we stand?" FEBS Letters **587**(12): 1693-1702.

Ben-Dov, N. and R. Korenstein (2012). "Enhancement of cell membrane invaginations, vesiculation and uptake of macromolecules by protonation of the cell surface." PLoS One **7**(4): e35204.

Ben-Dov, N. and R. Korenstein (2013). "Proton-induced endocytosis is dependent on cell membrane fluidity, lipid-phase order and the membrane resting potential." Biochim Biophys Acta **1828**(11): 2672-2681.

Biczak, R., P. Bałczewski, B. Pawłowska, B. Bachowska and P. Rychter (2014). "Comparison of Phytotoxicity of Selected Phosphonium Ionic Liquid." Ecological Chemistry and Engineering S **21**(2): 281-295.

Bilichak, A., J. Luu and F. Eudes (2015). "Intracellular delivery of fluorescent protein into viable wheat microspores using cationic peptides." Frontiers in Plant Science **6**.

Bolhassani, A. (2011). "Potential efficacy of cell-penetrating peptides for nucleic acid and drug delivery in cancer." Biochim Biophys Acta **1816**(2): 232-246.

Bondar, O. V., D. V. Saifullina, I. I. Shakhmaeva, I. I. Mavlyutova and T. I. Abdullin (2012). "Monitoring of the zeta potential of human cells upon reduction in their viability and interaction with polymers." Acta Naturae **4**(1): 78-81.

Brock, R. (2014). "The uptake of arginine-rich cell-penetrating peptides: putting the puzzle together." Bioconjug Chem **25**(5): 863-868.

Budak, H., J. Jiao, Y. Wang, J. N. Selvaraj, F. Xing and Y. Liu (2015). "Barley Stripe Mosaic Virus (BSMV) Induced MicroRNA Silencing in Common Wheat (Triticum aestivum L.)." Plos One **10**(5): e0126621.

Cardoso, A. M., S. Trabulo, A. L. Cardoso, S. Maia, P. Gomes, A. S. Jurado and M. C. Pedroso de Lima (2013). "Comparison of the Efficiency of Complexes Based on S4-PV Cell-Penetrating Peptides in Plasmid DNA and siRNA Delivery." Mol Pharm **10**(7): 2653-2666.

Charriere, F., E. Cuche, P. Marquet and C. Depeursinge (2006). Biological Cell (Pollen Grain) Refractive Index Tomography with Digital Holographic Microscopy. Conference on Three-Dimensional and Multidimensional Microscopy - Image Acquisition and Processing XIII, San Jose, CA.

Chatterjee, A. and S. P. Moulik (2005). "Studies on surfactant-biopolymer interaction. II. Interaction of cetyl trimethyl ammonium-, cetyl ethanolyl dimethyl ammonium-, cetyl diethanolyl methyl ammonium- and cetyl triphenyl phosphonium bromides and cetyl pyridinium chloride with calf thymus DNA." Indian Journal of Biochemistry & Biophysics **42**(4): 205-215.

Chichiriccò, G. and A. Poma (2015). "Penetration and Toxicity of Nanomaterials in Higher Plants." Nanomaterials **5**(2): 851-873.

Chuah, J. A., T. Yoshizumi, Y. Kodama and K. Numata (2015). "Gene introduction into the mitochondria of Arabidopsis thaliana via peptide-based carriers." Sci Rep **5**: 7751.

Chugh, A., E. Amundsen and F. Eudes (2009). "Translocation of cell-penetrating peptides and delivery of their cargoes in triticale microspores." Plant Cell Rep **28**(5): 801-810.

Chugh, A. and F. Eudes (2008). "Study of uptake of cell penetrating peptides and their cargoes in permeabilized wheat immature embryos." FEBS J **275**(10): 2403-2414.

Chugh, A., F. Eudes and Y. S. Shim (2010). "Cell-penetrating peptides: Nanocarrier for macromolecule delivery in living cells." IUBMB Life **62**(3): 183-193.

Ciesla, J., A. Bieganowski, M. Janczarek and T. Urbanik-Sypniewska (2011). "Determination of the electrokinetic potential of Rhizobium leguminosarum bv trifolii Rt24.2 using Laser Doppler Velocimetry--a methodological study." J Microbiol Methods **85**(3): 199-205.

Clima, L., E. L. Ursu, C. Cojocaru, A. Rotaru, M. Barboiu and M. Pinteala (2015). "Experimental design, modeling and optimization of polyplex formation between DNA oligonucleotides and branched polyethylenimine." Org Biomol Chem **13**(36): 9445-9456.

Crnolatac, I., L. M. Tumir, N. Y. Lesev, A. A. Vasilev, T. G. Deligeorgiev, K. Miskovic, L. Glavas-Obrovac, O. Vugrek and I. Piantanida (2013). "Probing the Structural Properties of DNA/RNA Grooves with Sterically Restricted Phosphonium Dyes: Screening of Dye Cytotoxicity and Uptake." Chemmedchem **8**(7): 1093-1103.

Cumming, J., D. W. Hawker, H. Chapman and K. Nugent (2010). "Sorption of Polymeric Quaternary Ammonium Compounds to Humic Acid." Water, Air, & Soil Pollution **214**(1-4): 5-11.

Dehkordi, M. N., A. K. Bordbar, P. Lincoln and V. Mirkhani (2012). "Spectroscopic study on the interaction of ct-DNA with manganese Salen complex containing triphenyl phosphonium groups." Spectrochim Acta A Mol Biomol Spectrosc **90**: 50-54.

Delaroche, D., B. Aussedat, S. Aubry, G. Chassaing, F. Burlina, G. Clodic, G. Bolbach, S. Lavielle and S. Sagan (2007). "Tracking a new cell-penetrating (W/R) nonapeptide, through an enzyme-stable mass spectrometry reporter tag." Anal Chem **79**(5): 1932-1938.

Deshayes, S., T. Plenat, G. Aldrian-Herrada, G. Divita, C. Le Grimellec and F. Heits (2004). "Primary amphipathic cell-penetrating peptides: Structural Requirements and Interactions with model membranes." Biochemistry **43**(24): 7698-7706.

Dey, D., S. Kumar, R. Banerjee, S. Maiti and D. Dhara (2014). "Polyplex formation between PEGylated linear cationic block copolymers and DNA: equilibrium and kinetic studies." J Phys Chem B **118**(25): 7012-7025.

Di Profio, P., R. Germani, L. Goracci, R. Grilli, G. Savelli and M. Tiecco (2010). "Interaction between DNA and cationic amphiphiles: a multi-technique study." Langmuir **26**(11): 7885-7892.

Dobrynin, A. and M. Rubinstein (2005). "Theory of polyelectrolytes in solutions and at surfaces." Progress in Polymer Science **30**(11): 1049-1118.

Dobrynin, A. V., A. Deshkovski and M. Rubinstein (2001). "Adsorption of Polyelectrolytes at Oppositely Charged Surfaces." Macromolecules **34**(10): 3421-3436.

Eggenberger, K., C. Mink, P. Wadhwani, A. S. Ulrich and P. Nick (2011). "Using the peptide BP100 as a cell-penetrating tool for the chemical engineering of actin f ilaments within living plant cells." Chembiochem **12**(1): 132-137.

El-Andaloussi, S., P. Jarver, H. J. Johansson and U. Langel (2007). "Cargo-dependent cytotoxicity and delivery efficacy of cell-penetrating peptides: a comparative study." Biochem J **407**(2): 285-292.

Ezzat, K., S. E. Andaloussi, E. M. Zaghloul, T. Lehto, S. Lindberg, P. M. Moreno, J. R. Viola, T. Magdy, R. Abdo, P. Guterstam, R. Sillard, S. M. Hammond, M. J. Wood, A. A. Arzumanov, M. J. Gait, C. I. Smith, M. Hallbrink and U. Langel (2011). "PepFect 14, a novel cell-penetrating peptide for oligonucleotide delivery in solution and as solid formulation." Nucleic Acids Res **39**(12): 5284-5298.

Fang, K., Y. Wang, T. Yu, L. Zhang, F. Baluška, J. Šamaj and J. Lin (2008). "Isolation of de-exined pollen and cytological studies of the pollen intines of Pinus bungeana Zucc. Ex Endl. and Picea wilsonii Mast." Flora - Morphology, Distribution, Functional Ecology of Plants **203**(4): 332-340.

Favretto, M. E., R. Wallbrecher, S. Schmidt, R. van de Putte and R. Brock (2014). "Glycosaminoglycans in the cellular uptake of drug delivery vectors - bystanders or active players?" J Control Release **180**: 81-90.

Ferrie, A. M. R. and K. L. Caswell (2010). "Isolated microspore culture techniques and recent progress for haploid and doubled haploid plant production." Plant Cell, Tissue and Organ Culture (PCTOC) **104**(3): 301-309.

Gimenez, M. J., F. Piston and S. G. Atienza (2011). "Identification of suitable reference genes for normalization of qPCR data in comparative transcriptomics analyses in the Triticeae." Planta **233**: 163-173.

Guterstam, P., F. Madani, H. Hirose, T. Takeuchi, S. Futaki, S. El Andaloussi, A. Graslund and U. Langel (2009). "Elucidating cell-penetrating peptide mechanisms of action for membrane interaction, cellular uptake, and translocation utilizing the hydrophobic counter-anion pyrenebutyrate." Biochim Biophys Acta **1788**(12): 2509-2517.

Halake, K., M. Birajdar, B. S. Kim, H. Bae, C. Lee, Y. J. Kim, S. Kim, H. J. Kim, S. Ahn, S. Y. An and J. Lee (2014). "Recent application developments of water-soluble synthetic polymers." Journal of Industrial and Engineering Chemistry **20**(6): 3913-3918.

Harrison, C. R., J. A. Sader and C. A. Lucy (2006). "Sulfonium and phosphonium, new ion-pairing agents with unique selectivity towards polarizable anions." J Chromatogr A **1113**(1-2): 123-129.

Hemp, S. T., M. H. Allen, Jr., M. D. Green and T. E. Long (2012). "Phosphonium-containing polyelectrolytes for nonviral gene delivery." Biomacromolecules **13**(1): 231-238.

Hemp, S. T., A. E. Smith, J. M. Bryson, M. H. Allen, Jr. and T. E. Long (2012). "Phosphonium-containing diblock copolymers for enhanced colloidal stability and efficient nucleic acid delivery." Biomacromolecules **13**(8): 2439-2445.

Herce, H. D., A. E. Garcia, J. Litt, R. S. Kane, P. Martin, N. Enrique, A. Rebolledo and V. Milesi (2009). "Arginine-rich peptides destabilize the plasma membrane, consistent with a pore formation translocation mechanism of cell-penetrating peptides." Biophys J **97**(7): 1917-1925.

Hidalgo-Alvarez, R., A. Martin, A. Fernandez, D. Bastos, F. Martinez and F. J. de las Nieves (1996). "Electrokinetic Properties, Colloidal Stability and Aggregation Kinetics of Polymer Colloids." Advances in Colloid and Interface Science **67**.

Holzberg, S., P. Brosio, C. Gross and G. P. Pogue (2002). "Barley stripe mosaic virus-induced gene silencing in a monocot plant." The Plant Journal **30**(3): 315-327.

Imani, R., S. H. Emami and S. Faghihi (2015). "Synthesis and characterization of an octaarginine functionalized graphene oxide nano-carrier for gene delivery applications." Phys. Chem. Chem. Phys. **17**(9): 6328-6339.

Jafari, M., W. Xu, R. Pan, C. M. Sweeting, D. N. Karunaratne and P. Chen (2014). "Serum stability and physicochemical characterization of a novel amphipathic peptide C6M1 for siRNA delivery." PLoS One **9**(5): e97797.

Jain, A., B. K. Yadav and A. Chugh (2015). "Marine antimicrobial peptide tachyplesin as an efficient nanocarrier for macromolecule delivery in plant and mammalian cells." FEBS J **282**(4): 732-745.

Jones, A. T. (2007). "Macropinocytosis: searching for an endocytic identity and role in the uptake of cell penetrating peptides." J Cell Mol Med **11**(4): 670-684.

Kadlecova, Z., Y. Rajendra, M. Matasci, L. Baldi, D. L. Hacker, F. M. Wurm and H. A. Klok (2013). "DNA delivery with hyperbranched polylysine: a comparative study with linear and dendritic polylysine." J Control Release **169**(3): 276-288.

Kagimoto, J., K. Fukumoto and H. Ohno (2006). "Effect of tetrabutylphosphonium cation on the physico-chemical properties of amino-acid ionic liquids." Chem Commun (Camb)(21): 2254-2256.

Kato, H., A. Nakamura and N. Noda (2014). "Determination of size distribution of silica nanoparticles: A comparison of scanning electron microscopy, dynamic light scattering, and flow field-flow fractionation with multiangle light scattering methods." Materials Express **4**(2): 144-152.

Kawamoto, S., T. Miyakawa, M. Takasu, R. Morikawa, T. Oda, H. Saito, S. Futaki and H. Nagao (2012). "Cell-penetrating peptide induces various deformations of lipid bilayer membrane: Inverted micelle, double bilayer, and transmembrane." International Journal of Quantum Chemistry **112**(1): 178-183.

Khondee, S., A. Baoum, T. J. Siahaan and C. Berkland (2011). "Calcium condensed LABL-TAT complexes effectively target gene delivery to ICAM-1 expressing cells." Mol Pharm **8**(3): 788-798.

Kim, S. S. and C. J. Douglas (2013). "Sporopollenin monomer biosynthesis in arabidopsis." Journal of Plant Biology **56**(1): 1-6.

Lakhwani, S. and M. N. Rahaman (1999). "Adsorption of polyvinylpyrrolidone (PVP) and its effect on the consolidation of suspensions of nanocrystalline CeO2 particles." Journal of Materials Science **34**: 3909-3912.

Lakshmanan, M., T. Yoshizumi, K. Sudesh, Y. Kodama and K. Numata (2015). "Double-stranded DNA introduction into intact plants using peptide-DNA complexes." Plant Biotechnology **32**(1): 39-45.

Lallemand, B., M. Erhardt, T. Heitz and M. Legrand (2013). "Sporopollenin biosynthetic enzymes interact and constitute a metabolon localized to the endoplasmic reticulum of tapetum cells." Plant Physiol **162**(2): 616-625.

Lalonde, S., M. Tegeder, M. Throne-Holst, W. B. Frommer and J. W. Patrick (2003). "Phloem loading and unloading of sugars and amino acids." Plant, Cell and Environment **26**(1): 37-56.

Lehto, T., R. Abes, N. Oskolkov, J. Suhorutsenko, D. M. Copolovici, I. Mager, J. R. Viola, O. E. Simonson, K. Ezzat, P. Guterstam, E. Eriste, C. I. Smith, B. Lebleu, A. Samir El and U. Langel (2010). "Delivery of nucleic acids with a stearylated (RxR)4 peptide using a non-covalent co-incubation strategy." J Control Release **141**(1): 42-51.

Li, Z.-y., Y. Liu, Y.-y. Zheng and R.-k. Xu (2014). "Zeta potential at the root surfaces of rice characterized by streaming potential measurements." Plant and Soil **386**(1-2): 237-250.

Liou, J. S., B. R. Liu, A. L. Martin, Y. W. Huang, H. J. Chiang and H. J. Lee (2012). "Protein Transduction in Human Cells is Enhanced by Cell-Penetrating Peptides Fused with an Endosomolytic HA2 Sequence." Peptides **37**(2): 273-284.

Lipatov, Y. S. (2002). "Polymer blends and interpenetrating polymer networks at the interface with solids." Progress in Polymer Science **27**(9): 1721-1801.

Liu, B. R., Y.-W. Huang, H.-J. Chiang and H.-J. Lee (2010). "Cell-Penetrating Peptide-Functionalized Quantum Dots for Intracellular Delivery." Journal of Nanoscience and Nanotechnology **10**(12): 7897-7905.

Liu, B. R., J. S. Liou, Y. J. Chen, Y. W. Huang and H. J. Lee (2013). "Delivery of nucleic acids, proteins, and nanoparticles by arginine-rich cell-penetrating peptides in rotifers." Mar Biotechnol (NY) **15**(5): 584-595.

Madani, F., S. Lindberg, U. Langel, S. Futaki and A. Graslund (2011). "Mechanisms of cellular uptake of cell-penetrating peptides." J Biophys **2011**: 414729.

Melnyk, C. W., A. Molnar and D. C. Baulcombe (2011). "Intercellular and systemic movement of RNA silencing signals." EMBO J **30**(17): 3553-3563.

Milletti, F. (2012). "Cell-penetrating peptides: classes, origin, and current landscape." Drug Discov Today **17**(15-16): 850-860.

Millili, P. G., J. A. Selekman, K. M. Blocker, D. A. Johnson, U. P. Naik and M. O. Sullivan (2010). "Structural and functional consequences of poly(ethylene glycol) inclusion on DNA condensation for gene delivery." Microscopy Research and Technique **73**(9): 866-877.

Minchin, R. F. and S. Yang (2010). "Endosomal disruptors in non-viral gene delivery." Expert Opinion on Drug Delivery **7**(3): 331-339.

Mizuno, T., M. Miyashita and H. Miyagawa (2009). "Cellular internalization of arginine-rich peptides into tobacco suspension cells: a structure-activity relationship study." J Pept Sci **15**(4): 259-263.

Mostafaei, M., B. Ghobadian, M. Barzegar and A. Banakar (2015). "Optimization of ultrasonic assisted continuous production of biodiesel using response surface methodology." Ultrason Sonochem **27**: 54-61.

Motta, S., P. Brocca, E. Del Favero, V. Rondelli, L. Cantù, A. Amici, D. Pozzi and G. Caracciolo (2013). "Nanoscale structure of protamine/DNA complexes for gene delivery." Applied Physics Letters **102**(5): 053703.

Muratovska, A., R. N. Lightowlers, R. W. Taylor, D. M. Turnbull, R. A. J. Smith, J. A. Wilce, S. W. Martin and M. P. Murphy (2001). "Targeting Peptide Nucleic Acid (PNA) Oligomers to Mitochondria Within Cells by Conjugation to Lipophilic Cations: Implications for Mitochondrial DNA Replication, Expression and Disease " Nucleic Acids Research **29**(9): 1852-1863.

Mäe, M., S. El Andaloussi, P. Lundin, N. Oskolkov, H. J. Johansson, P. Guterstam and U. Langel (2009). "A stearylated CPP for delivery of splice correcting oligonucleotides using a non-covalent co-incubation strategy." J Control Release **134**(3): 221-227.

Mäe, M., H. Myrberg, Y. Jiang, H. Paves, A. Valkna and U. Langel (2005). "Internalisation of cell-penetrating peptides into tobacco protoplasts." Biochim Biophys Acta **1669**(2): 101-107.

Mäger, I., E. Eiriksdottir, K. Langel, S. El Andaloussi and U. Langel (2010). "Assessing the uptake kinetics and internalization mechanisms of cell-penetrating peptides using a quenched fluorescence assay." Biochim Biophys Acta **1798**(3): 338-343.

Nam, H. Y., J. Kim, S. Kim, J. W. Yockman, S. W. Kim and D. A. Bull (2011). "Cell penetrating peptide conjugated bioreducible polymer for siRNA delivery." Biomaterials **32**(22): 5213-5222.

Nguyen, J., X. Xie, M. Neu, R. Dumitrascu, R. Reul, J. Sitterberg, U. Bakowsky, R. Schermuly, L. Fink, T. Schmehl, T. Gessler, W. Seeger and T. Kissel (2008). "Effects of cell-penetrating peptides and pegylation on transfection efficiency of polyethylenimine in mouse lungs." J Gene Med **10**(11): 1236-1246.

Numata, K., M. Ohtani, T. Yoshizumi, T. Demura and Y. Kodama (2014). "Local gene silencing in plants via synthetic dsRNA and carrier peptide." Plant Biotechnol J **12**(8): 1027-1034.

Ornelas-Megiatto, C., P. R. Wich and J. M. Frechet (2012). "Polyphosphonium polymers for siRNA delivery: an efficient and nontoxic alternative to polyammonium carriers." J Am Chem Soc **134**(4): 1902-1905.

Oskolkov, N., P. Arukuusk, D.-M. Copolovici, S. Lindberg, H. Margus, K. Padari, M. Pooga and Ü. Langel (2011). "NickFects, Phosphorylated Derivatives of Transportan 10 for Cellular Delivery of Oligonucleotides." International Journal of Peptide Research and Therapeutics **17**(2): 147-157.

Perevayazko, I. Y., M. Bauer, G. M. Pavlov, S. Hoeppener, S. Schubert, D. Fischer and U. S. Schubert (2012). "Polyelectrolyte complexes of DNA and linear PEI: formation, composition and properties." Langmuir **28**: 16167-16176.

Peuke, A. D., A. Gessler, S. Trumbore, C. W. Windt, N. Homan, E. Gerkema and H. Van As (2015). "Phloem flow and sugar transport in Ricinus communis L. is inhibited under anoxic conditions of shoot or roots." Plant Cell Environ **38**(3): 433-447.

Prabhu, S., S. R. Dennison, M. Mura, R. W. Lea, T. J. Snape and F. Harris (2014). "Cn-AMP2 from green coconut water is an anionic anticancer peptide." J Pept Sci **20**(12): 909-915.

Quebatte, G., E. Kitas and J. Seelig (2013). "riDOM, a cell-penetrating peptide. Interaction with DNA and heparan sulfate." J Phys Chem B **117**(37): 10807-10817.

Ranjbar, B. and P. Gill (2009). "Circular dichroism techniques: biomolecular and nanostructural analyses- a review." Chem Biol Drug Des **74**(2): 101-120.

Rodrigues, M., D. Andreu and N. C. Santos (2015). "Uptake and cellular distribution of nucleolar targeting peptides (NrTPs) in different cell types." Biopolymers **104**(2): 101-109.

Rodrigues, M., B. G. de la Torre, D. Andreu and N. C. Santos (2013). "Kinetic uptake profiles of cell penetrating peptides in lymphocytes and monocytes." Biochim Biophys Acta **1830**(10): 4554-4563.

Rosenbluh, J., S. K. Singh, Y. Gafni, A. Graessmann and A. Loyter (2004). "Non-endocytic penetration of core histones into petunia protoplasts and cultured cells: a novel mechanism for the introduction of macromolecules into plant cells." Biochim Biophys Acta **1664**(2): 230-240.

Sawahel, W. A. (2001). "Stable genetic transformation of cotton plants using polybrene-spermidine treatment." Plant Molecular Biology Reporter **19**(4): 377-377.

Shevchuk, I. A. and N. A. Klimenko (2010). "The change of the electrokinetic potential of Bacillus polymyxa IMV 8910 cells in interaction with ions of U(VI) and strontium." Journal of Water Chemistry and Technology **32**(1): 56-60.

Shi, J., H. Tan, X. H. Yu, Y. Liu, W. Liang, K. Ranathunge, R. B. Franke, L. Schreiber, Y. Wang, G. Kai, J. Shanklin, H. Ma and D. Zhang (2011). "Defective pollen wall is required for anther and microspore development in rice and encodes a fatty acyl carrier protein reductase." Plant Cell **23**(6): 2225-2246.

Shim, Y.-S., F. Eudes and I. Kovalchuk (2012). "dsDNA and protein co-delivery in triticale microspores." In Vitro Cellular & Developmental Biology - Plant **49**(2): 156-165.

Smith, R. J., R. W. Beck and L. E. Prevette (2015). "Impact of molecular weight and degree of conjugation on the thermodynamics of DNA complexation and stability of polyethylenimine-graft-poly(ethylene glycol) copolymers." Biophys Chem **203-204**: 12-21.

Steele, T. W., X. Zhao, P. Tarcha and T. Kissel (2012). "Factors influencing polycation/siRNA colloidal stability toward aerosol lung delivery." Eur J Pharm Biopharm **80**(1): 14-24.

Sun, D., H. I. Hussain, Z. Yi, R. Siegele, T. Cresswell, L. Kong and D. M. Cahill (2014). "Uptake and cellular distribution, in four plant species, of fluorescently labeled mesoporous silica nanoparticles." Plant cell reports **33**(8): 1389-1402.

Swiecicki, J.-M., A. Bartsch, J. Tailhades, M. Di Pisa, B. Heller, G. Chassaing, C. Mansuy, F. Burlina and S. Lavielle (2014). "The Efficacies of Cell-Penetrating Peptides in Accumulating in Large Unilamellar Vesicles Depend on their Ability To Form Inverted Micelles." Chembiochem **15**(6): 884-891.

Takechi, Y., H. Yoshii, M. Tanaka, T. Kawakami, S. Aimoto and H. Saito (2011). "Physicochemical mechanism for the enhanced ability of lipid membrane penetration of polyarginine." Langmuir **27**(11): 7099-7107.

Tanaka, K., T. Kanazawa, S. Horiuchi, T. Ando, K. Sugawara, Y. Takashima, Y. Seta and H. Okada (2013). "Cytoplasm-Responsive Nanocarriers Conjugated with a Functional Cell-Penetrating Peptide for Systemic siRNA Delivery." Int J Pharm **455**(1-2): 40-47.

Tsou, C. H., P. C. Cheng, C. M. Tseng, H. J. Yen, Y. L. Fu, T. R. You and D. B. Walden (2015). "Anther development of maize (Zea mays) and longstamen rice (Oryza longistaminata) revealed by cryo-SEM, with foci on locular dehydration and pollen arrangement." Plant Reprod **28**(1): 47-60.

Unnamalai, N., B. G. Kang and W. S. Lee (2004). "Cationic oligopeptide-mediated delivery of dsRNA for post-transcriptional gene silencing in plant cells." FEBS Lett **566**(1-3): 307-310.

Wang, S.-W., W. Liu and R. H. Colby (2011). "Counterion Dynamics in Polyurethane-Carboxylate Ionomers with Ionic Liquid Counterions." Chemistry of Materials **23**(7): 1862-1873.

Wang, Y.-H., Y.-C. Fu, H.-C. Chiu, C.-Z. Wang, S.-P. Lo, M.-L. Ho, P.-L. Liu and C.-K. Wang (2013). "Cationic nanoparticles with quaternary ammonium-functionalized PLGA–PEG-based copolymers for potent gene transfection." Journal of Nanoparticle Research **15**(11).

Wattraint, O., I. Saadallah, V. Silva-Pires, P. Sonnet and C. Sarazin (2013). "Influence of the insertion of a cationic peptide on the size and shape of nanoliposomes: a light scattering investigation." Int J Pharm **454**(2): 621-624.

Yamada, T., T. K. Das Gupta and C. W. Beattie (2013). "p28, an anionic cell-penetrating peptide, increases the activity of wild type and mutated p53 without altering its conformation." Mol Pharm **10**(9): 3375-3383.

Yamada, T., S. Signorelli, S. Cannistraro, C. W. Beattie and A. R. Bizzarri (2015). "Chirality switching within an anionic cell-penetrating peptide inhibits translocation without affecting preferential entry." Mol Pharm **12**(1): 140-149.

Yan, C. Y., J. W. Gu, D. P. Hou, H. Y. Jing, J. Wang, Y. Z. Guo, H. Katsumi, T. Sakane and A. Yamamoto (2015). "Synthesis of Tat tagged and folate modified N-succinyl-chitosan self-assembly nanoparticles as a novel gene vector." Int J Biol Macromol **72**: 751-756.

Zhang, W., J. Song, R. Liang, X. Zheng, J. Chen, G. Li, B. Zhang, K. Wang, X. Yan and R. Wang (2013). "Stearylated antimicrobial peptide [D]-K6L9 with cell penetrating property for efficient gene transfer." Peptides **46**: 33-39.

Zheng, C., L. Niu, W. Pan, J. Zhou, H. Lv, J. Cheng and D. Liang (2014). "Long-term kinetics of DNA interacting with polycations." Polymer **55**(10): 2464-2471.

Zhu, Y., R. Sheng, T. Luo, H. Li, W. Sun, Y. Li and A. Cao (2011). "Amphiphilic cationic [dendritic poly(L-lysine)]-block-poly(L-lactide)-block-[dendritic poly(L-lysine)]s in aqueous solution: self-aggregation and interaction with DNA as gene delivery carriers." Macromol Biosci **11**(2): 174-186.

Ziegler, A. and J. Seelig (2011). "Contributions of glycosaminoglycan binding and clustering to the biological uptake of the nonamphipathic cell-penetrating peptide WR9." Biochemistry **50**(21): 4650-4664.

Ziemienowicz, A., J. Pepper and F. Eudes (2015). "Applications of CPPs in Genome Modulation of Plants." Methods in molecular biology (Clifton, N.J.) **1324**: 417-434.

Ziemienowicz, A., Y. S. Shim, A. Matsuoka, F. Eudes and I. Kovalchuk (2012). "A novel method of transgene delivery into triticale plants using the Agrobacterium transferred DNA-derived nano-complex." Plant Physiol **158**(4): 1503-1513.

Zonin, E., R. Moscatiello, M. Miuzzo, N. Cavallarin, M. L. Di Paolo, D. Sandona, O. Marin, M. Brini, A. Negro and L. Navazio (2011). "TAT-mediated aequorin transduction: an alternative approach for effective calcium measurements in plant cells." Plant Cell Physiol **52**(12): 2225-2235.